Politecnico di Milano

Ingegneria dei Materiali

Laurea Magistrale

Investigation of a New Metallization Scheme for Front Ohmic Contacts to GaAs Intermediate Band Solar Cells

Andrea Li Bassi

Brittany Pattinson, 10427563

2014

© COPYRIGHT 2014

Brittany Pattinson. ALL RIGHTS RESERVED

Dedications

This work is dedicated to the two most inspirational women in my life, my grandmother and my mother. I love you both with all my heart.

Acknowledgments

There are a number of people without whom this thesis might not have been written, and to whom I am greatly indebted. First, I'd like to thank the members of my committee at Drexel University, Drs. Jonathan Spanier, Garritt Tucker, and Jason Baxter, and my advisor at Politecnico di Milano, Prof. Andrea Li Bassi, for their time and consideration. A special thank you goes to Dr. Spanier, who served as my advisor and provided me with much needed support and advice over the past years.

I must acknowledge the outstanding group at the Solar Energy Institute of the Polytechnic University of Madrid in Spain. I am incredibly grateful for the opportunity I had to work among such great minds and to conduct the majority of my research under the renowned Dr. Antonio Martí. This work may not have been completed successfully without the continued guidance I received from Dr. Alejandro Datas, who I thank for his patience and seemingly limitless ideas. I also owe many thanks to the countless others in the lab who helped me learn all the new techniques and concepts needed to finish my project. I owe thanks to Juan Villa for helping prepare the majority of my samples; to Esther López for explaining TLM to me more than once; to Irene Artacho for always helping me find what I needed around the lab; to Laura Barrutia for walking me through photolithography and for her constant encouragement; to Miguel Gómez for helping me fix things I swear I didn't break; and to everybody else who accepted me into their group and helped me feel at home 6,000 kilometers from home.

I would not have had the opportunity to study and conduct research abroad without the EAGLES program, which connects Drexel University with the Polytechnic

Universities in Madrid and Milan. I owe special thanks to Marcia Henisz of the study abroad office at Drexel, and Dr. Caroline Schauer, the graduate advisor of the MSE department at Drexel, for helping make sure I had everything in order to participate in the program.

I have to thank my loving parents for all the support they have provided me with throughout the years, both emotionally and financially. I could not have done the great things I've done or seen the world as I have without you both, I love you. I couldn't have completed this work without the love and support of all my family; thankfully, you won't have to ask me at any more family functions when I'm graduating! Many thanks are also owed to my friends: those who have been with me for years, and those I've made in the past two years all over Europe and the world. I hope to maintain contact and meet you all again somewhere. Without you, I might have graduated a year sooner.

Table of Contents

LIST OF TABLES viii

LIST OF FIGURES ix

ABSTRACT xiv

1. INTRODUCTION AND MOTIVATION 1

2. BACKGROUND 6

2.1. Basics of Intermediate Band Solar Cells 6

2.2. Metal-Semiconductor Contact 8

2.3. Ohmic Contact Resistance 11

2.3.1 Transmission Line Modeling (TLM) 12

2.4 Conventional Ohmic Contacts to p-GaAs 15

2.4.1 Au/Zn/Au Contacts 16

2.4.2 Other Gold-based Contacts 17

2.4.3 Non-Gold-based Contacts 19

2.5 Solar Cell Front Contact Materials 19

2.6 Contact Fabrication 20

2.6.1 Nickel Electroplating 21

2.6.2 Rapid Thermal Annealing 26

3 METHODS AND MATERIALS 26

3.1 Intermediate Band Solar Cell Fabrication 27

3.2 Photolithography 28

3.3 Thermal Evaporation 29

3.3.1 Cr/Au 29

3.3.2 Au/Zn/Au 29

3.3.3 Cr/Zn/Au 30

3.3.4 Nickel 30

3.4. Electroplating 30

3.5. Rapid Thermal Annealing 34

3.5.1 Thermally Evaporated Samples 34

3.5.2 Electrodeposited Samples 36

3.6. Transmission Line Modeling 36

3.7. Scanning Electron Microscopy 37

4. RESULTS AND DISCUSSION 38

4.1. Contact Resistance 38

4.1.1 Thermally Evaporated Samples (Non-Nickel), by Doping Level 38

4.1.2 Thermally Evaporated Nickel 56

4.1.3 Electrolytically Deposited Samples 59

4.2. Surface Topography 68

4.2.1 Thermally Evaporated Samples (Non-Nickel), by Doping Level 68

4.2.2 Electrolytically Deposited Samples 83

4.3. Contact Surface Composition 87

4.4. Discussion 90

5. CONCLUSION AND FUTURE RECOMMENDATIONS 96

LIST OF REFERENCES 99

List of Tables

1. Table 2.1 Work function values for metals studied in this research 12
2. Table 2.2 Literature review metallization scheme study results 16
3. Table 2.3 Watts nickel and nickel sulfamate electrolyte solution compositions ... 24
4. Table 3.1 Parameters applied to Ni electrolytic deposition on samples at both doping levels 34
5. Table 3.2 Annealing parameters for samples processed by thermal evaporation .. 35
6. Table 4.1 Minimum specific contact resistivities measured 39

List of Figures

1. Figure 2.1 Prototype of an IB solar cell implemented with InAs quantum dot layers [*9]*..7
2. Figure 2.2 Simplified bandgap diagram under illumination and forward bias [3] ..7
3. Figure 2.3 Band diagram before (a) and after (b) the metal and p-type semiconductor are brought into contact (*adapted from* [14]).................................9
4. Figure 2.4 Contact pad layout of typical TLM Device 13
5. Figure 2.5 Example of contact-contact resistance versus spacing graph used to extract contact resistance 14
6. Figure 3.1 Structure of intermediate band solar cells studied in this work...........28
7. Figure 3.2 Electrolytic deposition experiment set up. The electrical leads are attached at the other end to a Keithley SourceMeter® 2602 (not pictured)..........32
8. Figure 3.3 Sample holder used for GaAs IBSC wafers in electrolytic deposition experiment 32
9. Figure 4.1 Specific contact resistivity versus annealing temperature for p-GaAs (NA = 4.0 x 1016 cm-3) with thermally evaporated Au/Zn/Au contacts 40
10. Figure 4.2 Specific contact resistivity versus annealing temperature for p-GaAs (NA = 4.0 x 1016 cm-3) with thermally evaporated Cr/Zn/Au contacts 40
11. Figure 4.3 Specific contact resistivity for p-GaAs (NA = 4.0 x 1016 cm-3) with thermally evaporated Au/Zn/Au and Cr/Zn/Au contacts, after short time RTA ...41
12. Figure 4.4 Specific contact resistivity for p-GaAs (NA = 4.0 x 1016 cm-3) with thermally evaporated Au/Zn/Au and Cr/Zn/Au contacts, after long time RTA 42
13. Figure 4.5 Specific contact resistivity versus annealing temperature for p-GaAs (NA = 1.0 x 1019 cm-3) with thermally evaporated Au/Zn/Au contacts 43
14. Figure 4.6 Specific contact resistivity versus annealing temperature for p-GaAs (NA = 1.0 x 1019 cm-3) with thermally evaporated Cr/Zn/Au contacts 43
15. Figure 4.7 Specific contact resistivity for p-GaAs (NA = 1.0 x 1019 cm-3) with thermally evaporated Au/Zn/Au and Cr/Zn/Au contacts, after short time RTA ...44

16. Figure 4.8 Specific contact resistivity for p-GaAs (NA = 1.0 x 1019 cm-3) with thermally evaporated Au/Zn/Au and Cr/Zn/Au contacts, after long time RTA....45

17. Figure 4.9 Specific contact resistivity versus annealing temperature for p-GaAs (NA = 4.7 x 1019 cm-3) with thermally evaporated Cr/Au contacts 46

18. Figure 4.10 Specific contact resistivity versus annealing temperature for p-GaAs (NA = 4.7 x 1019 cm-3) with thermally evaporated Au/Zn/Au contacts 47

19. Figure 4.11 Specific contact resistivity versus annealing temperature for p-GaAs (NA = 4.7 x 1019 cm-3) with thermally evaporated Cr/Zn/Au contacts 48

20. Figure 4.12 Specific contact resistivity for p-GaAs (NA = 4.7 x 1019 cm-3) with thermally evaporated Cr/Zn/Au, Cr/Au, and Au/Zn/Au contacts, as-deposited ...49

21. Figure 4 13 Specific contact resistivity for p-GaAs (NA = 4.7 x 1019 cm-3) with thermally evaporated Cr/Zn/Au, Cr/Au, and Au/Zn/Au contacts, after short anneal by RTA...49

22. Figure 4.14 Specific contact resistivity for p-GaAs (NA = 4.7 x 1019 cm-3) with thermally evaporated Cr/Zn/Au, Cr/Au, and Au/Zn/Au contacts, after long anneal by RTA...50

23. Figure 4.15 Specific contact resistivity versus annealing temperature for p-GaAs (NA = 1.7 x 1020 cm-3) with thermally evaporated Cr/Au contacts 51

24. Figure 4.16 Specific contact resistivity versus annealing temperature for p-GaAs (NA = 1.7 x 1020 cm-3) with thermally evaporated Au/Zn/Au contacts 52

25. Figure 4.17 Specific contact resistivity versus annealing temperature for p-GaAs (NA = 1.7 x 1020 cm-3) with thermally evaporated Cr/Zn/Au contacts 53

26. Figure 4.18 Specific contact resistivity for p-GaAs (NA = 1.7 x 1020 cm-3) with thermally evaporated Cr/Au and Cr/Zn/Au contacts, as-deposited 54

27. Figure 4.19 Specific contact resistivity for p-GaAs (NA = 1.7 x 1020 cm-3) with thermally evaporated Cr/Zn/Au, Cr/Au, and Au/Zn/Au contacts, after short anneal by RTA...55

28. Figure 4.20 Specific contact resistivity for p-GaAs (NA = 1.7 x 1020 cm-3) with thermally evaporated Cr/Zn/Au, Cr/Au, and Au/Zn/Au contacts, after long anneal by RTA...55

29. Figure 4.21 Specific contact resistivities of thermally deposited Ni contacts to p-GaAs...56

30. Figure 4.22 Specific contact resistivities of contacts to p-GaAs (NA = 5.3 x 1018 cm-3) with thermally evaporated nickel contacts after annealing for short and long times 57

31. Figure 4.23 Specific contact resistivities of contacts to p-GaAs (NA = 3.0 x 1019 cm-3) with thermally evaporated nickel contacts after annealing for short and long times 58

32. Figure 4.24 Specific contact resistivities of contacts to p-GaAs (NA = 5.3 x 1018 cm-3) with nickel contacts electrolytically deposited with a target thickness of 2500 Å...59

33. Figure 4.25 Specific contact resistivities of contacts to p-GaAs (NA = 5.3 x 1018 cm-3) with nickel contacts electrolytically deposited with a target thickness of 5000 Å...60

34. Figure 4.26 Specific contact resistivities of contacts to p-GaAs (NA = 5.3 x 1018 cm-3) with nickel contacts electrolytically deposited at a current density of 2.5 mA/cm2...61

35. Figure 4.27 Specific contact resistivities of contacts to p-GaAs (NA = 5.3 x 1018 cm-3) with nickel contacts electrolytically deposited at a current density of 5 mA/cm2...62

36. Figure 4.28 Specific contact resistivities of contacts to p-GaAs (NA = 5.3 x 1018 cm-3) with nickel contacts electrolytically deposited at a current density of 5 mA/cm2 and subsequently annealed by RTA 63

37. Figure 4.29 Specific contact resistivities of contacts to p-GaAs (NA = 5.3 x 1018 cm-3) with nickel contacts electrolytically deposited at a current density of 2.5 mA/cm2 and subsequently annealed by RTA 63

38. Figure 4.30 Specific contact resistivities of contacts to p-GaAs (NA = 3.0 x 1019 cm-3) with nickel contacts electrolytically deposited with a target thickness of 2500 Å...64

39. Figure 4.31 Specific contact resistivities of contacts to p-GaAs (NA = 3.0 x 1019 cm-3) with nickel contacts electrolytically deposited with a target thickness of 5000 Å...65

40. Figure 4.32 Specific contact resistivities of contacts to p-GaAs (NA = 3.0 x 1019 cm-3) with nickel contacts electrolytically deposited at a current density of 2.5 mA/cm2...66

41. Figure 4.33 Specific contact resistivities of contacts to p-GaAs (NA = 3.0 x 1019 cm-3) with nickel contacts electrolytically deposited at a current density of 5 mA/cm2 67

42. Figure 4.34 Specific contact resistivities of contacts to p-GaAs (NA = 3.0 x 1019 cm-3) with nickel contacts electrolytically deposited at a current density of 2.5 mA/cm2 and subsequently annealed by RTA 68

43. Figure 4.35 SEM micrograph of Au/Zn/Au contact to p-GaAs (NA = 4.0 x 1016 cm-3) after 60 seconds of RTA at 400ºC 69

44. Figure 4.36 SEM micrograph of Au/Zn/Au contact to p-GaAs (NA = 4.0 x 1016 cm-3) after 60 seconds of RTA at 450ºC 69

45. Figure 4.37 SEM micrograph of Cr/Zn/Au contact to p-GaAs (NA = 4.0 x 1016 cm-3) after 30 seconds of RTA at 500ºC 70

46. Figure 4.38 SEM micrograph of Cr/Zn/Au contact to p-GaAs (NA = 4.0 x 1016 cm-3) after 30 seconds of RTA at 550ºC (10,000X) 71

47. Figure 4.39 SEM micrograph of Cr/Zn/Au contact to p-GaAs (NA = 4.0 x 1016 cm-3) after 30 seconds of RTA at 550ºC (1,000X) 71

48. Figure 4.40 SEM micrograph of Cr/Au contact to p-GaAs (NA = 4.0 x 1016 cm-3) after 60 seconds of RTA at 450ºC (5,000X) 72

49. Figure 4.41 SEM micrograph of Cr/Zn/Au contact to p-GaAs (NA = 1.0 x 1019 cm-3) after 30 seconds of RTA at 500ºC (5,000X) 73

50. Figure 4.42 SEM micrograph of Cr/Zn/Au contact to p-GaAs (NA = 1.0 x 1019 cm-3) after 30 seconds of RTA at 550ºC (5,000X) 74

51. Figure 4.43 SEM micrograph of Au/Zn/Au contact to p-GaAs (NA = 4.7 x 1019 cm-3) after 60 seconds of RTA at 450ºC (10,000X) 75

52. Figure 4.44 SEM micrograph of Au/Zn/Au contact to p-GaAs (NA = 4.7 x 1019 cm-3) after 60 seconds of RTA at 500ºC (10,000X) 75

53. Figure 4.45 SEM micrograph of Cr/Au contact to p-GaAs (NA = 4.7 x 1019 cm-3) after 60 seconds of RTA at 400ºC (10,000X) 76

54. Figure 4.46 SEM micrograph of Cr/Au contact to p-GaAs (NA = 4.7 x 1019 cm-3) after 60 seconds of RTA at 450ºC (10,000X) 77

55. Figure 4.47 SEM micrograph of Cr/Zn/Au contact to p-GaAs (NA = 1.7 x 1020 cm-3), as deposited (1,000X) 78

56. Figure 4.48 SEM micrograph of Au/Zn/Au contact to p-GaAs (NA = 1.7 x 1020 cm-3), after 60 seconds of RTA at 450°C (10,000X) 79

57. Figure 4.49 SEM micrograph of Au/Zn/Au contact to p-GaAs (NA = 1.7 x 1020 cm-3), after 60 seconds of RTA at 500°C (10,000X) 79

58. Figure 4.50 SEM micrograph of Cr/Zn/Au contact to p-GaAs (NA = 1.7 x 1020 cm-3), after 30 seconds of RTA at 500°C (10,000X) 80

59. Figure 4.51 SEM micrograph of Cr/Zn/Au contact to p-GaAs (NA = 1.7 x 1020 cm-3), after 30 seconds of RTA at 550°C (10,000X) 81

60. Figure 4.52 SEM micrograph of Cr/Au contact to p-GaAs (NA = 1.7 x 1020 cm-3), after 60 seconds of RTA at 450°C (5,000X) 82

61. Figure 4.53 SEM micrograph of Cr/Au contact to p-GaAs (NA = 1.7 x 1020 cm-3), after 60 seconds of RTA at 500°C (5,000X) 82

62. Figure 4.54 Nickel contacts, as-deposited by electrolytic deposition at 5 mA/cm2 to p-GaAs (NA = 5.3 x 1018 cm-3) (5,000X) 84

63. Figure 4.55 Nickel contacts by electrolytic deposition at 5 mA/cm2 to p-GaAs (NA = 5.3 x 1018 cm-3) after 60 seconds of annealing at 350°C (5,000X) 84

64. Figure 4.56 Nickel contacts by electrolytic deposition at 5 mA/cm2 to p-GaAs (NA = 5.3 x 1018 cm-3) after 60 seconds of annealing at 400°C (5,000X) 85

65. Figure 4.57 Nickel contacts, as-deposited by electrolytic deposition at 2.5 mA/cm2 to p-GaAs (NA = 3.0 x 1019 cm-3) (5,000X)...................................... 86

66. Figure 4.58 Nickel contacts, as-deposited by electrolytic deposition at 5 mA/cm2 to p-GaAs (NA = 3.0 x 1019 cm-3) (5,000X) 86

67. Figure 4.59 X-ray spectra measured by EDS on thermally evaporated Au/Zn/Au contact to p-GaAs (NA = 1.7 x 1020 cm-3) 88

68. Figure 4.60 X-ray spectra measured by EDS on thermally evaporated Cr/Au contact to p-GaAs (NA = 1.7 x 1020 cm-3) at positions indicated in the accompanying SEM micrograph 89

69. Figure 4.61 X-ray spectra measured by EDS on thermally evaporated Cr/Zn/Au contact to p-GaAs (NA NA = 1.7 x 1020 cm-3) at positions indicated in the accompanying SEM micrograph.. 90

ABSTRACT

Investigation of a New Metallization Scheme for Front
Ohmic Contacts to GaAs Intermediate Band Solar Cells

Brittany Pattinson

Dr. Johnathan Spanier

Various metallization schemes for front contact to GaAs intermediate band solar cells (IBSCs) have been investigated by specific contact resistivity measurements and surface topography examination by scanning electron microscopy. GaAs IBSCs were fabricated by molecular beam epitaxy (MBE) according to the established process for these cells. Contacts were fabricated on the cells by thermal evaporation and electrolytic deposition in a transmission line model (TLM) pattern for contact resistance measurement.

In order to compare the effect of wafer doping on specific contact resistivity, three different metallization schemes (Cr/Au, Au/Zn/Au, and Cr/Zn/Au) were each deposited by thermal evaporation onto wafers of four different doping levels (N_A = 4.0 x 10^{16}, 1.0 x 10^{19}, 4.7 x 10^{19}, 1.7 x 10^{20} cm^{-3}). The investigation of these wafers mainly concerned the formation of low resistance ohmic contacts with the Cr/Zn/Au metallization, which has not been extensively studied. In order to compare the two deposition methods, Ni contacts were deposited onto wafers of two different doping levels (N_A = 5.3 x 10^{18} and 3.0 x 10^{19} cm^{-3}) by both thermal evaporation and electrolytic deposition. Emphasis was placed on obtaining low resistance ohmic contact to the p-GaAs material by electrolytically depositing nickel.

All contacts were heat treated by rapid thermal annealing (RTA) to investigate the effect of annealing temperature and time on specific contact resistivity. After annealing

contacts on wafers with low doping ($N_A \leq 1.0$ x 10^{19} cm^{-3}), ohmic contacts were realized. In more highly doped wafers, ohmic contacts were realized upon deposition. Cr/Zn/Au contacts were always characterized by specific contact resistivities comparable to those of the typical Cr/Au and Au/Zn/Au contacts. The lowest resistances measured on contacts to p-GaAs with $N_A = 4.0$ x 10^{16} cm^{-3} wafers were 1.09 x 10^{-2} and 1.96 x 10^{-2} Ωcm^2 for Au/Zn/Au and Cr/Zn/Au, respectively. For contacts to p-GaAs with $N_A = 1.0$ x 10^{19} cm^{-3}, the lowest measured resistances were 8.48 x 10^{-4} for Au/Zn/Au and 8.76 x 10^{-4} for Cr/Zn/Au. Ohmic contacts to p-GaAs with $N_A = 4.7$ x 10^{19} cm^{-3} were characterized by minimum contact resistances of 1.03 x 10^{-4}, 1.53 x 10^{-4}, and 1.51 x 10^{-4} Ωcm^2, for Cr/Au, Au/Zn/Au, and Cr/Zn/Au, respectively. For ohmic contacts to p-GaAs with $N_A = 1.7$ x 10^{20} cm^{-3}, the lowest measured specific contact resistivities were 5.82 x 10^{-5}, 1.55 x 10^{-4}, and 7.25 x 10^{-5} Ωcm^2, for Cr/Au, Au/Zn/Au, and Cr/Zn/Au, respectively.

Ni contacts deposited by electrolysis displayed ohmic behavior upon deposition. The specific contact resistivities of these samples were lowered after annealing, in the case of contacts to the more lowly doped wafer ($N_A = 5.3$ x 10^{18} cm^{-3}). The lowest specific contact resistivities measured on Ni contacts by electrolytic deposition were 9.91 x 10^{-4} and 1.74 x 10^{-4} Ωcm^2 on wafers of $N_A = 5.3$ x 10^{18} cm^{-3} and $N_A = 3.0$ x 10^{19} cm^{-3}, respectively. These resistance values were comparable to those measured on Ni contacts deposited by thermal evaporation.

CHAPTER 1

MOTIVATION

As the adverse effects of climate change become more prevalent, the global demand for cleaner, renewable energies rises. According to the Intergovernmental Panel of Climate Change, human activity has induced an increase in greenhouse gas concentration and has subsequently caused most of the observed increase in global temperature over the last 50 years [1]. Stabilization of atmospheric CO_2 concentrations would require widespread implementation of energy production sources which are carbon-neutral, i.e., nuclear power and renewable energies. An obvious solution would be to harness the power of the sun, which produces 58,000 TW-hours of energy a year, about 2000 times more than annual human consumption [2]. Currently, only a small fraction of the global energy consumed is being supplied by the sun. The need for cost effective and high efficiency method of solar energy conversion is becoming greater with each passing year.

Solar photovoltaic (PV) sales have experienced impressive growth in recent years; however, the prices are still too high for it to be a viable competitor with other commercially available energy production technologies. New research in so-called “third generation” photovoltaics is aimed at producing highly efficient PV technologies at lower costs. Among these third generation PVs are intermediate-band solar cells (IBSCs). While far from commercial availability, IBSCs have the potential to convert unprecedented amounts of sunlight to useable energy [3].

At the center of this research is a novel IBSC design being studied at the Solar Energy Institute of the Polytechnic University of Madrid in Spain. A new metallization scheme for the front contact to this p-type GaAs based IBSC can prove to be more effective in achieving ohmic contact with low specific contact resistivity, compared with the Cr/Au contacts already being fabricated onto these devices. Specific contact resistivity is directly related to the series resistance, a parameter which degrades the output power of a solar cell. Reducing this value as low as possible can potentially increase the efficiency of the cell by maintaining a low resistive power-loss component. [4]

The metallization scheme currently being used in these cells was chosen mainly for its good adhesion properties and the fact that it can be used to achieve non-alloyed, low specific resistance ohmic contact to p-type GaAs. An initial Cr layer is a good choice for contacting to this substrate because chromium's lattice parameter (0.288 nm) is about half that of GaAs (0.565 nm), which encourages good adhesion due to perfect matching at the interface [5]. No other metallization schemes have been thoroughly investigated for contacting to this material. The aim of this research is to determine whether there exists an alternate combination of metals used in forming ohmic contacts to p-type GaAs which is able to achieve a low contact resistance without degrading the semiconductor material itself. Determination of an optimum semiconductor doping level, contact metallization scheme, and annealing process is desired. Additionally, various methods of forming metal contacts will be investigated. Thermal evaporation and electrolytic deposition of metals will be studied in this work in order to determine which processes can be used to produce satisfactory ohmic contacts to the IBSCs.

There is a possibility to reduce the specific contact resistivity value achieved by front ohmic contacts on p-GaAs for IBSCs without increasing the cost of processing typically involved in fabricating these cells. Previously, studies have been performed by other research groups on ohmic contacting to p-GaAs with Au/Zn/Au and Cr/Au, but not with Cr/Zn/Au via thermal evaporation (in this work, the metallization schemes will be named “Metal 1/Metal 2, etc.,” such that Metal 1 is the metal in contact with the substrate, followed by Metal 2, and so on). The results of this study may lead to implementation of a new metallization scheme for front ohmic contacts in the fabrication of IBSCs based on p-type GaAs. The results of this study also have the potential to encourage further research on the thermally evaporated Cr/Zn/Au metallization scheme for other GaAs devices, if positive results are achieved.

A literature review will be carried out concerning the theory of ohmic contacting to semiconductor devices, specifically to GaAs. Review of conventional p-type GaAs contacts will be useful in justifying the choice of metallization schemes studied. Pre-existing studies of chosen materials will be reviewed to give insight on process parameters to use during contact fabrication. Various methods of contact deposition onto the substrate will be studied, in order to validate the choices of thermal evaporation and electrolytic deposition.

Conventionally, the Au/Zn metallization scheme is considered the most successful option for ohmic contacting to p-type GaAs, due to the very high diffusion coefficient of Zn [6]. A Au basis for the contact is known to be advantageous due to its good adhesion to GaAs, as well as its ease of deposition and promotion of low specific contact resistivity

[7]. Ultimately, though, a Au based metallization scheme may be detrimental to the specific contact resistivity. It has been shown that an excessive amount of Au interdiffusion and Ga outdiffusion may occur at high temperatures, limiting the Zn interdiffusion [7]. This is a motivation to study a new metallization scheme which uses a different base metal, such as Cr, along with Zn.

Previously, low contact resistances have been achieved using a Au/Zn/Au scheme on p-type GaAs devices; the same results should be achieved over a range of doping levels on the material used in this study. Additionally, Cr/Au contacts have been suitable in the past for the material under investigation, so Cr/Zn/Au should also produce satisfactory, if not improved, results. It is assumed that the chosen metallization schemes will form ohmic contacts with the p-type GaAs material. This has been true for similar metallization schemes for other research groups working with GaAs. Additionally, the semiconductor material will be highly doped, which promotes ohmic contacting in itself.

Three different metallization schemes will be evaporated onto p-GaAs at varying levels of doping; the samples will be annealed for varying times and temperatures. The specific contact resistivities of the contacts will be measured and compared. The Transmission Line Model (TLM) method will be used to evaluate the specific contact resistivity values. This is the most commonly used method for determination of this parameter. The p-type GaAs material will be the main focus of the study, as metallization schemes for contacting to n-type GaAs have been studied to a greater extent in the past.

The motivation for studying electrolytic deposition is its ease of implementation and the reduced economic risks associated with this technique. As this deposition method

has not been thoroughly investigated for IBSCs, this research will only concern the plausibility of creating ohmic contacts to the substrate with nickel, which is widely deposited by this method. Ni metallization systems have been studied most notably on p-type GaN substrates; it is of interest to know whether similar results can be realized with this metal, deposited onto p-GaAs.

CHAPTER 2

BACKGROUND

2.1 Basics of Intermediate Band Solar Cells

The intermediate band solar cell (IBSC) concept is a relatively new one, IBSCs being considered "third-generation" photovoltaics (PV). The main goal of third-generation PVs is cost reduction, which may be achieved by using cheaper or less PV materials and/or exploiting photons for more work. IBSCs aim to exploit photons for more work, in the sense that these cells are designed to utilize low-, intermediate-, and high-energy photons for energy production. Under maximum sun concentration, the theoretical limiting efficiency limit of IBSCs is 63.2%, exceeding that for both a single gap solar cell (40.7%) and for a tandem of two solar cells (55.4%) [3].

A schematic of the IBSC under investigation in this work is illustrated in Figure 2.1. This structure is based on a typical pn-junction with an isolated intermediate layer formed by a periodic array of InAs quantum dots (QDs). Upon illumination, electron-hole pairs are generated. Above-band gap energy photons promote electrons from the valence band (VB) to the conduction band (CB) directly, as is the case in a conventional semiconductor solar cell. Below band gap energy photons, on the other hand, are able to promote electrons from the VB to the intermediate band (IB) and from the IB to the CB. These transitions are illustrated in Figure 2.2. The implication of the IB is that is must contain the Fermi level, as it is required to be partially filled with electrons. Carriers are

only extracted via the VB and CB, through selective contacting to the n-emitter (for electron extraction) and p-emitter (for hole extraction). [8]

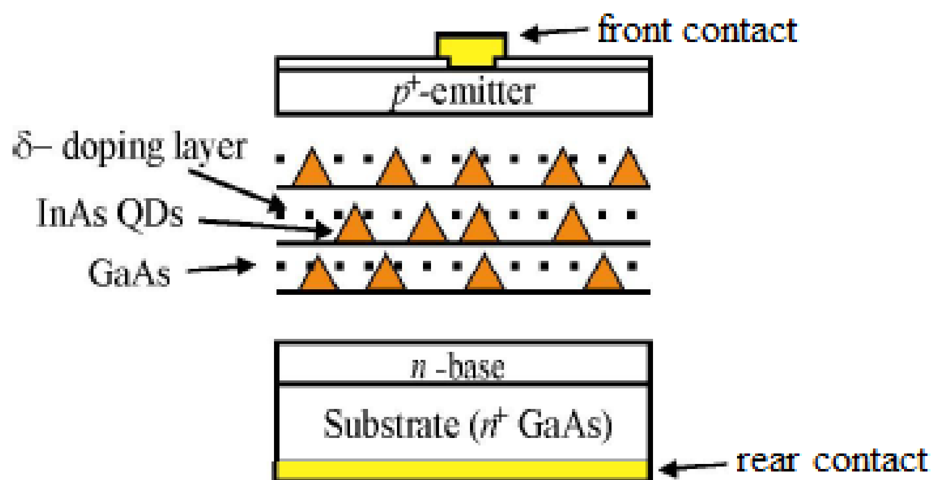

Figure 2.1 Prototype of an IB solar cell implemented with InAs quantum dot layers [9]

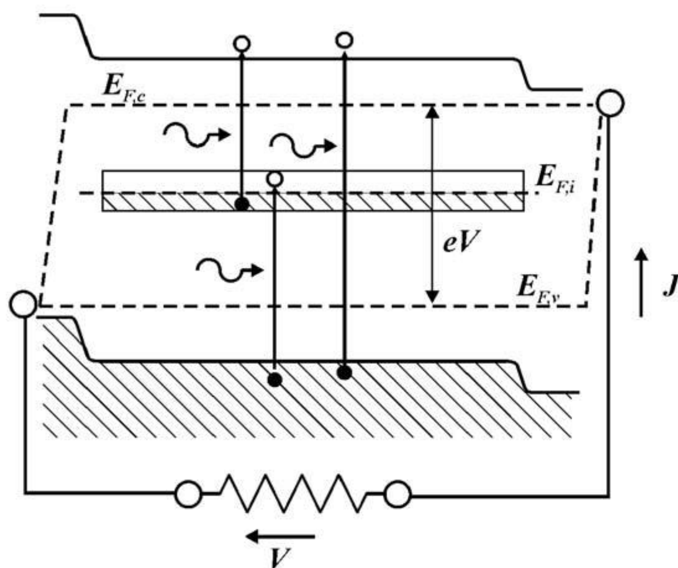

Figure 2.2 Simplified bandgap diagram under illumination and forward bias [3]

The generated photocurrent flows from the cell via the electrical contacts on the front and rear sides of the cell, to which an external load is applied. Normally, the rear contact covers the whole back side of the cell, whereas the front contact is made up of a fine-lined pattern to reduce shading loses. An anti-reflection coating will be applied to further reduce optical losses. Additional electrical losses arise due to series and parallel resistances in the cell.

2.2 Metal-semiconductor Contact

Metallization systems are essentially responsible for providing electrical pathways between the external circuits and the active region of the semiconductor. Contact resistance is an important concern when considering the front side metallization of solar cells. To understand this parameter, it is worth briefly presenting the current flow mechanisms at the metal-semiconductor interface. Two generic contact types, Schottky and ohmic, are formed when metals and semiconductors come into close contact. While low-resistance ohmic contacts are ideal for use in solar cells, Schottky contacts will be presented for the purpose of comparison. Schottky contacts are formed when the metal work function is greater than the n-type semiconductor work function, or lower than the p-type semiconductor work function.

Schottky diodes were first explained by Schottky in the 1930's, when he predicted the theory of rectification for these devices [10]. Known as the Schottky effect, this theory explains that the individual Fermi levels of the metal and the semiconductor are adjusted to become identical on either side of the metal-semiconductor interface upon

metal deposition, as is depicted in Figure 2.3. This adjustment leads to long-range band bending in the bulk semiconductor in order to satisfy the charge neutrality requirement, by which, the ionization of adjacent impurities of opposite charge is demanded [11]. This so-called stabilization of the Fermi level positions at the interface gives rise to a potential barrier to carrier movement across the interface [12]. This barrier is called the Schottky barrier and its height ϕ_B is given, in the ideal case, as

$$\phi_B = \phi_M - \chi$$

where ϕ_M is the metal work function (minimum energy needed to eject an electron) and χ is the semiconductor electron affinity (energy from the conduction band minimum to the vacuum level). It has been shown experimentally that the Schottky barrier height is less dependent on the metal, and more so on the presence of electric states due changing surface dipole contributions [13].

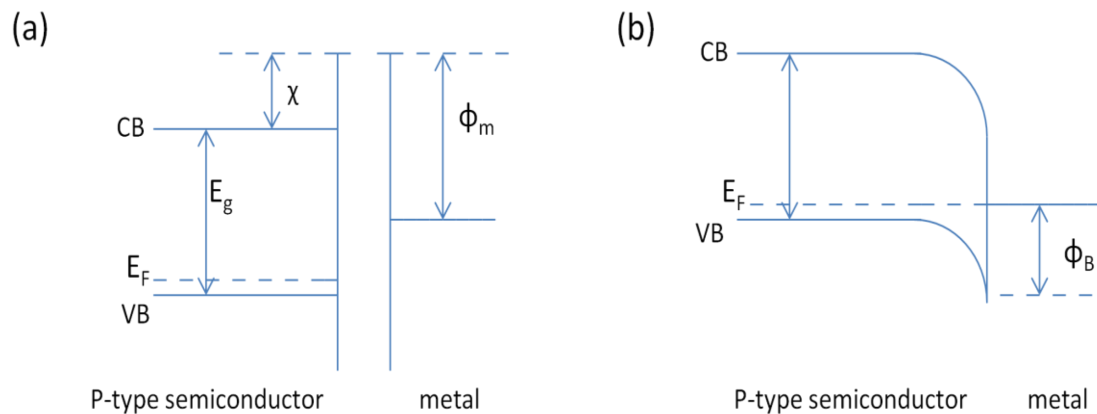

Figure 2.3 Band diagram before (a) and after (b) the metal and p-type semiconductor are brought into contact (*adapted from* [14])

As mentioned, in the presence of a Schottky contact, holes (in the case of p-type semiconductors) and electrons (in the case of n-type semiconductors) face a barrier to free movement and tunneling is quite difficult. Thus, current flow in Schottky diodes is governed by thermionic emission, where carrier flow occurs under/over the barrier.

Following Ohm's law, ohmic contacts have a linear current-voltage behavior, which implies a low barrier to current conduction at the metal-semiconductor interface [15]. This type of contact is also characterized by a low resistance, and can be achieved by depositing a metal directly on a highly doped semiconductor layer, which increases the probability of tunneling. Ohmic contacts can also be achieved through barrier height reduction by use of a heterostructure, to enhance thermionic emission [16]. In this work, the goal is to produce an ohmic contact through the former of these methods.

As the semiconductor impurity level is increased, quantum-mechanical tunneling through a narrowed barrier becomes the dominant form of conduction, and is referred to as thermionic-field emission; this is in opposition to the conduction method in Schottky contacts, where thermionic emission occurs under/over a lowered barrier [6]. In the case of a highly doped semiconductor directly adjacent to the metal, the depletion region in the semiconductor becomes thin enough to allow quantum mechanical tunneling through the barrier, even at its base; this current transport mechanism is known as field emission [17]. Thus, doping of the surface region of semiconductors with relatively high barrier heights, such as GaAs, which has a barrier height approximately one-third of the band gap (E_g = 1.43 V), can be an effective strategy for achieving ohmic contacts [6, 11].

2.3 Ohmic Contact Resistance

For solar cells, a satisfactory ohmic contact is required to have a low resistance to carrier flow, to be linear and non-injecting, and to possess qualities such as smooth surfaces, environmental stability, and ease of fabrication [11]. An especially important parameter in ohmic contact evaluation is the specific contact resistivity, which is the contact resistance per unit contact area. If a contact is characterized by non-negligible resistances, it will contribute to poor device performance, as the output power of the cell will be degraded. Additionally, the longevity of solar cells may be degraded by the potential aging characteristics of high resistance ohmic contacts [4]. Specific contact resistivity depends greatly on the impurity concentration in the semiconductor, the metal-semiconductor barrier height, the carrier effective mass, and the temperature [7].

As GaAs possesses a large barrier to electrons (0.8V), it can be difficult to achieve ohmic contact to the material. The easiest way to make a good ohmic contact to GaAs is through heavy doping of the semiconductor, which will modify the depletion region to be several nanometers thick, enabling charge carriers to tunnel through the barrier. In order to achieve the high doping levels needed (in excess of 5×10^{19} cm^{-3}) to achieve an adequately low specific contact resistivity (on the order of 10^{-6} Ωcm^2) for high performance devices, special growth conditions must be controlled with fabrication techniques such as molecular beam epitaxy. [11]

In addition to the significance of doping levels, the importance of the work functions of the semiconductor and the metals to be deposited must be considered. The work function describes the amount of energy required to remove an electron from the

solid surface to a point immediately outside the surface; alternatively, it is described as the energy needed to remove an electron from the Fermi level to the vacuum level. For p-type semiconductors, it is desirable to use metals for ohmic contacts which have work functions greater than that of the semiconductor material. Inoue et al. have studied the work function of GaAs on the (0 0 1) surface and found the value to be 4.77 eV [18]. The work functions of the metals studied in this research are presented in Table 2.1.

Table 2.1 Work function values for metals studied in this research

Metal	Work function (eV) [19]
Au	5.1
Cr	4.5
Zn	4.3
Ni	5.15

2.3.1 Transmission Line Modeling (TLM)

Originally proposed by Shockley [20], and improved upon by Berger [21], the transmission line modeling method (TLM) is the most commonly used method of determining the specific contact resistivity at a metal-semiconductor interface. TLM is based on the measurement of the total resistance between two contact pads of equal dimension separated by a pre-defined distance. Critical data are extracted from the plot of the total resistance as a function of the separation distance. The total resistance measured between any two contact pads during a TLM experiment is twice the contact resistance plus the resistance of the semiconductor layer:

$$R = 2R_c + R_{SS}\frac{L}{W},$$

where $R_c$is the contact resistance, R_{SS} is the semiconductor sheet resistance between the contact pads (a known material parameter), L is the distance between the two pads, and W is the width of the pad, as shown in Figure 2.4.

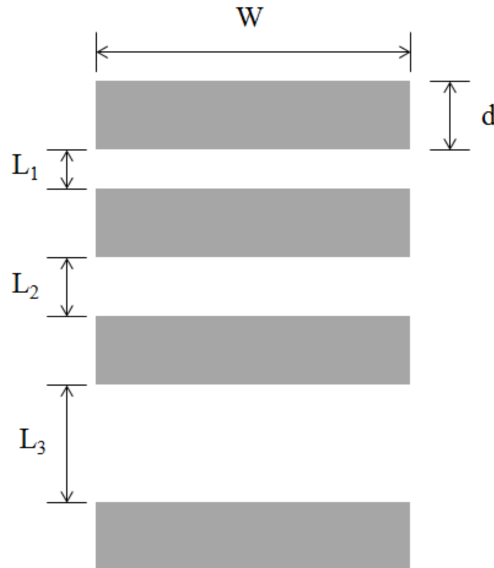

Figure 2.4 Contact pad layout of typical TLM Device

Assuming zero metal resistance, the contact resistance is given by

$$R_c = \frac{R_{SC} L_t}{W} \coth \frac{d}{L_t},$$

where R_{SC} is the semiconductor sheet resistance below the contact, d is the length of the contact pad, and L_t is the transfer length, defined as

$$L_t = \sqrt{\frac{\rho_c}{R_{SC}}},$$

ρ_c being the specific contact resistivity. The transfer length is a measure of how far the current travels from the metal to the semiconductor. R_C can be found by fitting a linear regression line to the plot of the total contact-to-contact resistance versus contact spacing, as in Figure 2.5.

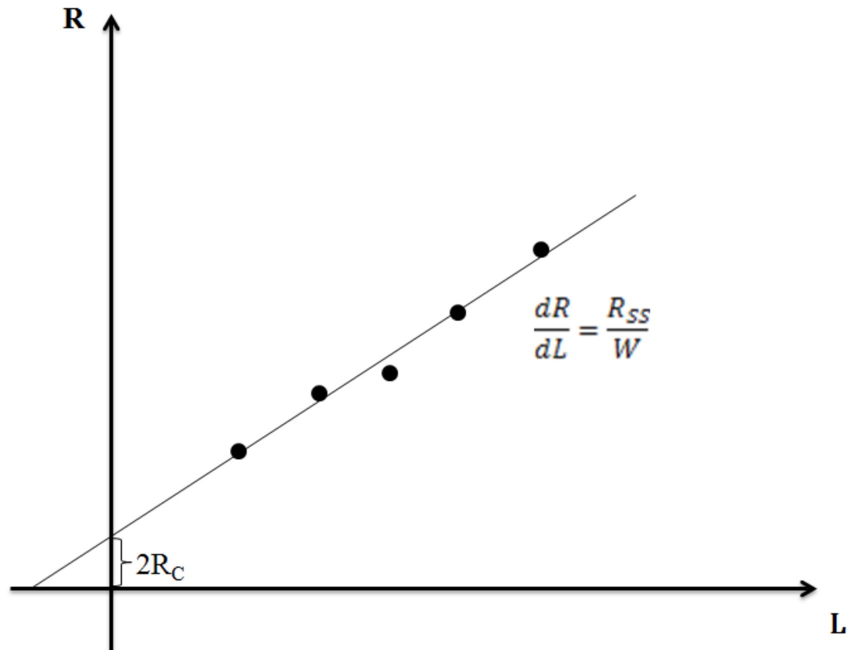

Figure 2.5 Example of contact-contact resistance versus spacing graph used to extract contact resistance

To determine the values of L_t and R_{SC}, one must determine a quantity known as the end resistance, R_e, unless it is assumed to be negligible. Fundamentally, the end resistance is the ratio of the voltage at the end of the contact to the current entering at the front of the contact. Maintaining the assumption that the metal resistance is zero, the end resistance is given by

$$R_e = \frac{L_t R_{SC}}{W \sinh \frac{d}{L_t}} = \frac{R_c}{\cosh \frac{d}{L_t}}.$$

The reliability of this expression depends on the transfer length and the contact length being of the same order.

2.4 Conventional Ohmic Contacts to p-GaAs

The most widely used ohmic contacts to p-type GaAs are gold-based metallizations. The basic contact scheme is designed such that a suitable dopant is supplied to the semiconductor (most commonly used are zinc, beryllium, or manganese as acceptors and germanium and silicon as donors), and, in some cases, an additional material is introduced to modify the Au-semiconductor reaction (notable elements serving this purpose are nickel, palladium, titanium, chromium, and silver). Gold-based metallization schemes are advantageous in ohmic contacting in many aspects: (1) these metallization schemes routinely allow for low specific contact resistivities; (2) a high resistance against corrosion has been found in these systems; (3) they are proven to be highly compatible with standard evaporation and photolithographic techniques; (4) reliability up to 10^9 has been established at room temperature. Gold-based metallization systems also present some disadvantages, including: (1) high reactivity with III-V semiconductors, which is sometimes undesirable; (2) surface inhomogeneity; (3) poor adhesion to oxidized surfaces. [12] For these reasons, it is useful to study both gold- and non-gold-based metallization schemes for ohmic contacting to p-GaAs. The results of the following studies are presented in Table 2.2.

Table 2.2 Literature review metallization scheme study results

p-GaAs Doping Level (cm^{-3})	Metallization Scheme	Layer Thicknesses (Å)	Minimum Specific Contact Resistivity ($\Omega \cdot cm^2$)	Heat Treatment
3×10^{17}	Au/Zn/Au	200/100-700/2000	3×10^{-6}	15 sec RTA, 350ºC
4×10^{19}	Au/Zn/Au	300/300/1000	3.6×10^{-6}	60 sec RTA, 400ºC
8×10^{17}	Au/Zn/Au	200/100/600	$\sim 10^{-5}$	3 min furnace annealing, 320ºC
2.9×10^{18}	Cr/Au	500/500	$\sim 10^{-5}$	1 min furnace annealing, 430ºC
	Au/Mn/Ni/Au	40/40/10/200	4.6×10^{-8}	40 sec RTA, 380ºC
2×10^{20}	Ti/Pt/Au		2.8×10^{-8}	1 sec VRTP, 400ºC
	Ni/Pd/Au	800/1200/2000	2.1×10^{-6}	1 min furnace annealing, 300ºC
	Ni/Au	1500/1500	4.7×10^{-5}	1 min furnace annealing, 420ºC
	Sn/Ni/Al	500/500/1000	1.2×10^{-4}	20 sec RTA, 750ºC

2.4.1 Au/Zn/Au Contacts

Lu et al. studied a Au (200 Å)/Zn (100-700 Å)/Au (2000 Å) system and investigated the effects of rapid thermal annealing (RTA) on these samples. In their study, it was found that the interaction of Au with Ga to form α-AuGa was crucial for the creation of ohmic contacts to GaAs. The proper reaction occurred after annealing at 300°C, allowing the transition from rectifying to ohmic contacts. The group obtained a minimum specific contact resistivity of approximately 3×10^{-6} Ωcm^2 for Be-doped p-GaAs with $N_a = 3 \times 10^{17}$ cm^{-3} after 15 seconds of RTA at 350°C. [22]

Kren et al. conducted a study similar to that of Lu et al.; however, Kren et al. investigated their Au (300 Å)/Zn (300 Å)/Au (1000 Å) system on C-doped p-GaAs with $N_a = 4 \times 10^{19}$ cm^{-3}. The thin Au layer was evaporated onto the GaAs first in order to improve the adhesion of the evaporated Zn to the sample. The group achieved ohmic

contact without annealing, and found a decrease in contact resistance with annealing. The group attributed the resistance decrease to the doping of the material under the contact by Zn during the annealing. The minimum specific contact resistivity achieved by this group was 3.6 x 10^{-6} Ωcm^2 after 60 seconds of RTA at 400°C. [23]

Kaminska et al. investigated pure Au (800 Å), pure Zn (3500 Å), and Au (200 Å)/Zn (100 Å)/Au (600 Å) contacts to GaAs wafers Zn-doped to a concentration of 8 x 10^{17} cm^{-3}. In the study, pure Au did not form an ohmic contact with the p-GaAs. Pure Zn formed an ohmic contact after heat treating at 220°C for 3 minutes. Prolonged annealing of these samples proved to be detrimental to the contact resistance; this effect was correlated with the growth of a Zn_3As_2 phase at the metal-semiconductor interface. Ohmic contact was achieved with the Au/Zn/Au metallization after annealing at 300°C for 3 minutes; the lowest specific contact resistivity attained with this system was in the 10^{-5} Ωcm^2 range, after annealing between 320 and 460°C. The group concluded that the presence of Zn is necessary to produce a highly doped GaAs region under the metal after outdiffusion of Ga from the semiconductor creates vacancies to be filled (by the Zn). [24]

2.4.2 Other Gold-based Contacts

Castanedo et al. formed ohmic contacts to p-GaAs with a Cr/Au bilayer contact. The group thermally evaporated the Cr (500 Å)/Au (500 Å) contact to Zn-doped GaAs with N_a = 2.9 x 10^{18}. After annealing the samples, ohmic contacts were achieved; the lowest specific contact resistivity (~ 10^{-5} Ωcm^2) was achieved after furnace annealing at 430ºC for one minute. The group found that the Cr behaved similarly to the Zn in the

aforementioned Au/Zn contacts, in that it diffuses into the GaAs where the Ga and As has outdiffused; this reaction was found to have occurred both with and without annealing.

In an attempt to introduce Mn as a suitable dopant in the standard Au-based contact scheme, Thiery et al. fabricated Au (40 Å)/Mn (40 Å)/Ni (10 Å)/Au (200 Å) contacts to p-GaAs. The minimum specific contact resistivity obtained in the study was 4.6×10^{-8} Ωcm^2 after RTA at 380°C for 40 seconds. The group attributes the low specific resistivity value to the tunneling, which they hypothesize is due to the formation of a mixed zone composed of Ni, As, and Ga, and to the high semiconductor doping by the Mn diffusion into the GaAs. [25]

With the goal of achieving a non-alloyed ohmic contact to p-GaAs, Stareev et al. studied the Ti/Pt/Au metallization system. The Ti film was intended to function as an adhesive barrier layer, while the Pt was introduced to prevent excessive Au penetration into the underlying layers. The group studied Be- and Zn-doped GaAs, both with $N_a = 2 \times 10^{20}$ cm^{-3}. The as-deposited contacts to p-GaAs achieved a specific contact resistivity value of 1.7×10^{-5} Ωcm^2. Very rapid thermal processing (VRTP) was carried out for each sample in order to retain the crystalline properties of the semiconductor. In the case of p-GaAs, VRTP at 400°C for one second reduced the specific contact resistivity to 2.8×10^{-8} Ωcm^2. [26]

Wu et al. studied Ni/Pd/Au and Ni/Au contacts to p-GaAs. Their investigation focused on the effect of the thickness of the Ni and Pd layers on the specific contact resistivity. The optimum thicknesses for the Ni/Pd/Au contact metals were 800 Å, 1200 Å, and 2000 Å, respectively; this metallization scheme achieved its lowest specific

resistivity of 2.1 x 10^{-6} Ωcm^2 after annealing for one minute at 300°C. Both the Ni and Pd were found to have diffused into the p-GaAs significantly, while both Ga and As outdiffused. For the Ni (1500 Å)/Au (1500 Å) ohmic contact, a specific resistance of about 4.7 x 10^{-5} Ωcm^2 was obtained after one minute of annealing at 420°C. [27]

2.4.3 Non-Gold-based Contacts

Prasad aimed to fabricate a metallization scheme that would be suitable for both n-type and p-type GaAs in his research on the Sn/Ni/Al system. By thermal evaporation, a metallization system of 500 Å of Sn, followed by 500 Å of Ni and 1000 Å of Al was deposited onto the semiconductor surface. Ohmic contacts to p-GaAs were realized pre- and post-anneal. The lowest specific contact resistivity value of 1.2 x 10^{-4} Ωcm^2 was obtained after 20 seconds of RTA at 750°C. [28]

2.5 Solar Cell Front Contact Materials

For years, the silicon solar cell front contacting scheme has been fabricated by screen-printed silver. With the aim of increasing cell efficiencies and decreasing manufacturing costs, new materials and methods have been investigated for contacting to these cells. Cheaper materials such as nickel and copper have been gaining interest recently in the field. Combined with economic plating technologies, these metals have the potential to replace Ag as a front contact metal to Si PVs. [29]

Lee et al. formed Ni/Cu front contacts to Si solar cells by plating techniques and found an improvement in cell efficiency of 0.8% compared to cells with the same contact scheme deposited by screen printing. The group acknowledged that Cu and Ni have both

found applications in various semiconductor electronics, hence the motivation to apply these metals to solar cells. Noting that Cu has the ability to degrade cell performance due to its being a deep-level impurity in Si, the group proposed the use of Ni as a barrier layer between the Cu and Si. Ni was chosen in this study for its low bulk resistance and low thermal temperature. [30]

2.6 Contact Fabrication

Typically, ohmic contacts to semiconductors are fabricated by vacuum deposition techniques, such as thermal evaporation, electron beam evaporation, or, more rarely, sputtering. As evaporation techniques provide a high purity deposition method which causes minimal damage to the semiconductor surface, they are the techniques of choice for most metal deposition on GaAs. In order to reduce the possibility of contamination of the semiconductor on which metals are being deposited, a high vacuum level, on the order of 10^{-6} Torr must be maintained. Electron beam evaporation causes minimal damage to the semiconductor surface, as the energetic ions produced cannot be accelerated to the sample surface to effectively cause lattice damage; this technique is typically used when the required temperatures are too high for thermal evaporation. Sputtering, on the other hand, is able to produce more damage to the substrate surface and also requires extensive surface cleaning prior to deposition to ensure a good adhesion. Thermal evaporation is the deposition technique of choice for low-melting temperature metals when minimum surface damage is desired. This technique is one of the oldest and most widely used vacuum deposition processes. [31]

Plating techniques including electroplating, pulse plating, and electroless plating can also be used. Electroplating has been regularly used as a deposition technique for forming gold contacts to GaAs devices; it is a low temperature process which requires simple, inexpensive equipment [32]. Compared to thermal evaporation of Au, this technique is much more economical. Harris et al. estimate that electroplating a layer of Au 2 μm thick onto a 1.0 cm^2 surface requires 0.15 mg of Au, as the metal only precipitates in places where it is actually used; on the other hand, thermal evaporation of the same amount requires 36 mg, due to its indirect nature of evaporation. The group found comparable contact resistances between electroplated and thermally evaporated gold contacts to their GaAs-based concentrator solar cells [33]. Pulsed electrodeposition is advantageous for its offering of easy deposit structure and morphology control; however, the power supplies for pulse plating are relatively expensive. Electroless plating offers the opportunity to reduce manufacturing time and lower equipment costs, compared with vacuum deposition techniques. Electroless plating may present a problem when alternating metal layers are desired, though, as there is no ideal switching mechanism between deposition solutions [34].

2.6.1 Nickel Electroplating

Nickel plating is a well established technique used for decorative, engineering, and electroforming purposes that has been studied since the beginning of the 20th century. In the process, a layer of nickel is electrolytically deposited onto a conductive substrate surface. The two electrodes involved in the process are the soluble metal anode, where dissolution takes place, and the cathode, where the metal deposition occurs. The

electrodes are placed in conductive, aqueous nickel salt solution, and a direct current is passed between them. The solution contains nickel in the form of positively charged divalent ions (Ni^{+}). Metallic nickel (Ni^{0}) conversion from the reaction of the nickel ions with two electrons occurs at the cathode when current is introduced to the system. At the anode, metallic nickel is dissolved to form divalent ions; hence, the reverse reaction occurs at the cathode:

$$Ni^{2+} + 2e^{-} \leftrightarrow Ni^{0}$$

The efficiency of the nickel deposition depends on the additional reactions occurring at the cathode and the anode. At the cathode, a small amount of the current is consumed by hydrogen ion discharge from water, reducing the cathode efficiency from 100 to about 92-97%. The anode efficiency is normally 100%; however, in some cases, where the pH of the solution is too high, hydroxyl ions are discharged in preference to the nickel dissolution and oxygen evolution occurs at the anode. If oxygen evolution occurs at the anode, the anode becomes passive and nickel dissolution is inhibited. [35]

The amount of the nickel deposited on the cathode in grams, *m* can be estimated by considering the applied current and the deposition time, according to Faraday's law:

$$m = \frac{M}{nF} aIt,$$

where *M* is the molecular weight, *n* is the number of electrons involved in the electrochemical reaction, *F* is Faraday's constant (96,500 C), *a* is the current efficiency ratio (cathode/anode efficiency), *I* is the current flowing through the solution, and *t* is the deposition time [34]. For nickel,

$$m = 109.5\ aIt.$$

Dividing this equation by the density of nickel and the deposition surface area yields the equation for average deposit thickness:

$$s = \frac{109.5\ aIt}{dA},$$

where s is the deposit thickness, d is the density of nickel, and A is the area of the surface to be electroplated [34]. Clearly, the thickness of the deposit depends directly on the current density applied to the bath, I/A.

The thickness calculated by the above equation is an average value, due to the fact that the current density distribution is generally non-uniform across the cathode surface. The current density distribution is largely determined by geometric factors in the nickel plating process; this includes the shape of the part, its placement relative to the anode, and the dimensions of the system. Thickness uniformity is difficult to achieve in nickel plating due to the presence of recessed areas on the cathode surface, which inevitably receive less current than more prominent areas. The cathode polarization, the cathode efficiency and electrical conductivity of the solution also influence the current distribution. These factors all contribute to the throwing power of the electrolytic solution. An electrolyte with a high throwing power has the capability to form a uniform deposit across the surface of the cathode. In order to improve the throwing power of nickel electroplating solutions, one can lower the current density, increase the solution conductivity, raise the pH and temperature of the solution, and increase the distance between electrodes [34].

Many nickel plating solutions are commercially available for nickel deposition, but the two most commonly used are Watts and sulfamate solutions. The compositions of the two solutions are presented in Table 2.3. The Watts solution is relatively inexpensive and easily controlled. The main nickel ion source in the solution is the nickel sulfate, which also limits the cathode current density. Nickel chloride serves to increase electrical conductivity of the solution and improve the uniformity of the deposit thickness. Boric acid acts as a buffer and affects the deposit appearance. The operating conditions (pH, temperature, current density) of the deposition by Watts solution affect deposit properties, such as hardness, tensile strength, and internal stress. [35]

Table 2.3 Watts nickel and nickel sulfamate electrolyte solution compositions

	Electrolyte Composition, g/L [35]	
	Watts Nickel	Nickel Sulfamate
Nickel Sulfate, $NiSo_4 \cdot 6H_2O$	225 to 400	
Nickel Sulfamate, Ni $(SO_3NH_2)_2$		300 to 450
Nickel Chloride, $NiCl_2 \cdot 6H_2O$	30 to 60	0 to 30
Boric Acid, H_3BO_3	30 to 45	30 to 45

Nickel sulfamate solutions are chosen for use in electroforming because they enable high rates of deposition and exhibit superior throwing power. These solutions also permit lower operating temperatures because of their high solubility, which leads to a higher nickel metal concentration. To minimize anode passivity at high current densities, nickel chloride is sometimes added to nickel sulfamate solutions. Nickel sulfamate

solutions are relatively expensive and especially useful for applications which demand deposits with low residual stress. [35]

The anode usually used in nickel plating processes is a soluble nickel anode. The anode chosen influences the metal distribution and is responsible for distributing current to the parts to be plated. A simple method of satisfying the anode requirements is to suspend the nickel metal bar from a hook and immerse it in the plating solution, without the hook penetrating the solution surface. To ensure that no anode residues enter the solution and cause roughness in the deposit on the cathode, the nickel anode materials can be encased in cloth anode bags; this prevention technique was not practiced in the current study. Recently, the simple nickel metal bar anode has been largely replaced in practice by small nickel pieces loaded into a titanium mesh basket. The titanium baskets are advantageous in that they ensure a uniform anode area, which helps regulate current distribution and promote consistent thickness across the deposit area. [35]

The main controllable parameters in nickel electroplating are the pH and temperature of the plating solution, and the current density in the bath. Benhenda et al. studied the effects on deposit topography of current density and temperature in Ni deposition on copper from a Watts bath [36]. In their study, it was found that a dense structure with a low roughness could be obtained while operating at low temperature (30°C) and low current density (20 mA/cm^2); however, these samples exhibited a higher contact resistance than those plated at 60°C. In their research of Ni plating from acid sulfate solution onto stainless steel cathodes, Holm et al. found that increasing the electrolyte temperature (from 40 to 60°C) and pH (from 2.0 to 3.5) improved the current efficiency [37].

2.6.2 Rapid Thermal Annealing (RTA)

Heat treatment is often required after initial contact deposition. Normally, post-deposition annealing is meant to improve contact adhesion, but may also serve to lower the contact resistance, if certain alloying reactions are promoted by high temperatures. Care must be taken in annealing, however, as some unwanted compounds may form upon heating. Rapid heating and cooling can be exploited to lower the contact resistance by preventing unwanted compounds to form during heating and cooling transitions. This attribute makes rapid thermal annealing (RTA) desirable for heat treatment of ohmic contacts, especially when contacts are formed on especially reactive substrates.

CHAPTER 3

METHODS AND MATERIALS

3.1 Intermediate Band Solar Cell Fabrication

During processing steps, GaAs devices are highly susceptible to contamination from environmental pollutants and thus must be fabricated in clean room environments. The bulk of the IBSC fabrication process takes place in a molecular beam epitaxy (MBE) machine. This machine must be kept at low vacuum (10^{-9} Torr range) to enable better control over growth conditions. With MBE, Be-doped GaAs layers are grown on an N^+ GaAs substrate. The IBSC structure is depicted in Figure 3.1. The first layer grown on the substrate is a 200 nm Si-doped GaAs layer, followed by Si-doped AlGaAs layers (~600 nm total) acting as the back surface field and base layers. Next, the QD stack is added, isolated by AlGaAs layers. Be-doped AlGaAs layers are added to serve as the emitter and window layers before the Be-AlAs stop-etching layer and Be-GaAs contact layers are grown.

Be – GaAs	3 nm	contact layers
Be – GaAs (N=10^{20})	30 nm	
Be – GaAs (N=$2x10^{18}$-10^{19})	40 nm	
Be – GaAs (N=$2x10^{18}$)	227nm	
Be – AlAs (N=$7,4x10^{18}$)	5 nm	Stop-etching
Be – GaAs (N=$2x10^{18}$)	5 nm	
Be – $Al_{0.78}Ga_{0.22}As$ (N=$5,4x10^{18}$)	30 nm	window
Be – $Al_{0.35}Ga_{0.65}As$ (N=10^{18})	200 nm	emitter
$Al_{0.35}Ga_{0.65}As$	70 nm	QD stack
$Al_{0.35}Ga_{0.65}As$	130 nm	
Si – $Al_{0.35}Ga_{0.65}As$ (N=$5x10^{17}$)	500 nm	base
Si – $Al_{0.41}Ga_{0.59}As$ (N=$2,6x10^{18}$)	105 nm	BSF
Si – GaAs (N=$2x10^{18}$)	200 nm	
N+ - GaAs substrate		

Figure 3.1 Structure of intermediate band solar cells studied in this work

3.2 Photolithography

For fabrication of the front contact layer to the cell, a photolithography patterning step must be carried out. The negative photoresist NR9-3000PY was used in this process. This resist was chosen for its good resolution capability, fast development time, and easy removal. Once applied to the GaAs wafer, the resist was spun down and a UV assisted patterning was carried out. For the purpose of electrical characterization, the photolithographic mask used was that of a typical TLM device pattern. Each TLM device printed contained ten equal sized rectangular pads (0.8 mm x 0.2 mm) spaced 0.005, 0.01, 0.015, 0.02, 0.025, 0.03, 0.035, 0.04, and 0.045 mm apart. After UV exposure and a post-exposure bake step, the wafer was dipped in resist developer RD6 for 30 seconds to remove the unexposed resist material and then rinsed thoroughly in DI water to remove excess developer.

3.3 Thermal Evaporation

Thermal evaporation is the method currently used in the processing of front ohmic contacts to the IBSC material under investigation in the study. The starting materials employed in this study were in the form of elemental pellets in the case of gold, zinc, and nickel, and were in the form of pure metal bars in the case of chromium. Immediately before the deposition, both the metal starting materials and the samples were cleaned in an HCl/H_20 (1:1) solution to remove native oxides. All depositions were performed under a vacuum on the order of 10^{-6} Torr.

3.3.1 Cr/Au

Cr/Au contacts were deposited on wafers of three different doping levels: N_A = 4 x 10^{16} cm^{-3}, 4.7 x 10^{19} cm^{-3}, and 1.7 x 10^{20} cm^{-3}. The target contact thickness for these samples was Cr: 300 Å, Au: 2000 Å, with the real values being 309 Å and 2034 Å, respectively. The Cr was deposited at a rate from 1.7 to 2 Å/s, while the Au was deposited from 18 to 20 Å/s.

3.3.2 Au/Zn/Au

Au/Zn/Au contacts were deposited on wafers of four different doping levels: N_A = 1 x 10^{19} cm^{-3}, 4 x 10^{16} cm^{-3}, 4.7 x 10^{19} cm^{-3}, and 1.7 x 10^{20} cm^{-3}. The target contact thickness for these samples was Au: 300 Å, Zn: 300 Å, Au: 2000 Å, with the real values being 319 Å, 315 Å, and 2026 Å, respectively. The first layer of Au was deposited at 15 Å/s, the Zn layer from 6 to 12 Å/s, and the final Au layer from 10 to 15 Å/s.

3.3.3 Cr/Zn/Au

Cr/Zn/Au contacts were deposited on wafers of four different doping levels: N_A = 1 x 10^{19} cm^{-3}, 4 x 10^{16} cm^{-3}, 4.7 x 10^{19} cm^{-3}, and 1.7 x 10^{20} cm^{-3}. The target contact thickness for these samples was Cr: 50 Å, Zn: 300 Å, Au: 2000 Å, with the real values being 53 Å, 304 Å, and 2034 Å, respectively. The Cr layer was deposited at 1.5 Å/s, the Zn layer from 1 to 2 Å/s, and the Au layer from 14 to 20 Å/s.

3.3.4 Nickel

For the purpose of comparison to the electrolytically deposited samples, nickel contacts were deposited by thermal evaporation on wafers of two different doping levels: N_A = 5.3 x 10^{18} cm^{-3} and 3.0 x 10^{19} cm^{-3}. The samples were deposited under a vacuum of 10^{-6} Torr at a rate of 3.2 Å/sec. The target thickness for these deposits was 800 Å, with the real thickness being 930 Å.

3.4 Electroplating

The electroplating process had not previously been used in this lab to fabricate contacts to IBSCs, so this research concerned the implementation of a working electroplating experiment set up and process development. The only metal deposited by this method was nickel. A Watts nickel electrolyte was employed in this study.

The experiment set up is depicted in Figure 3.2. The deposition was carried out in a 250 mL glass beaker situated on a hot plate, which kept the electrolyte at a temperature of 50-60°C. The anode used in the process was a Ni metal bar, directly clamped to the

positive electrical lead and suspended in the solution. A sample holder for the cathode (GaAs wafer) was designed and produced using a plastic base (Figure 3.3). A copper metal bar was attached to the plastic base to hold the sample in place and provide the required conductivity to the sample. The Cu was largely covered with negative resist NR9 and laboratory tape in order to concentrate the conductivity to the tip in contact with the sample; also left uncovered was the top of the metal bar, which was the location of the negative electric lead attachment. The sample holder was suspended from a laboratory stand and clamp and placed above the beaker such that the sample and not the Cu tip was submerged in the electrolyte.

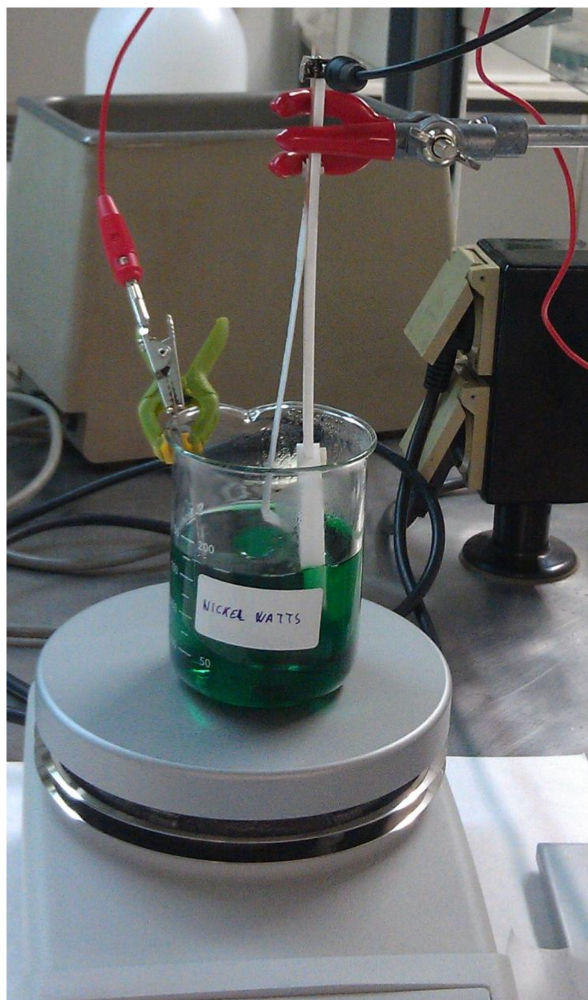

Figure 3.2 Electrolytic deposition experiment set up. The electrical leads are attached at the other end to a Keithley SourceMeter® 2602 (not pictured)

Figure 3.3 Sample holder used for GaAs IBSC wafers in electrolytic deposition experiment

The current introduced to the system was sourced by a Keithley SourceMeter® 2602, which was controlled through an NI LabVIEW interface. A step current method was employed to obtain electrochemical equilibrium by overcoming the assumed activation polarization. First, a constant current density of 0.008 mA/cm^2 was applied for two minutes, followed by two minutes each of 0.015 and 1.75 mA/cm^2 before the current density required for the particular sample (2.5 or 5 mA/cm^2) was applied for the appropriate amount of time to obtain the desired thickness (based only on the final current applied). The first three current density and time values were chosen arbitrarily; due to time constraints and sample limitations, no other current values were investigated.

All depositions in this work were carried out at 50-60°C under a medium-speed agitation, produced by a magnetic stir bar in the solution. The doping levels of the samples processed by this method were 5.3×10^{18} and 3.0×10^{19} cm^{-3}. The effects of both the current density and the deposition times were studied in this work. The current density values chosen were 2.5 and 5 mA/cm^2. These values were chosen based on the work of Ward et al. on Ni/Au contacts for GaAs based concentrator solar cells [38]. The deposition times chosen were determined by the use of Faraday's law on the assumption of 100% current efficiency to obtain nominal thicknesses of 2500 Å and 5000 Å. Four samples of each doping level were processed, varying the current density and deposition time; the deposition parameters of each sample are displayed in Table 3.1.

Table 3.1 Parameters applied to Ni electrolytic deposition on samples at both doping levels

Current Applied (mA)	Current Density (mA/cm^2)	Deposition Time (s)	Desired Thickness (Å)
2.54	2.5	293	2500
2.54	2.5	585	5000
5.12	5	146	2500
5.12	5	293	5000

3.5 Rapid Thermal Annealing (RTA)

The Surface Science Integration Solaris 75 manual loading rapid thermal processing system was used for the RTA carried out on the samples in this study. All annealing was preceded by a 30 second nitrogen gas purge and carried out under a constant flow of forming gas. The temperature was ramped up after the N_2 purge at a rate of 30°C/second, and ramped back down at the highest rate possible.

3.5.1 Thermally Evaporated Samples

Each of the samples produced by thermal evaporation was subsequently sectioned and treated by RTA. Each whole sample from evaporation yielded eight or ten smaller samples, each containing two TLM devices for contact resistance measurement. Annealing times and temperatures were varied according to Table 3.2. These temperature ranges and times were chosen based on various literature sources.

A temperature range of 350-500°C was set for the annealing of Cr/Au contacts; this is the same temperature range used by Castanedo et al. in their study of the same contact scheme to p-GaAs ($N_A = 2.9 \times 10^{18}$ cm^{-3}) [39]. Castanedo et al. employed RTA on their samples for one and two minutes, with the lower resistance values being obtained

after just one minute of annealing; hence, in this study, 30 and 60 second annealing times at these temperatures were investigated.

The Au/Zn/Au contacts were annealed in the range 350-500°C; this range is comparable to that used in the study of Au/Zn/Au contacts to p-GaAs (N_A = 3.0 x 10^{17} cm^{-3}) by Lu et al., who performed RTA from 375-500°C for 5 to 20 seconds [22]. Kaminska et al. also studied RTA on Au/Zn/Au contacts to p-GaAs, using the range of 200-500°C for 3-10 minutes; the group found the lowest resistances between 320-460°C for three minutes [24].

As Cr/Zn/Au contacts to p-GaAs have not been previously studied, the temperature range and annealing times were chosen based on those of the Cr/Au and Au/Zn/Au metallization schemes. For Ni contacts, the annealing times and temperatures were based on a combination of the previous works described and the work of Ho et al., who studied Ni/Au contacts to p-GaN using furnace annealing for ten minutes from 300-600°C [40].

Table 3.2 Annealing parameters for samples processed by thermal evaporation

	Cr/Au	Cr/Zn/Au	Au/Zn/Au	Ni (N_A = 3.0 x 10^{19} cm^{-3})	Ni (N_A = 5.3 x 10^{18} cm^{-3})
300°C				60, 120 sec	60, 100 sec
350°C	30, 60 sec		60, 120 sec	60, 120 sec	60, 100 sec
400°C	30, 60 sec	30, 60 sec	60, 120 sec	60, 120 sec	60, 100 sec
450°C	30, 60 sec	30, 60 sec	60, 120 sec	60, 120 sec	60, 100 sec
500°C	30, 60 sec	30, 60 sec	60, 120 sec	60, 120 sec	60, 100 sec
550°C		30, 60 sec			

3.5.2 Electrodeposited Samples

Some Ni electrodeposited samples were annealed by RTA from 350-550°C for 60, 100, and 120 seconds. After initial contact resistance measurements showed no improvement after annealing, no further RTA processing was carried out on these samples.

3.6 Transmission Line Modeling (TLM)

The four-terminal TLM method was applied to all samples for contact resistance measurement before and after annealing. The probe system was accompanied by an optical microscope and attached to a Keithley SourceMeter® 2400. The resistance measurements were obtained at a source current range of 0.01 mA to 1 mA with a programmed compliance voltage of 5 mV. These are the standard parameters used when measuring contact resistance of contacts to the GaAs IBSCs studied in this research.

Current-voltage curves were obtained at each measurement of neighboring pads. For every TLM device, nine curves were obtained. The inverse slope of each of the nine curves corresponded to the resistance values used in the plot of resistance versus pad spacing used to obtain contact resistance values. Half of the y-intercept of the best fit line to the resistance versus pad spacing plot was taken as the contact resistance value; this value was divided by the contact area to obtain the specific contact resistivity value for each TLM device.

In some cases, contact end resistances (R_e) were obtained and incorporated in the specific contact resistivity calculations. This value was not obtained for all samples due to instrument and/or user error which resulted in negative values of R_e. To perform the contact end resistance measurement, the four probes were applied to two contact pads separated by one pad. The same procedure was applied to determine the specific contact resistivity, with an additional calculation for the transfer length and end resistance.

3.7 Scanning Electron Microscopy (SEM)

Scanning electron microscopy was performed on select samples[1]. The purpose of this testing was to examine the surface topography of the contact and attempt to correlate surface features to specific contact resistivity values measured. SEM observations were made on a Zeiss Supra 50VP under high vacuum.

---

[1] Samples had been transported from Universidad Politécnica de Madrid in Spain to Drexel University in Philadelphia, PA prior to SEM examination. Not all samples were able to be taken from Spain for further testing.

CHAPTER 4

RESULTS AND DISCUSSION

4.1 Specific Contact Resistivity[2]

4.1.1 Thermally Evaporated Samples (Non-Nickel), by Doping Level

4.1.1.1 $N_A = 4.0 \times 10^{16}$ cm^{-3}

All three metallization schemes were deposited on samples of the lowest doping level studied, 4.0×10^{16} cm^{-3}. All as-deposited contacts exhibited rectifying behavior; this was expected, due to the low doping of the wafer. Contacts of Cr/Au remained rectifying after annealing by RTA. After annealing samples with Cr/Zn/Au and Au/Zn/Au, ohmic contacts were realized. Predictably, contacts deposited on wafers of this doping level exhibited the highest specific contact resistivity of all the wafers.

The specific contact resistivities of the Au/Zn/Au contacts are plotted versus annealing temperature in Figure 4.1. All contact resistivities were on the order of 10^{-2} Ωcm^2. After 60 seconds of annealing ("short anneal"), there was a clear drop in specific contact resistivity (0.0111 Ωcm^2) from 400 to 450ºC, corresponding to the lowest measured resistivity, 1.09×10^{-2} Ωcm^2. A more subtle resistivity change in samples annealed at these temperatures can be seen in those annealed for 120 seconds ("long anneal"). In this case, once again, the lowest resistivity value was obtained after RTA at 450ºC, in which case $\rho_c = 1.10 \times 10^{-2}$ Ωcm^2.

---

[2] The minimum specific contact resistivity results discussed in this section are presented in Table 4.1

Table 4.1 Minimum specific contact resistivities measured

Deposition Method	Doping Level (cm^{-3})	Metallization Scheme	Thickness (Å)	Minimum Specific Contact Resistivity ($\Omega \cdot cm^2$)	Annealing Parameters
Thermal Evaporation	4.0×10^{16}	Au/Zn/Au	319/315/2026	1.09×10^{-2}	60 seconds, 450°C
		Cr/Zn/Au	53/304/2034	1.96×10^{-2}	60 seconds, 500°C
	1.0×10^{19}	Au/Zn/Au	319/315/2026	8.48×10^{-4}	60 seconds, 350°C
		Cr/Zn/Au	53/304/2034	8.76×10^{-4}	30 seconds, 500°C
	4.7×10^{19}	Cr/Au	309/2034	1.03×10^{-4}	as-deposited
		Au/Zn/Au	319/315/2026	1.53×10^{-4}	as-deposited
		Cr/Zn/Au	53/304/2034	1.51×10^{-4}	as-deposited
	1.7×10^{20}	Cr/Au	309/2034	5.82×10^{-5}	as-deposited
		Au/Zn/Au	319/315/2026	1.55×10^{-4}	120 seconds, 450°C
		Cr/Zn/Au	53/304/2034	7.25×10^{-5}	as-deposited
	5.3×10^{18}	Ni	930	1.69×10^{-3}	60 seconds, 500°C
	3.0×10^{19}	Ni	930	4.58×10^{-4}	60 seconds, 350°C
Electrolytic Deposition	5.3×10^{18}	Ni	2500	1.18×10^{-3}	60 seconds, 450°C
		Ni	5000	9.91×10^{-4}	60 seconds, 450°C
	3.0×10^{19}	Ni	2500	1.74×10^{-4}	as-deposited
		Ni	5000	1.90×10^{-4}	as-deposited

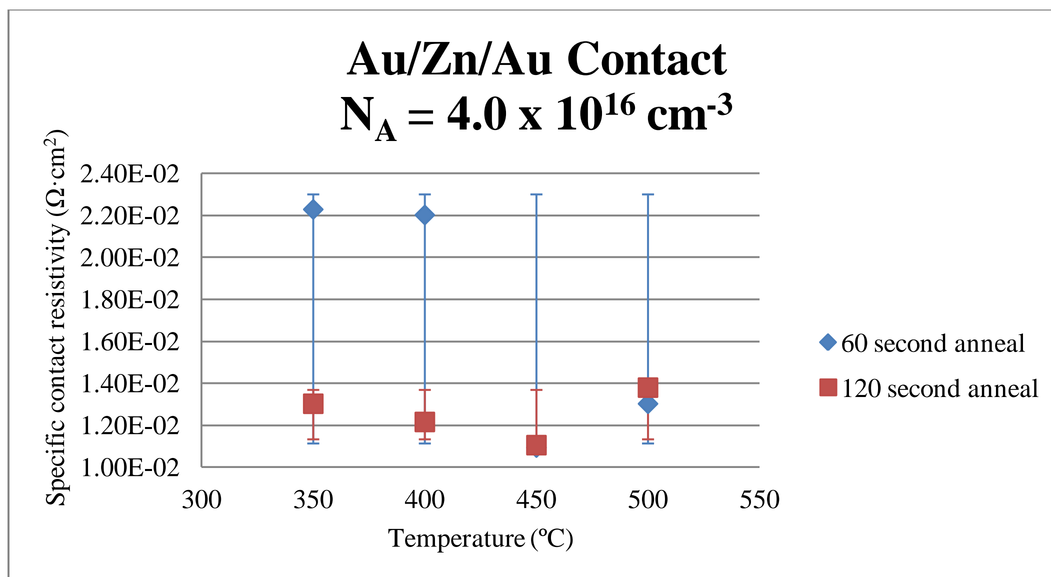

Figure 4.1 Specific contact resistivity versus annealing temperature for p-GaAs ($N_A = 4.0 \times 10^{16}$ cm^{-3}) with thermally evaporated Au/Zn/Au contacts

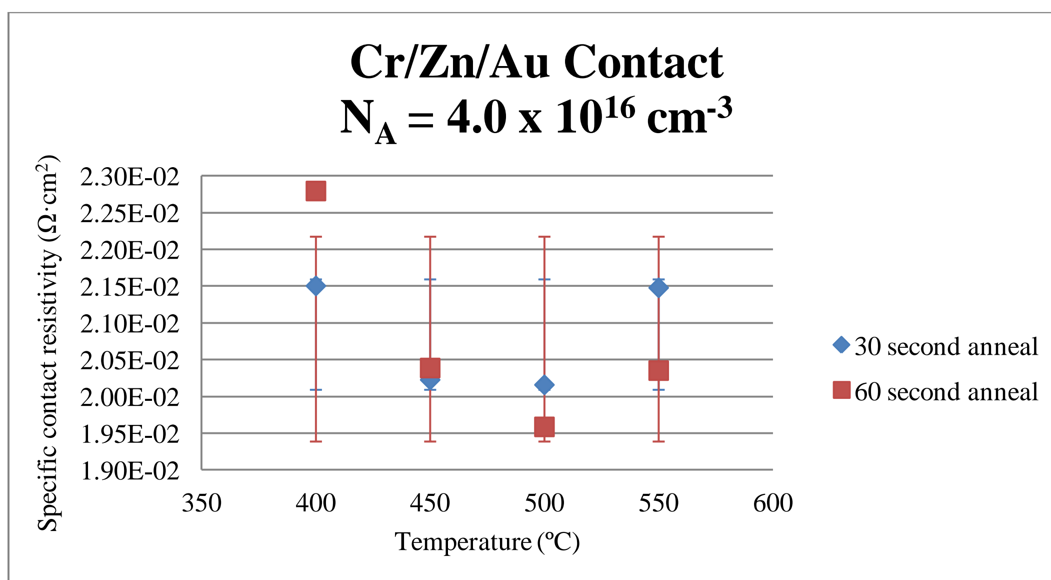

Figure 4.2 Specific contact resistivity versus annealing temperature for p-GaAs ($N_A = 4.0 \times 10^{16}$ cm^{-3}) with thermally evaporated Cr/Zn/Au contacts

The specific contact resistivities of the Cr/Zn/Au contacts are plotted versus annealing temperature in Figure 4.2. All specific contact resistivities were on the order of

10^{-2} Ωcm^2. In samples annealed for both 30 seconds ("short anneal") and 60 seconds ("long anneal"), the minimum specific contact resistivity was obtained after annealing at 500ºC. The minimum specific contact resistivity obtained after 60 seconds of annealing (1.96 x 10^{-2} Ωcm^2) was slightly lower than that obtained after 30 seconds of annealing (2.02 x 10^{-2} Ωcm^2).

Comparisons of the two metallization schemes are shown in Figure 4.3 and Figure 4.4 for short and long annealing times, respectively. It is clear that the Au/Zn/Au contacts promote a lower specific contact resistivity, overall. These contacts also produced resistivity values with a larger standard deviation than those of Cr/Zn/Au.

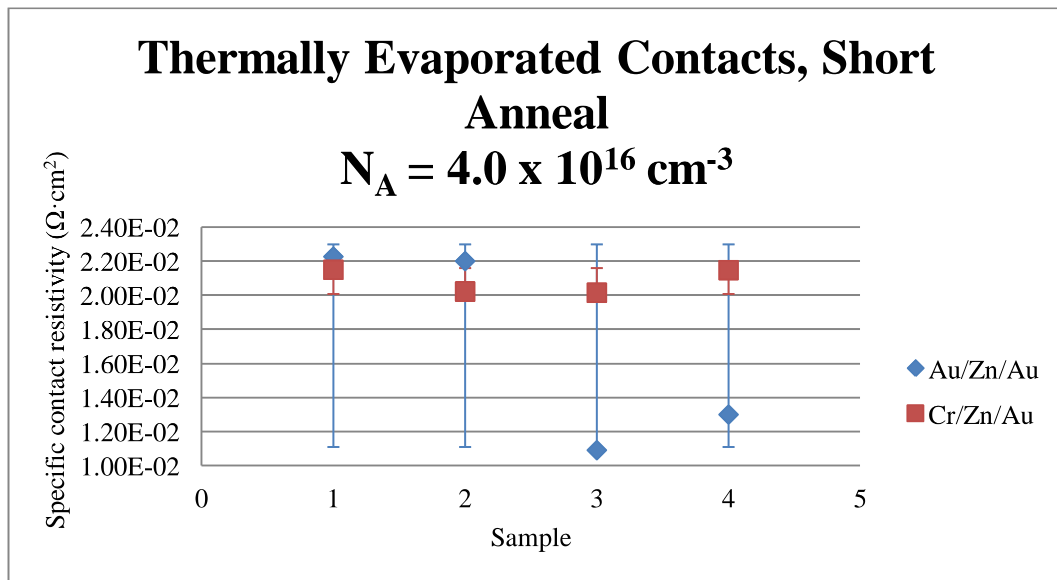

Figure 4.3 Specific contact resistivity for p-GaAs (N_A = 4.0 x 10^{16} cm^{-3}) with thermally evaporated Au/Zn/Au and Cr/Zn/Au contacts, after short time RTA

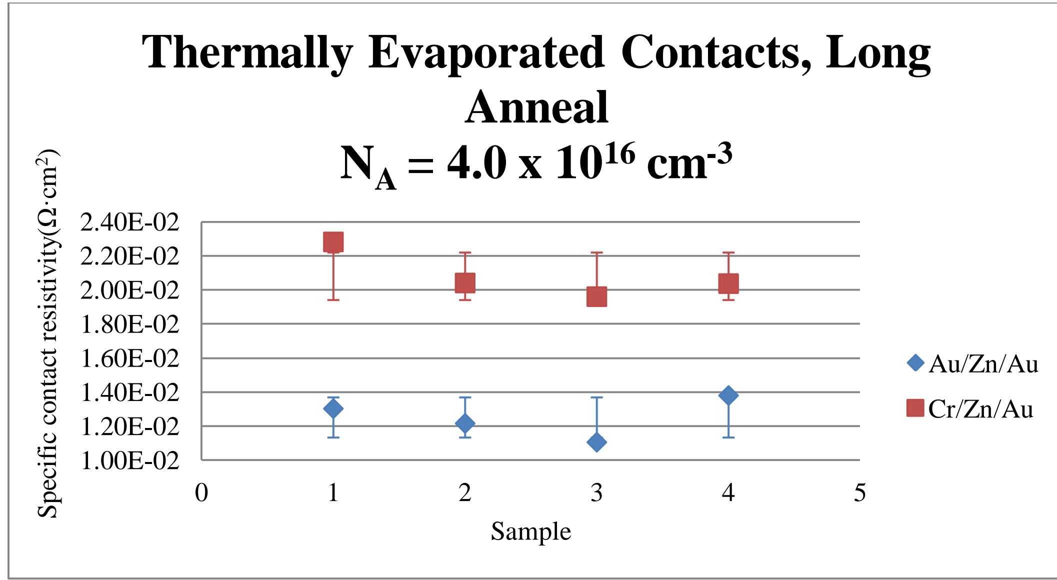

Figure 4.4 Specific contact resistivity for p-GaAs ($N_A = 4.0 \times 10^{16}$ cm^{-3}) with thermally evaporated Au/Zn/Au and Cr/Zn/Au contacts, after long time RTA

4.1.1.2 $N_A = 1.0 \times 10^{19}$ cm^{-3}

Two metallization schemes were deposited on samples doped to 1.0×10^{19} cm^{-3}: Au/Zn/Au and Cr/Zn/Au. All as-deposited contacts exhibited rectifying behavior. After annealing, ohmic contacts were realized on all samples. Predictably, contacts deposited on wafers of this doping level exhibited relatively high specific contact resistivities.

The specific contact resistivities of the Au/Zn/Au contacts are plotted versus annealing temperature in Figure 4.5. All specific contact resistivities were on the order of 10^{-4} to 10^{-3} Ωcm^2. After annealing (in both short and long anneal cases), there was a clear increase in specific contact resistivity from 450ºC to 500ºC. Contacts annealed from 350ºC to 450ºC all yielded similar specific contact resistivities, from 8.48×10^{-4} Ωcm^2 to 8.74×10^{-4} Ωcm^2 for samples annealed for 60 seconds and from 8.82×10^{-4} Ωcm^2 to 9.14

x 10^{-4} Ωcm^2 for samples annealed for 120 seconds. The lowest resistivity value was obtained at 350°C after short anneal and at 400°C after long anneal.

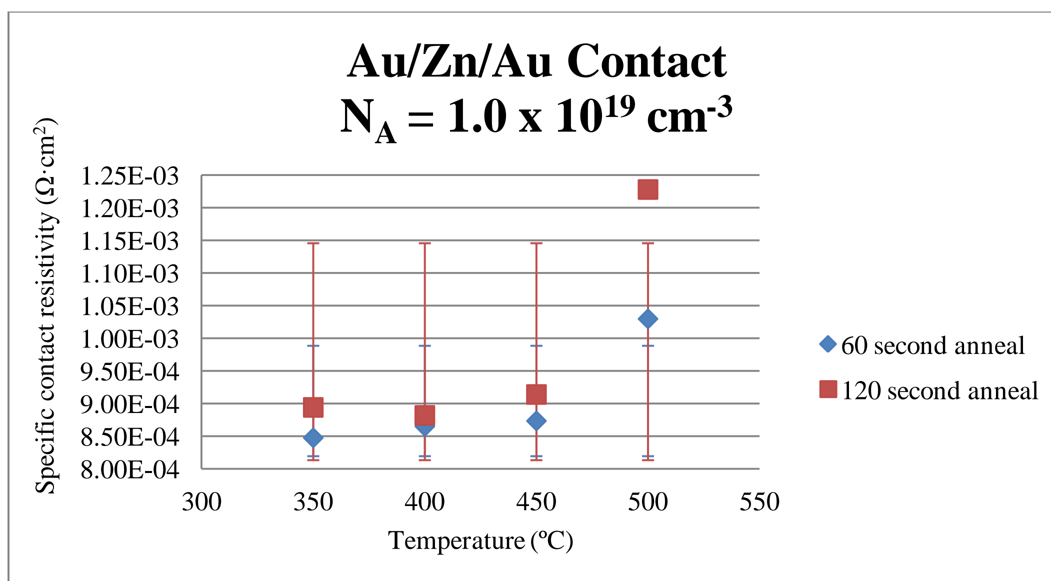

Figure 4.5 Specific contact resistivity versus annealing temperature for p-GaAs ($N_A = 1.0 \times 10^{19}$ cm^{-3}) with thermally evaporated Au/Zn/Au contacts

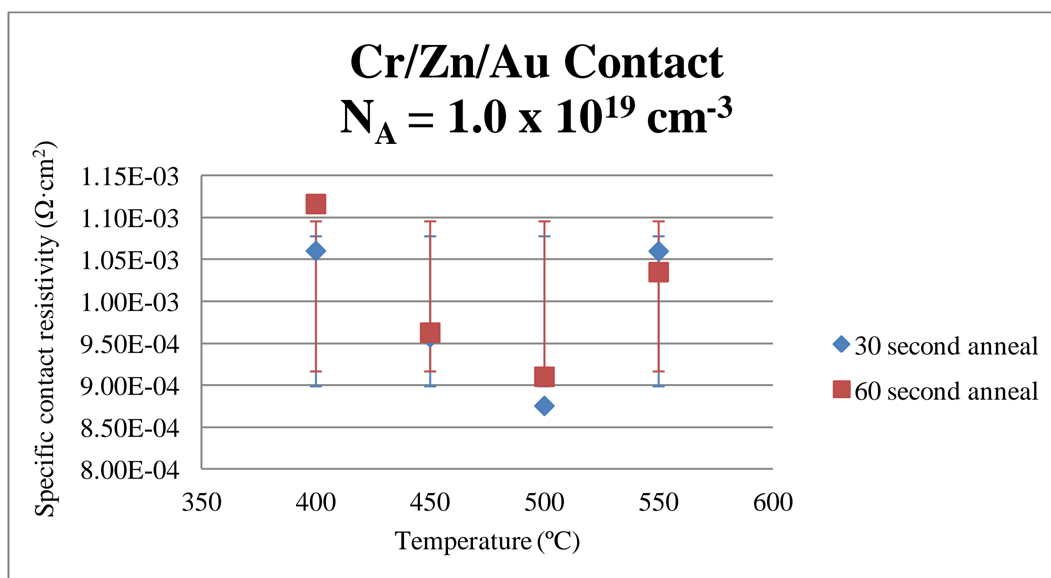

Figure 4.6 Specific contact resistivity versus annealing temperature for p-GaAs (**$N_A = 1.0 \times 10^{19}$ cm^{-3}**) with thermally evaporated Cr/Zn/Au contacts

The specific contact resistivities of the Cr/Zn/Au contacts are plotted versus annealing temperature in Figure 4.6. All contact resistivities were on the order of 10^{-4} to 10^{-3} Ωcm^2. In samples annealed for both 30 seconds and 60 seconds, the minimum specific contact resistivity was obtained at 500ºC. The minimum specific contact resistivity obtained after 30 seconds of annealing (8.76×10^{-4} Ωcm^2) was slightly lower than that obtained after 60 seconds of annealing (9.10×10^{-4} Ωcm^2).

Comparisons of the two metallization schemes are shown in Figure 4.7 and Figure 4.8 for short and long annealing times, respectively. The Au/Zn/Au contacts promote a lower specific contact resistivity, overall. These contacts produced resistivity values with a larger standard deviation than those of Cr/Zn/Au after long time annealing; with the opposite being true after short time annealing.

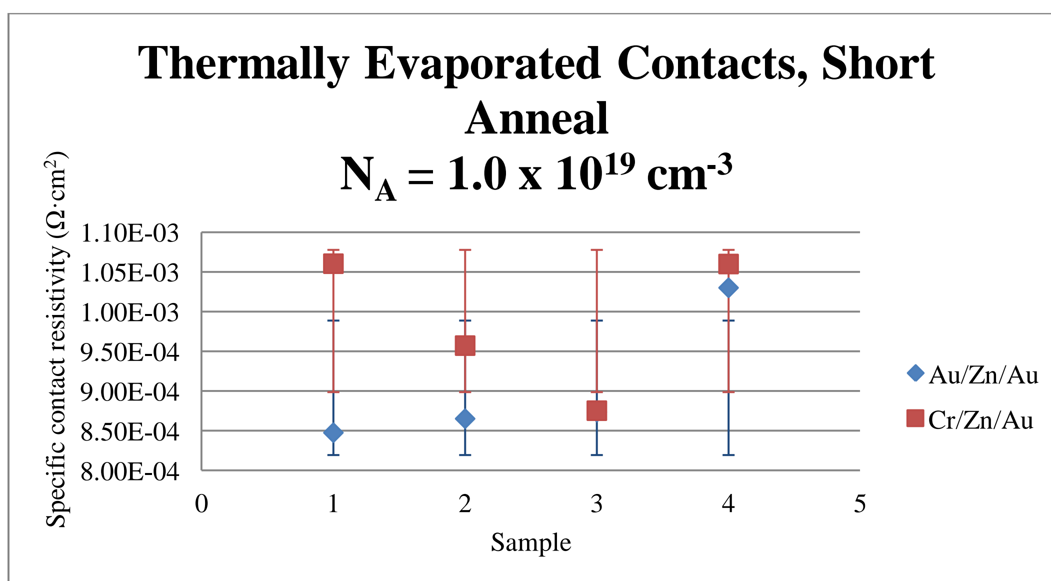

Figure 4.7 Specific contact resistivity for p-GaAs ($N_A = 1.0 \times 10^{19}$ cm^{-3}) with thermally evaporated Au/Zn/Au and Cr/Zn/Au contacts, after short time RTA

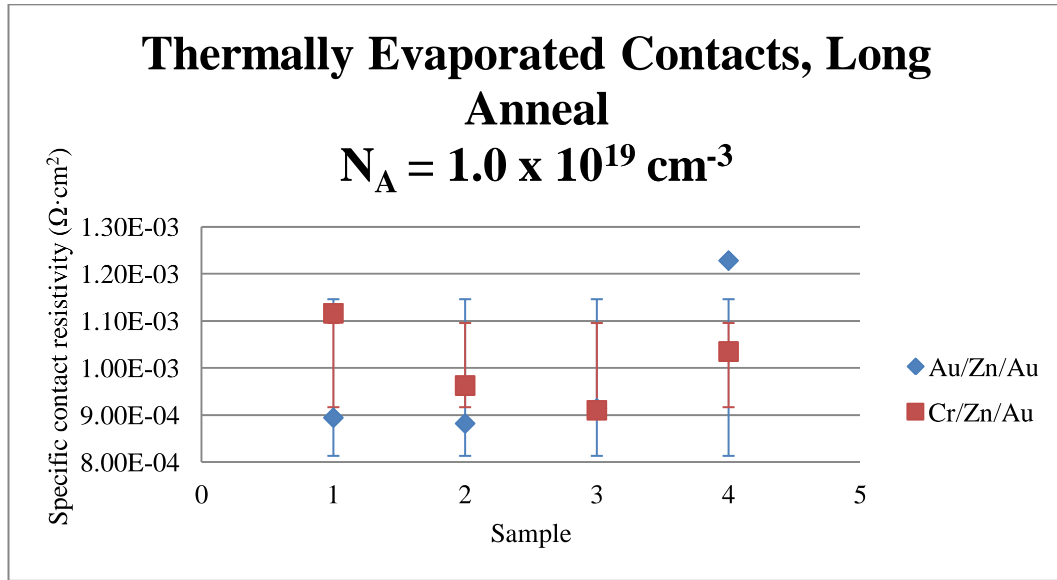

Figure 4.8 Specific contact resistivity for p-GaAs ($N_A = 1.0 \times 10^{19}$ cm^{-3}) with thermally evaporated Au/Zn/Au and Cr/Zn/Au contacts, after long time RTA

4.1.1.3 $N_A = 4.7 \times 10^{19}$ cm^{-3}

All metallization schemes were deposited on samples doped to 4.7 x 10^{19} cm^{-3}. All as-deposited contacts exhibited ohmic behavior. Specific contact resistivities including R_e were determined for all samples, except for those with Cr/Au contacts annealed for 60 seconds and for those with Au/Zn/Au contacts as deposited.

The specific contact resistivities of the Cr/Au contacts are plotted versus annealing temperature in Figure 4.9. The “pre-anneal” values plotted are the average of the specific contact resistivity values measured pre-anneal of those samples annealed (for short and long times) at the corresponding temperatures. All contact resistivities were on the order of 10^{-4} Ωcm^2. As-deposited contacts exhibited the lowest specific contact resistivities. After annealing at 350ºC and 400ºC, contacts annealed for longer times were more resistant than those annealed for a short time; the opposite is true for those annealed at

450ºC and 500ºC. The lowest resistivity obtained was on an as-deposited contact, with a value of 1.03 x 10^{-4} Ωcm^2.

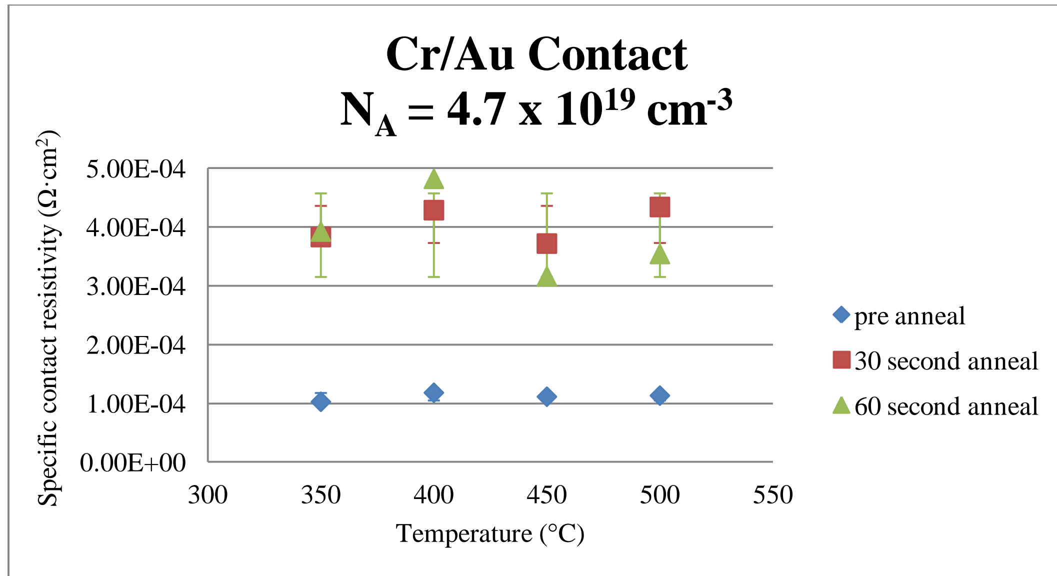

Figure 4.9 Specific contact resistivity versus annealing temperature for p-GaAs (N_A = 4.7 x 10^{19} cm^{-3}) with thermally evaporated Cr/Au contacts

The specific contact resistivities of the Au/Zn/Au contacts are plotted versus annealing temperature in Figure 4.10. The "pre-anneal" values plotted are the average of the contact resistivity values measured pre-anneal of those samples annealed for a long time at the corresponding temperatures. All contact resistivities were on the order of 10^{-4} Ωcm^2. The lowest specific contact resistivities measured were on contacts as-deposited. Almost all resistivities obtained after 120 seconds of annealing were lower than those obtained after 60 seconds of annealing (with the exception of the samples annealed at 500ºC). The lowest specific contact resistivity obtained was 1.53 x 10^{-4} Ωcm^2, in an as-deposited sample.

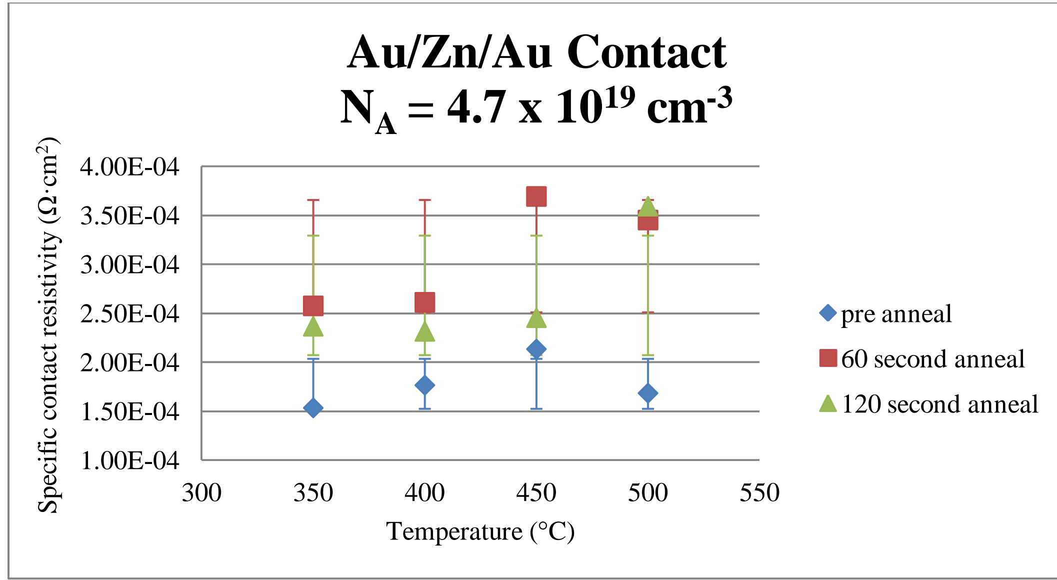

Figure 4.10 Specific contact resistivity versus annealing temperature for p-GaAs (N_A = 4.7 x 10^{19} cm^{-3}) with thermally evaporated Au/Zn/Au contacts

The specific contact resistivities of the Cr/Zn/Au contacts are plotted versus annealing temperature in Figure 4.11. The "pre-anneal" values plotted are the average of the contact resistivity values measured pre-anneal of those samples annealed (for short and long times) at the corresponding temperatures. All contact resistivities were on the order of 10^{-4} Ωcm^2. The lowest specific contact resistivities measured were on contacts as-deposited. Resistivity values measured on samples after annealing at both short and long times differed at the most by only 3.3 x 10^{-5} Ωcm^2 (specifically, for those samples annealed at 400ºC). The lowest specific contact resistivity obtained was 1.51 x 10^{-4} Ωcm^2, in an as-deposited sample.

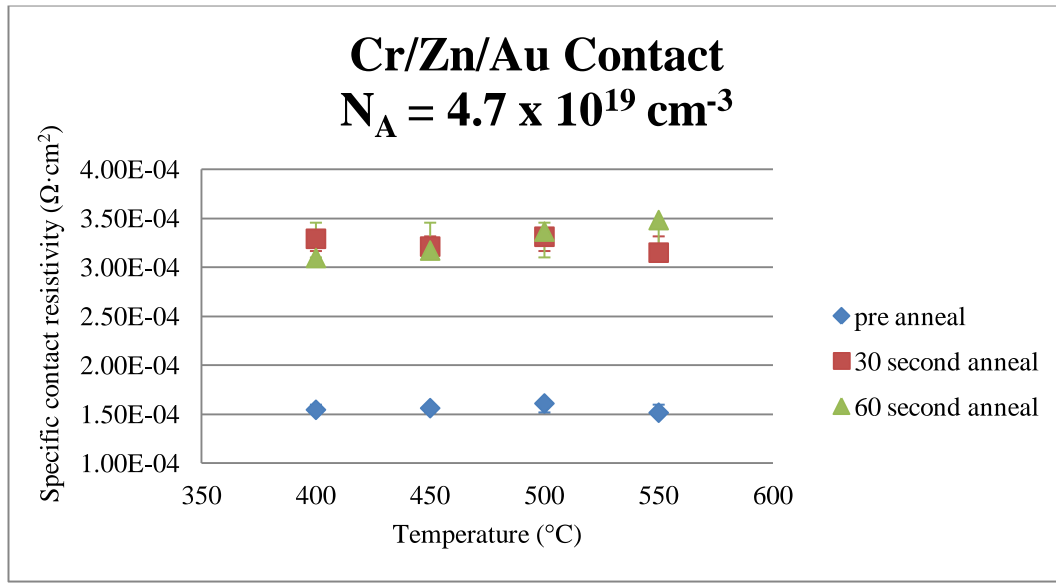

Figure 4.11 Specific contact resistivity versus annealing temperature for p-GaAs (N_A = 4.7 x 10^{19} cm^{-3}) with thermally evaporated Cr/Zn/Au contacts

Comparisons of the three metallization schemes are shown in Figure 4.12, Figure 4 13, and Figure 4.14, for pre-anneal, short anneal, and long anneal, respectively. The Cr/Au contacts had the lowest specific contact resistivities in the as-deposited samples; Au/Zn/Au contacts were the most highly resistant of the contacts as-deposited on the samples. Measured resistivities of Cr/Au contacts increased by about three to four times from their pre-anneal values after both short and long anneal times. In the samples annealed for a shorter time, it was found that Au/Zn/Au contacts displayed the lowest resistivities at the two lower annealing temperatures, with resistivities rising above those of the Cr/Zn/Au contacts at the two higher annealing temperatures. For the contacts annealed at longer times, Au/Zn/Au contacts were almost always the least resistant.

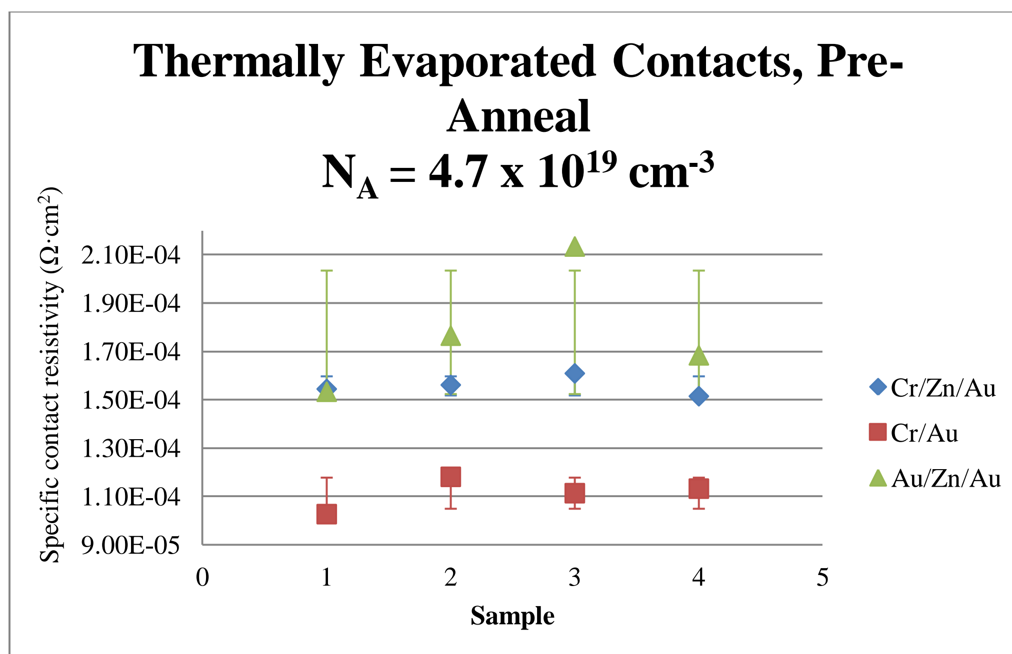

Figure 4.12 Specific contact resistivity for p-GaAs (N_A = 4.7 x 10^{19} cm^{-3}) with thermally evaporated Cr/Zn/Au, Cr/Au, and Au/Zn/Au contacts, as-deposited

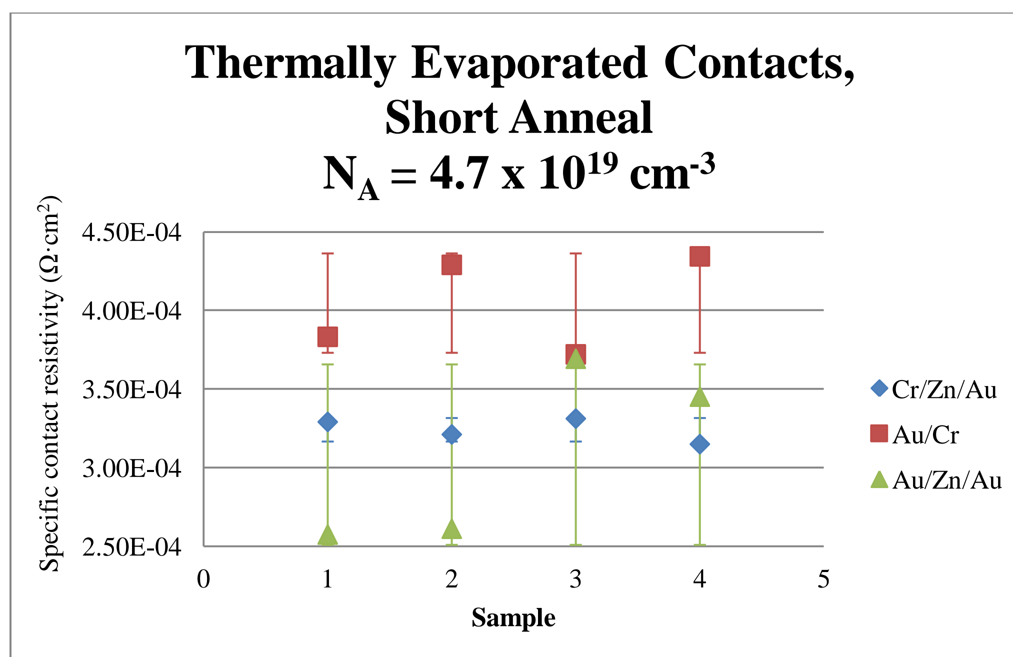

Figure 4 13 Specific contact resistivity for p-GaAs (N_A = 4.7 x 10^{19} cm^{-3}) with thermally evaporated Cr/Zn/Au, Cr/Au, and Au/Zn/Au contacts, after short anneal by RTA

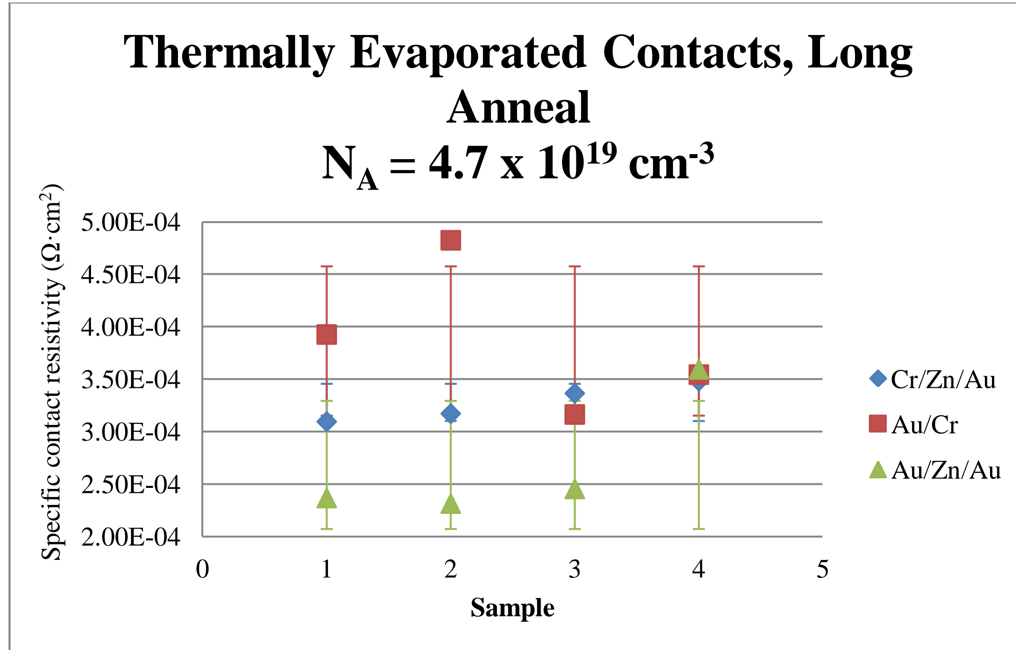

Figure 4.14 Specific contact resistivity for p-GaAs ($N_A = 4.7 \times 10^{19}$ cm^{-3}) with thermally evaporated Cr/Zn/Au, Cr/Au, and Au/Zn/Au contacts, after long anneal by RTA

4.1.1.4 $N_A = 1.7 \times 10^{20}$ cm^{-3}

All metallization schemes were deposited on samples of the highest doping level studied, 1.7×10^{20} cm^{-3}. All as-deposited contacts exhibited ohmic behavior, except for those of Au/Zn/Au. Specific contact resistivities including R_e were determined for all samples with ohmic behavior.

The specific contact resistivities of the Cr/Au contacts are plotted versus annealing temperature in Figure 4.15. The “pre-anneal” values plotted are the average of the contact resistivity values measured pre-anneal of those samples annealed (for short and long times) at the corresponding temperatures. All contact resistivities post-anneal were on the order of 10^{-4} Ωcm^2; contact resistivities of as-deposited samples were on the order of 10^{-5} Ωcm^2. The lowest resistivities obtained after anneal at both short and long times were of

contacts annealed at 400ºC. The lowest specific contact resistivity obtained was on an as-deposited contact, with a value of 5.82×10^{-5} Ωcm^2.

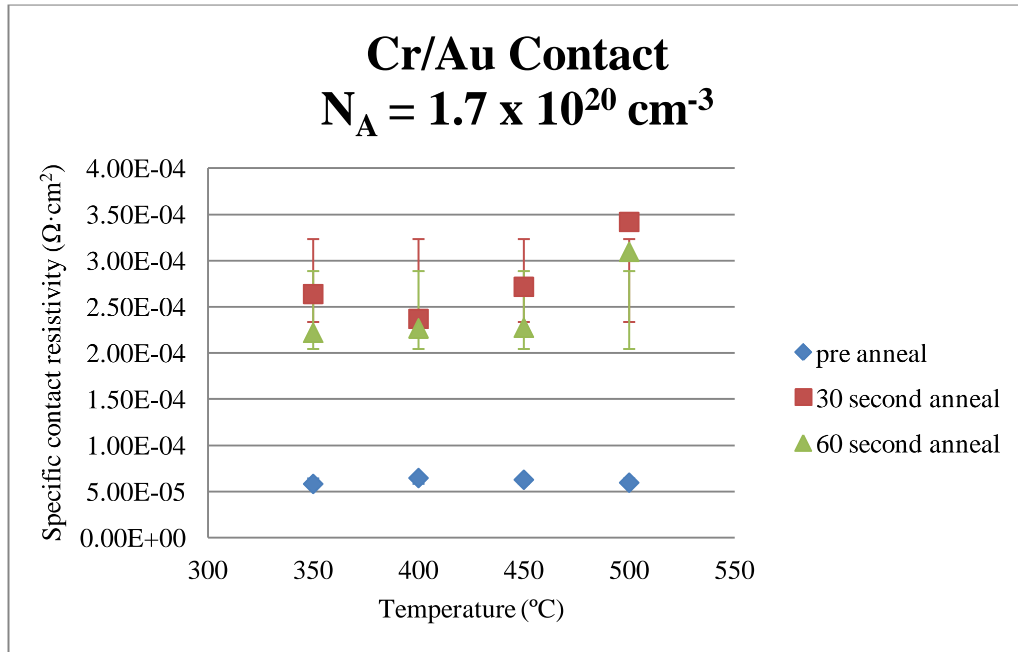

Figure 4.15 Specific contact resistivity versus annealing temperature for p-GaAs ($N_A = 1.7 \times 10^{20}$ cm^{-3}) with thermally evaporated Cr/Au contacts

The specific contact resistivities of the Au/Zn/Au contacts are plotted versus annealing temperature in Figure 4.16. All contact resistivities were on the order of 10^{-4} Ωcm^2. After annealing (in both the short and long anneal cases), there was a clear increase in specific contact resistivity from 450ºC to 500ºC. Contacts annealed from 350ºC to 450ºC all yielded similar specific contact resistivities, from 1.63×10^{-4} Ωcm^2 to 1.78×10^{-4} Ωcm^2 for samples annealed for 60 seconds and from 1.55×10^{-4} Ωcm^2 to 1.65×10^{-4} Ωcm^2 for samples annealed for 120 seconds. The lowest measured resistivity value was 1.55×10^{-4} Ωcm^2, obtained after annealing at 450ºC for 120 seconds.

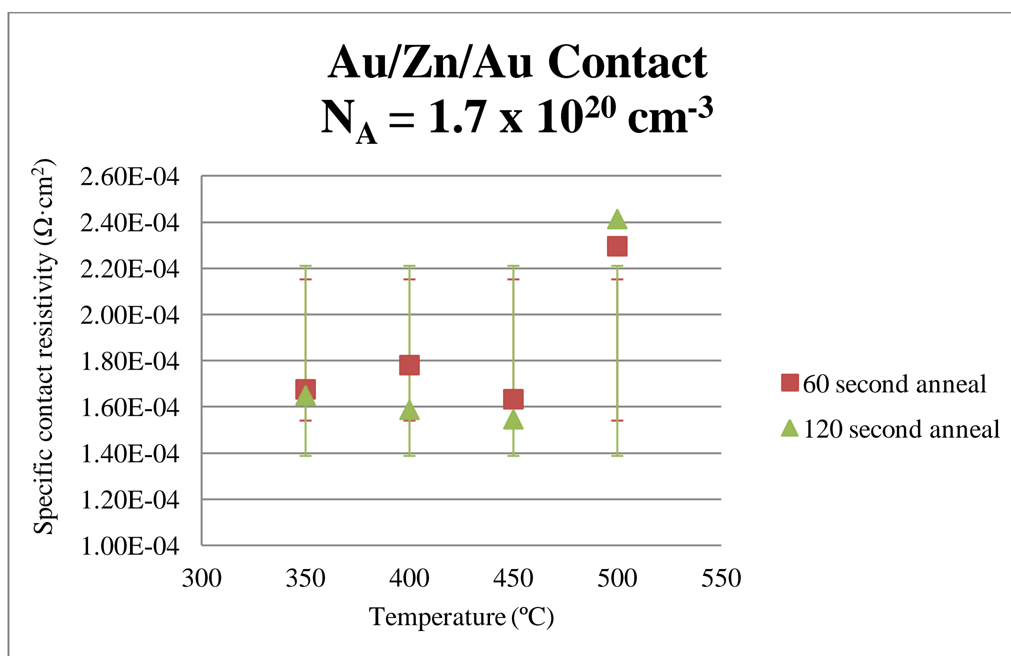

Figure 4.16 Specific contact resistivity versus annealing temperature for p-GaAs (N_A = 1.7 x 10^{20} cm^{-3}) with thermally evaporated Au/Zn/Au contacts

The specific contact resistivities of the Cr/Zn/Au contacts are plotted versus annealing temperature in Figure 4.17. The "pre-anneal" values plotted are the average of the contact resistivity values measured pre-anneal of those samples annealed (for short and long times) at the corresponding temperatures. All contact resistivities, post anneal were on the order of 10^{-4} Ωcm^2; contact resistivities of as-deposited samples were on the order of 10^{-5} Ωcm^2. After annealing (in both the short and long anneal cases), there was a clear increase in specific contact resistivity from 500ºC to 550ºC. Contacts annealed from 400ºC to 500ºC all yielded similar specific contact resistivities, from 2.04 x 10^{-4} Ωcm^2 to 2.14 x 10^{-4} Ωcm^2 for samples annealed for 30 seconds and from 1.99 x 10^{-4} Ωcm^2 to 2.23

x 10^{-4} Ωcm^2 for samples annealed for 60 seconds. The lowest measured specific contact resistivity value was 7.25 x 10^{-5} Ωcm^2, obtained in an as-deposited sample.

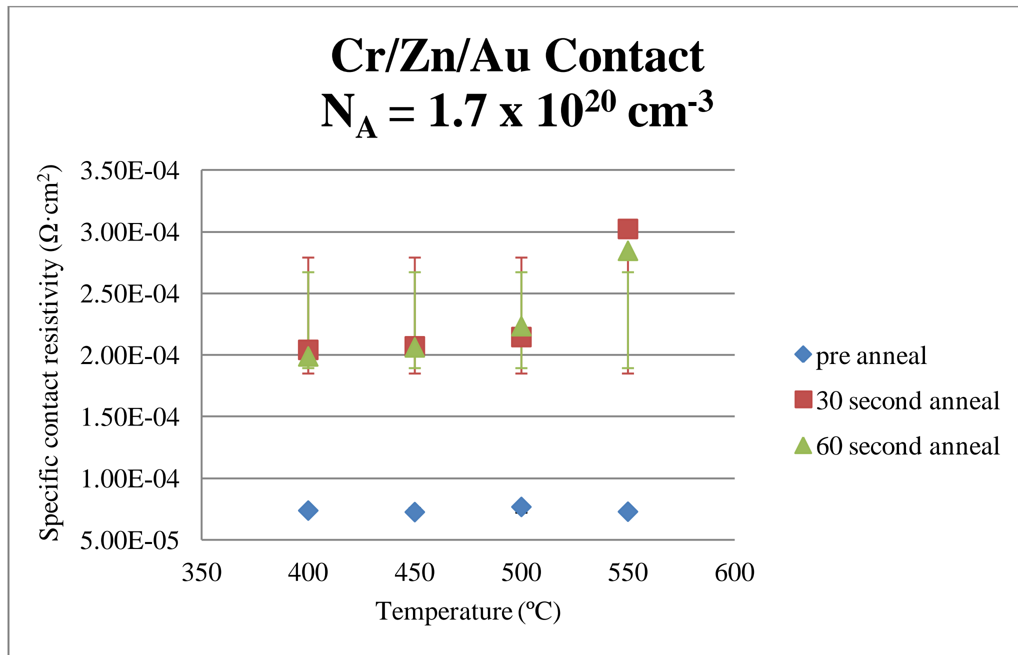

Figure 4.17 Specific contact resistivity versus annealing temperature for p-GaAs (N_A = 1.7 x 10^{20} cm^{-3}) with thermally evaporated Cr/Zn/Au contacts

Comparisons of the three metallization schemes are shown in Figure 4.18, Figure 4.19, and Figure 4.20, for pre-anneal, short anneal, and long anneal, respectively. The Cr/Au contacts had the lower specific contact resistivities in the as-deposited samples. Measured resistivities of Cr/Au contacts increased by about three to four times from their pre-anneal values after both short and long anneal times. In the samples annealed for a shorter time, it was found that Au/Zn/Au contacts displayed the lowest resistivities, and Cr/Au contacts displayed the highest. For the contacts annealed at longer times,

Au/Zn/Au contacts were always the least resistant, and Cr/Au contacts were always the most resistant.

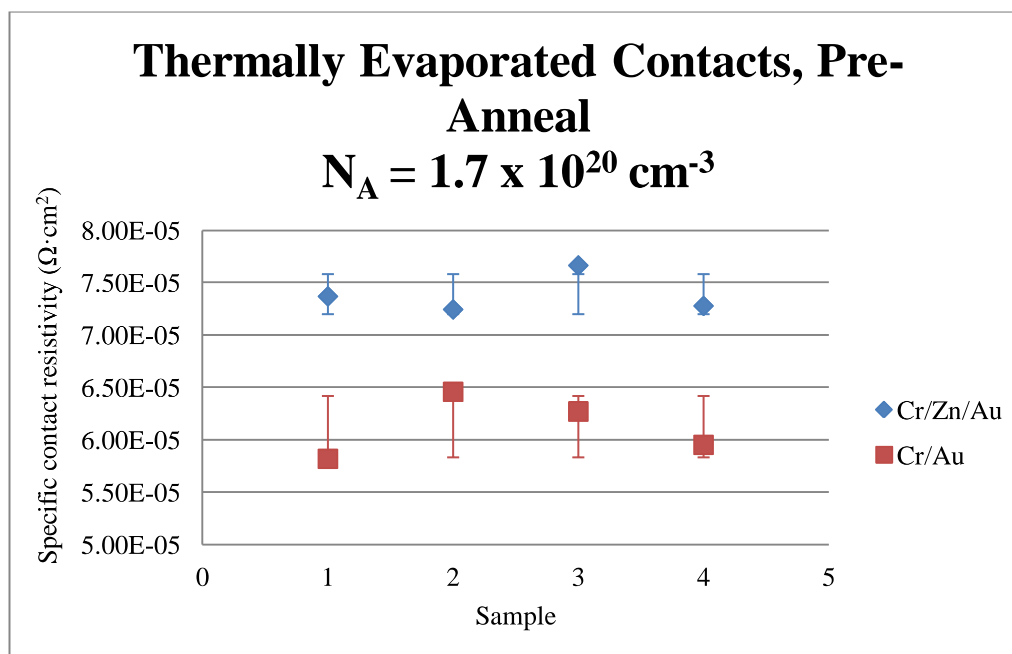

Figure 4.18 Specific contact resistivity for p-GaAs ($N_A = 1.7 \times 10^{20}$ cm^{-3}) with thermally evaporated Cr/Au and Cr/Zn/Au contacts, as-deposited

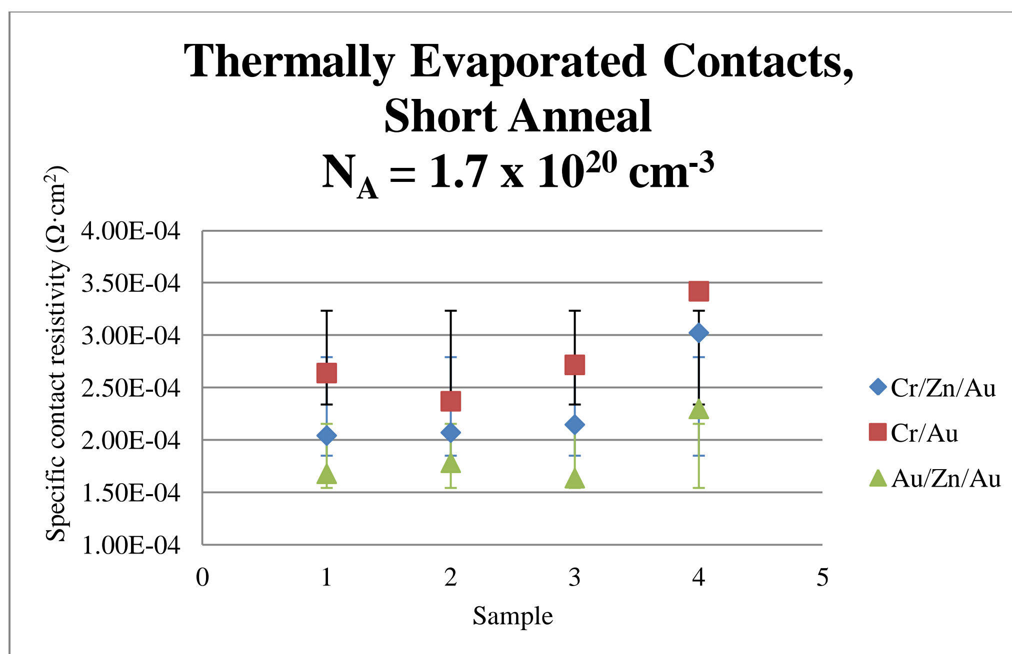

Figure 4.19 Specific contact resistivity for p-GaAs (N_A = 1.7 x 10^{20} cm^{-3}) with thermally evaporated Cr/Zn/Au, Cr/Au, and Au/Zn/Au contacts, after short anneal by RTA

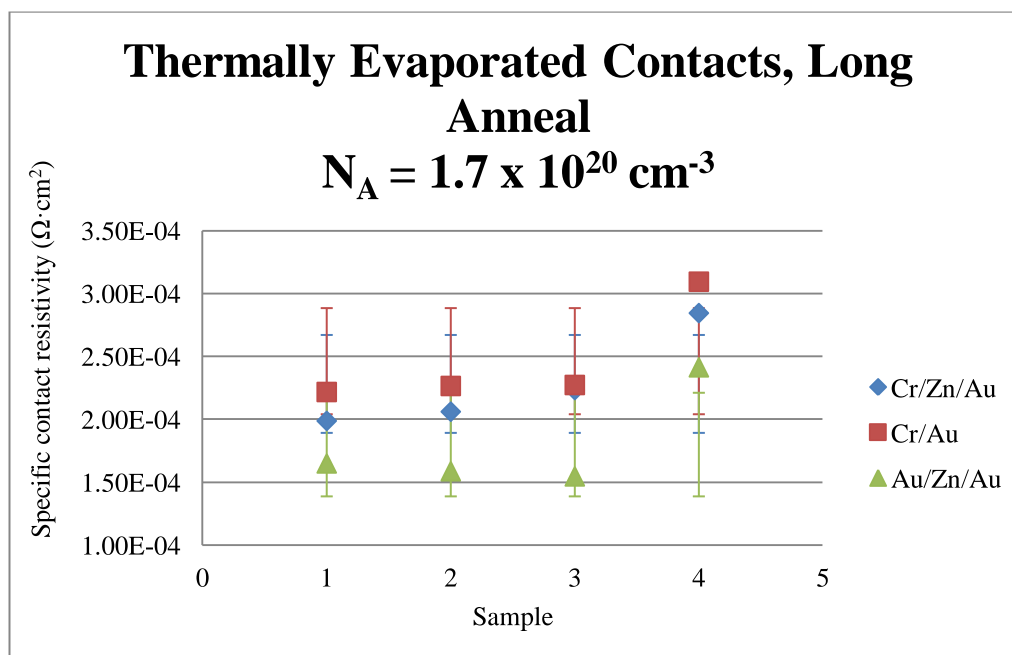

Figure 4.20 Specific contact resistivity for p-GaAs (N_A = 1.7 x 10^{20} cm^{-3}) with thermally evaporated Cr/Zn/Au, Cr/Au, and Au/Zn/Au contacts, after long anneal by RTA

4.1.2 Thermally Evaporated Nickel

Nickel deposits were thermally evaporated onto two wafers, of doping N_A = 5.3 x 10^{18} cm^{-3} and N_A = 3.0 x 10^{19} cm^{-3}. The samples were annealed from 300ºC to 550ºC (in 50ºC increments) for 60 and 100 seconds (N_A = 5.3 x 10^{18} cm^{-3}) and 60 and 120 seconds (N_A = 3.0 x 10^{19} cm^{-3}). A comparison of contacts as-deposited on the two different wafers is displayed in Figure 4.21. As was expected, contacts to the wafer of the higher doping level exhibited lower specific contact resistivities (on the order of 10^{-4} Ωcm^2, compared to 10^{-3} Ωcm^2).

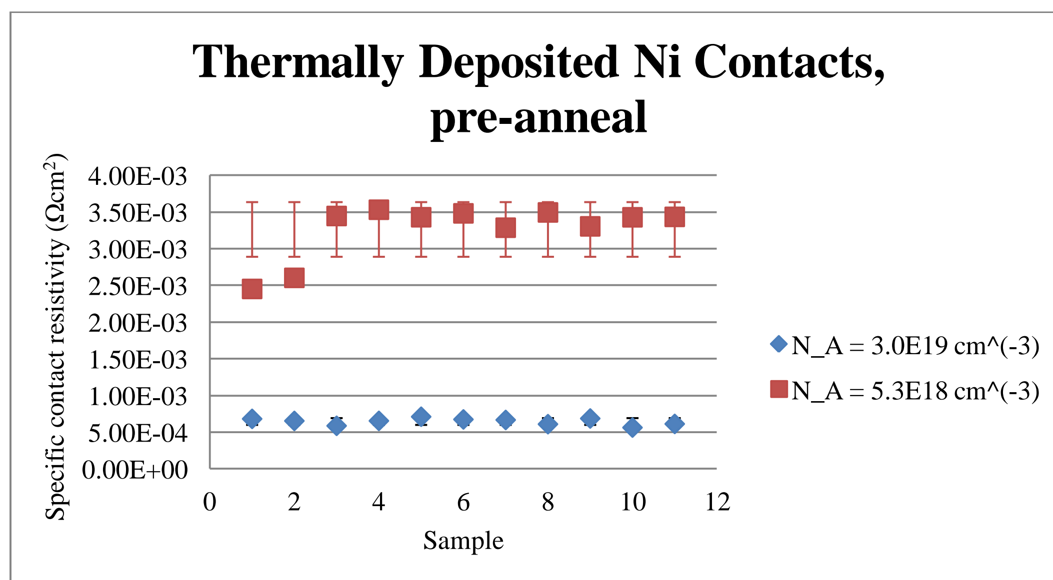

Figure 4.21 Specific contact resistivities of thermally deposited Ni contacts to p-GaAs

The specific contact resistivities of the Ni contacts to the wafer with N_A = 5.3 x 10^{18} cm^{-3} are plotted versus annealing temperature in Figure 4.22. The "pre-anneal" values plotted are the average of the contact resistivity values measured pre-anneal of those

samples annealed (for short and long times) at the corresponding temperatures. The results plotted at 300°C are outliers, based on standard deviation error bars, and will not be considered in the discussion. All contact resistivity values measured were on the order of 10^{-3} Ωcm^2. The as-deposited contacts were all more highly resistant than those after annealing. Specific contact resistivity values measured after annealing at 60 seconds and 100 seconds were very similar, with the lowest resistivities being measured after annealing at 500ºC (1.69 x 10^{-3} Ωcm^2 and 1.85 x 10^{-3} Ωcm^2, respectively).

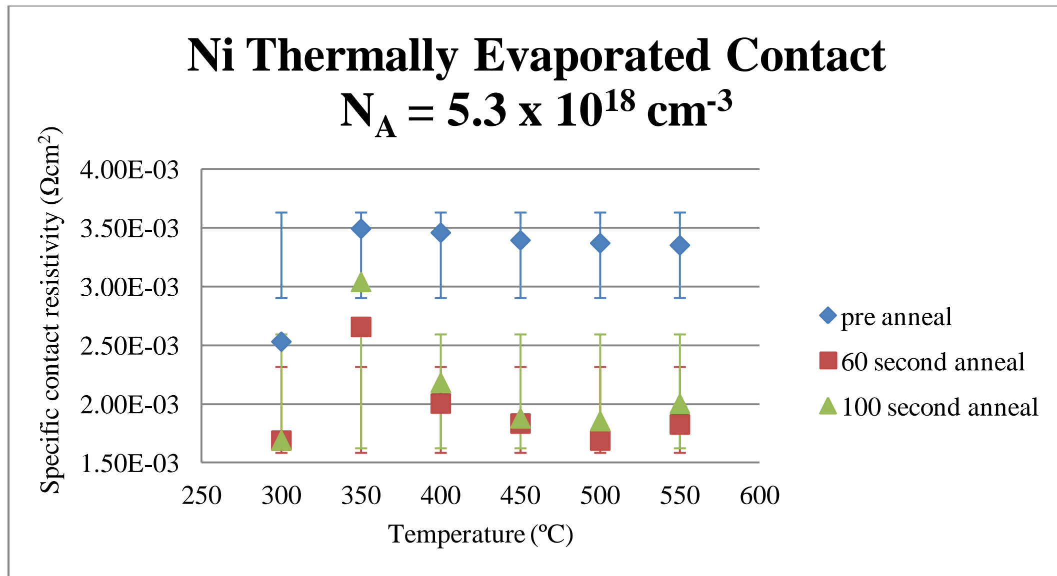

Figure 4.22 Specific contact resistivities of contacts to p-GaAs (N_A = 5.3 x 10^{18} cm^{-3}) with thermally evaporated nickel contacts after annealing for short and long times

The specific contact resistivities of the Ni contacts to the wafer with N_A = 3.0 x 10^{19} cm^{-3} are plotted versus annealing temperature in Figure 4.23. The "pre-anneal" values plotted are the average of the contact resistivity values measured pre-anneal of those samples annealed (for short and long times) at the corresponding temperatures. Most specific contact resistivity values measured were on the order of 10^{-4} Ωcm^2. After

annealing at 300ºC and 350ºC for both short and long times, contact resistivities decreased from those measured on as-deposited contacts. The resistivity continued to decrease from those of the as-deposited contacts after 60 seconds of annealing at 400ºC and 450ºC. Specific contact resistivities increased from those measured on the as-deposited contacts after short and long time annealing at 500ºC and 550ºC. The lowest measured resistivity was 4.58 x 10^{-4} Ωcm^2, obtained after annealing at 350ºC for 60 seconds.

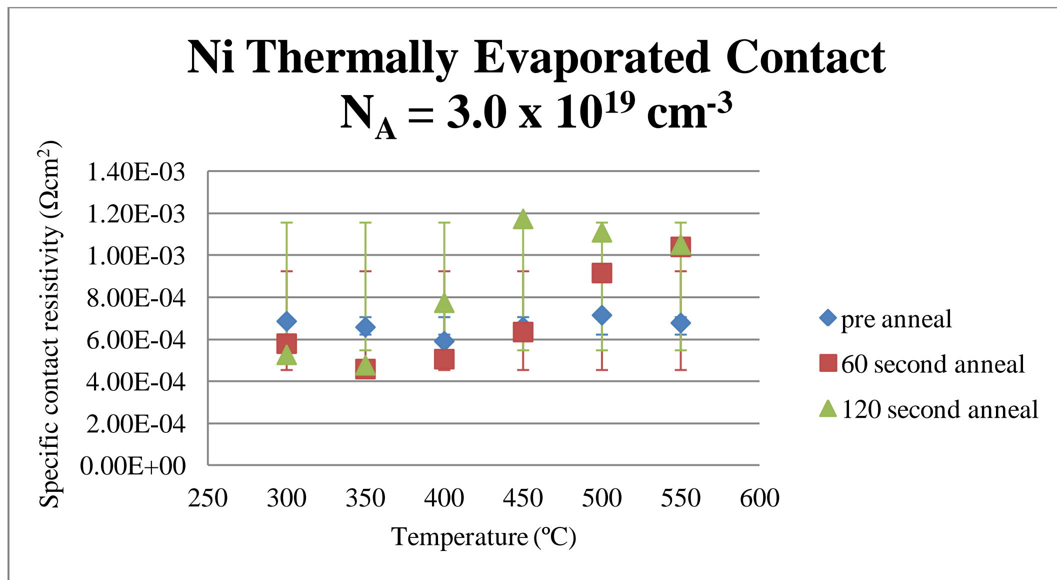

Figure 4.23 Specific contact resistivities of contacts to p-GaAs (N_A = 3.0 x 10^{19} cm^{-3}) with thermally evaporated nickel contacts after annealing for short and long times

4.1.3 Electrolytically Deposited Samples

4.1.3.1 $N_A = 5.3 \times 10^{18}$ cm^{-3}

A comparison of specific contact resistivities measured on contacts deposited at both 2.5 mA/cm^2 and 5 mA/cm^2 with a target thickness of 2500 Å is displayed in Figure 4.24. Almost all measured values of contacts deposited at 5 mA/cm^2 are lower than those of contacts deposited at 2.5 mA/cm^2. All specific contact resistivities are on the order of 10^{-3} Ωcm^2. Resistivity values obtained for samples 1 and 3 deposited at 2.5 mA/cm^2 appear to be outliers, based on standard deviation error bars, and will not be considered in the discussion of the results. The minimum specific contact resistivity measured on samples deposited at 2.5 mA/cm^2 was 3.02×10^{-3} Ωcm^2; and that on samples deposited at 5 mA/cm^2 was 2.76×10^{-3} Ωcm^2.

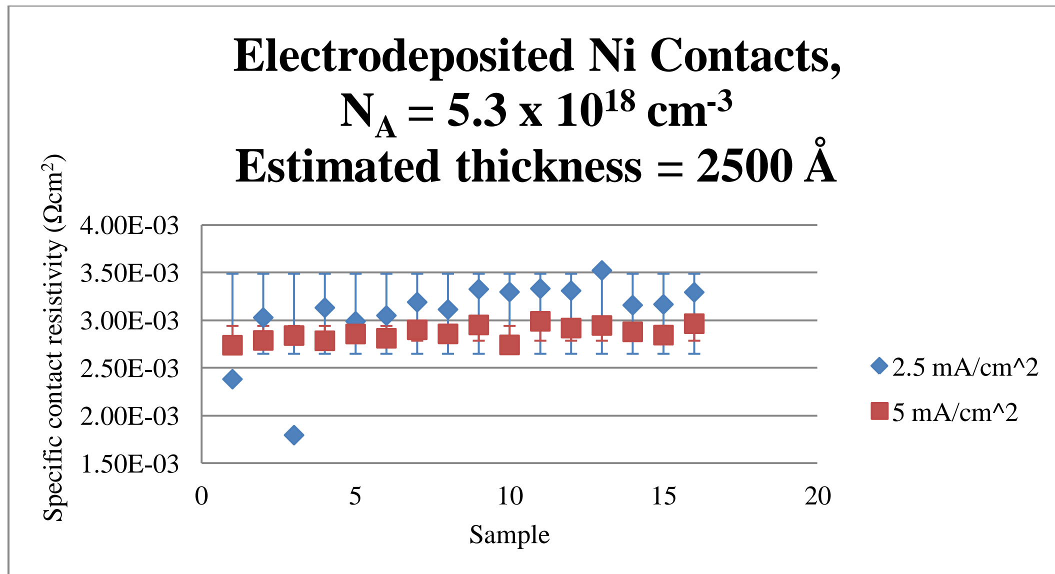

Figure 4.24 Specific contact resistivities of contacts to p-GaAs ($N_A = 5.3 \times 10^{18}$ cm^{-3}) with nickel contacts electrolytically deposited with a target thickness of 2500 Å

A comparison of specific contact resistivities measured on contacts deposited at both 2.5 mA/cm^2 and 5 mA/cm^2 with a target thickness of 5000 Å is displayed in Figure 4.25. Almost all measured values of contacts deposited at 5 mA/cm^2 are lower than those of contacts deposited at 2.5 mA/cm^2. All specific contact resistivities are on the order of 10^{-3} Ωcm^2. Resistivity values obtained for sample 10 deposited at 2.5 mA/cm^2 and for samples 1, 2, and 6 deposited at 5 mA/cm2 appear to be outliers, based on standard deviation error bars, and will not be considered in the discussion of the results. The minimum specific contact resistivity measured on samples deposited at 2.5 mA/cm^2 was 3.01 x 10^{-3} Ωcm^2; and that on samples deposited at 5 mA/cm^2 was 2.77 x 10^{-3} Ωcm^2.

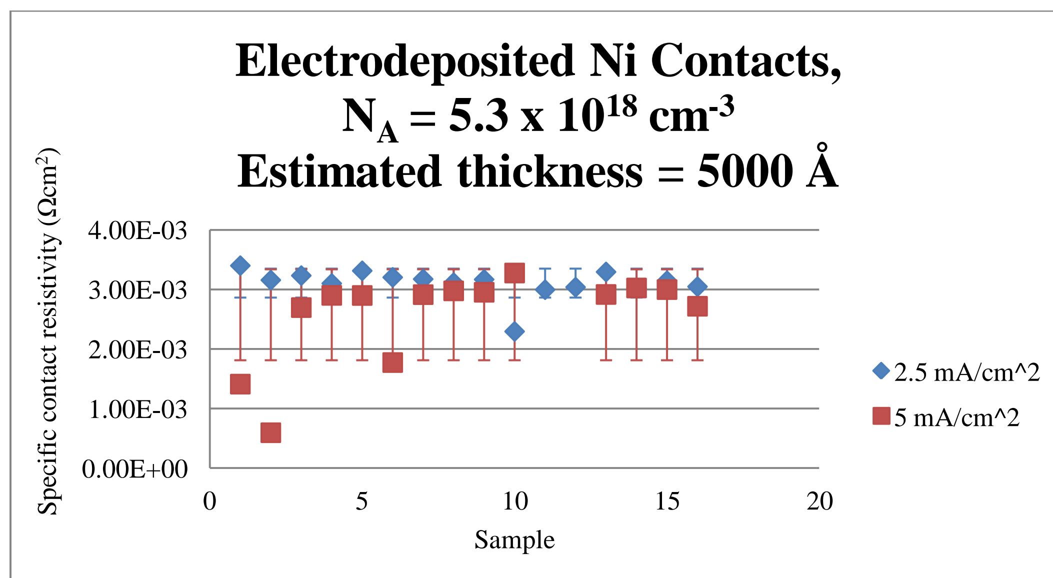

Figure 4.25 Specific contact resistivities of contacts to p-GaAs (N_A = 5.3 x 10^{18} cm^{-3}) with nickel contacts electrolytically deposited with a target thickness of 5000 Å

A comparison of specific contact resistivities measured on contacts deposited with target thickness of both 2500 Å and 5000 Å at a current density of 2.5 mA/cm^2 is

displayed in Figure 4.26. There is no clear difference in contact resistivities obtained for samples of different thicknesses. Resistivity values obtained for sample 10 (target thickness 5000 Å) and for samples 1 and 3 (target thickness 2500 Å) appear to be outliers, based on standard deviation error bars, and will not be considered in the discussion of the results.

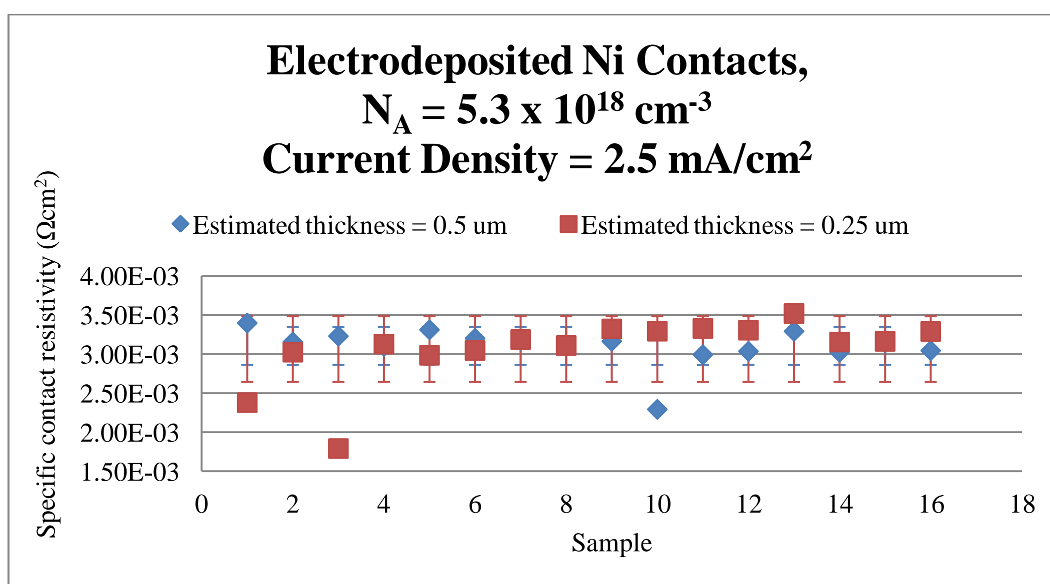

Figure 4.26 Specific contact resistivities of contacts to p-GaAs ($N_A = 5.3 \times 10^{18}$ cm^{-3}) with nickel contacts electrolytically deposited at a current density of 2.5 mA/cm^2

A comparison of specific contact resistivities measured on contacts deposited with target thickness of both 2500 Å and 5000 Å at a current density of 5 mA/cm^2 is displayed in Figure 4.27. There is no clear difference in contact resistivities obtained for samples of different thicknesses. Resistivity values obtained for samples 1, 2, and 6 (target thickness 5000 Å) appear to be outliers, based on standard deviation error bars, and will not be considered in the discussion of the results.

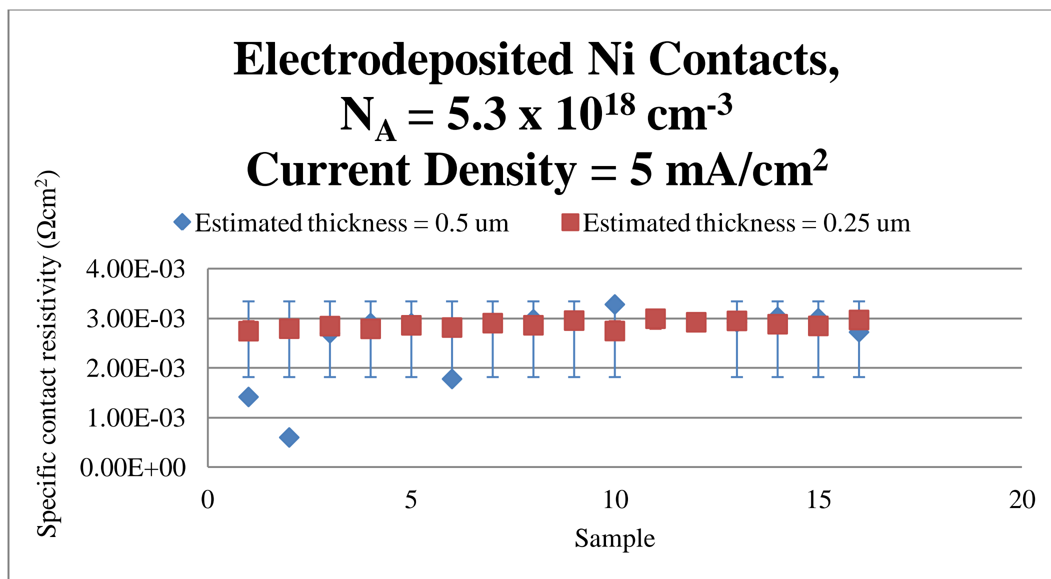

Figure 4.27 Specific contact resistivities of contacts to p-GaAs (N_A = 5.3 x 10^{18} cm^{-3}) with nickel contacts electrolytically deposited at a current density of 5 mA/cm^2

Some samples deposited at 5 mA/cm^2 to a target thickness of 2500 Å were annealed and measured for specific contact resistivity. The results are displayed in Figure 4.28. The “pre-anneal” values plotted are the average of the specific contact resistivity values measured pre-anneal of those samples annealed at the corresponding temperatures. The specific contact resistivity is seen to decrease after annealing, with the lowest value (9.91 x 10^{-4} Ωcm^2) being measured after 60 seconds of annealing at 450°C.

Samples deposited at 2.5 mA/cm^2 to a target thickness of 5000 Å were annealed and measured for specific contact resistivity. The results are displayed in Figure 4.29. The “pre-anneal” values plotted are the average of the contact resistivity values measured pre-anneal of those samples annealed at the corresponding temperatures. The specific contact resistivity is seen to decrease after annealing, with the lowest value (1.18 x 10^{-3} Ωcm^2) being measured after 60 seconds of annealing at 450°C.

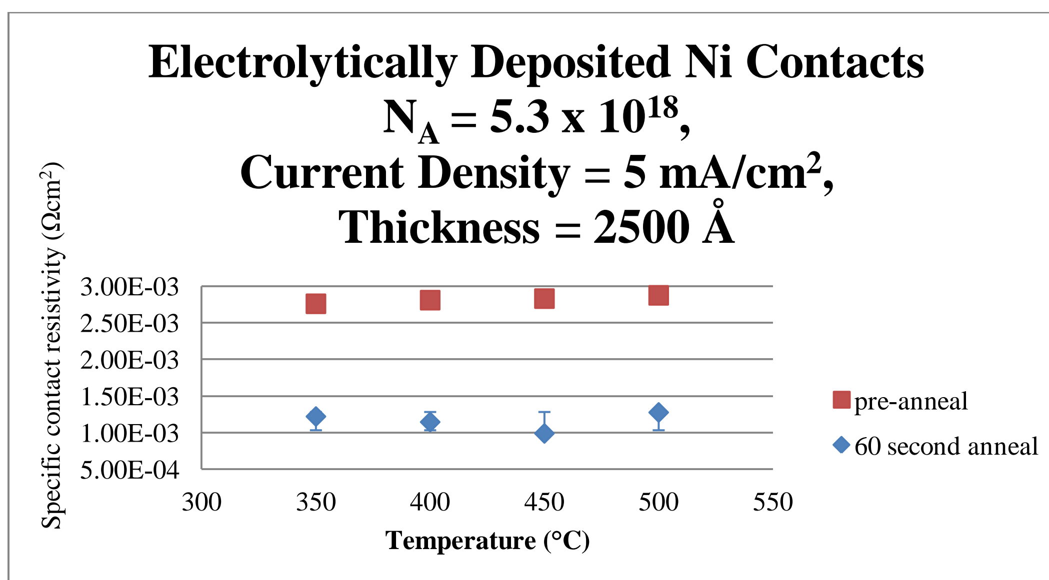

Figure 4.28 Specific contact resistivities of contacts to p-GaAs ($N_A = 5.3 \times 10^{18}$ cm^{-3}) with nickel contacts electrolytically deposited at a current density of 5 mA/cm^2 and subsequently annealed by RTA

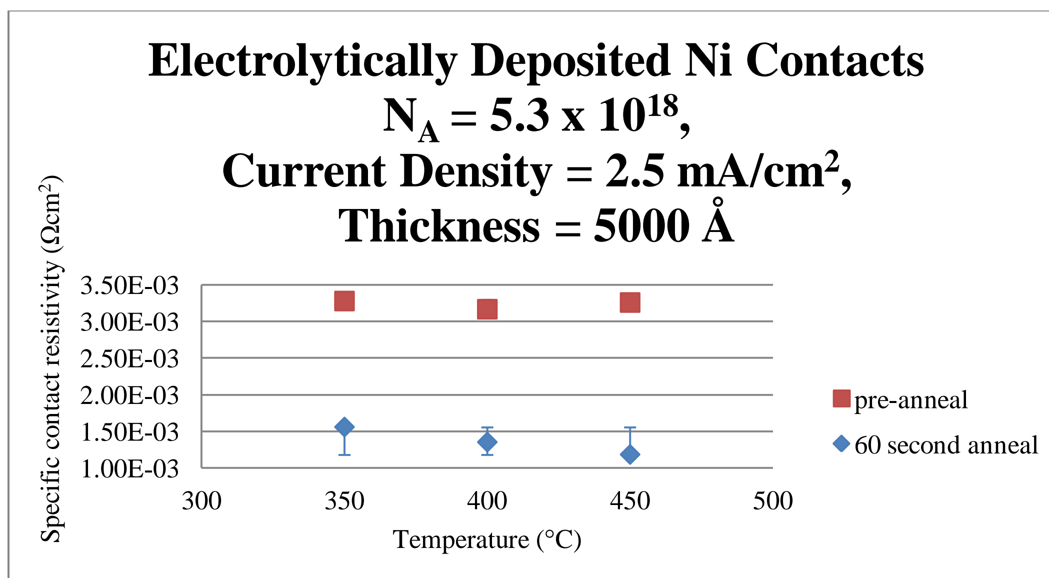

Figure 4.29 Specific contact resistivities of contacts to p-GaAs ($N_A = 5.3 \times 10^{18}$ cm^{-3}) with nickel contacts electrolytically deposited at a current density of 2.5 mA/cm2 and subsequently annealed by RTA

4.1.3.2 $N_A = 3.0 \times 10^{19}$ cm^{-3}

A comparison of specific contact resistivities measured on contacts deposited at both 2.5 mA/cm^2 and 5 mA/cm^2 with a target thickness of 2500 Å is displayed in Figure 4.30. Almost all measured values of contacts deposited at 5 mA/cm^2 are lower than those of contacts deposited at 2.5 mA/cm^2. All specific contact resistivities are on the order of 10^{-4} Ωcm^2. Resistivity values obtained for samples 14 to 16 deposited at 2.5 mA/cm^2 and sample 1 deposited at 5 mA/cm^2 appear to be outliers, based on standard deviation error bars, and will not be considered in the discussion of the results. The minimum specific contact resistivity measured on samples deposited at 2.5 mA/cm^2 was 2.32×10^{-4} Ωcm^2; and that on samples deposited at 5 mA/cm^2 was 1.75×10^{-4} Ωcm^2.

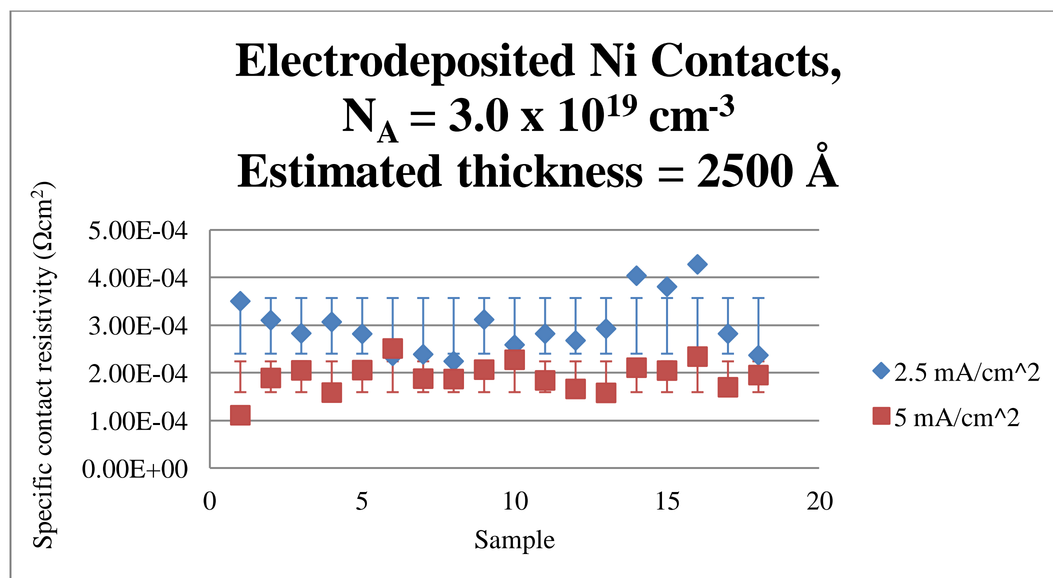

Figure 4.30 Specific contact resistivities of contacts to p-GaAs ($N_A = 3.0 \times 10^{19}$ cm^{-3}) with nickel contacts electrolytically deposited with a target thickness of 2500 Å

A comparison of specific contact resistivities measured on contacts deposited at both 2.5 mA/cm^2 and 5 mA/cm^2 with a target thickness of 5000 Å is displayed in Figure

4.31. Almost all measured values of contacts deposited at 5 mA/cm^2 are lower than those of contacts deposited at 2.5 mA/cm^2. All specific contact resistivities are on the order of 10^{-4} Ωcm^2. Resistivity values obtained for samples 9, 10, 12, and 18 deposited at 2.5 mA/cm^2 and samples 3, 8, and 10 deposited at 5 mA/cm^2 appear to be outliers, based on standard deviation error bars, and will not be considered in the discussion of the results. The minimum specific contact resistivity measured on samples deposited at 2.5 mA/cm^2 was 2.44 x 10^{-4} Ωcm^2; and that on samples deposited at 5 mA/cm^2 was 1.90 x 10^{-4} Ωcm^2.

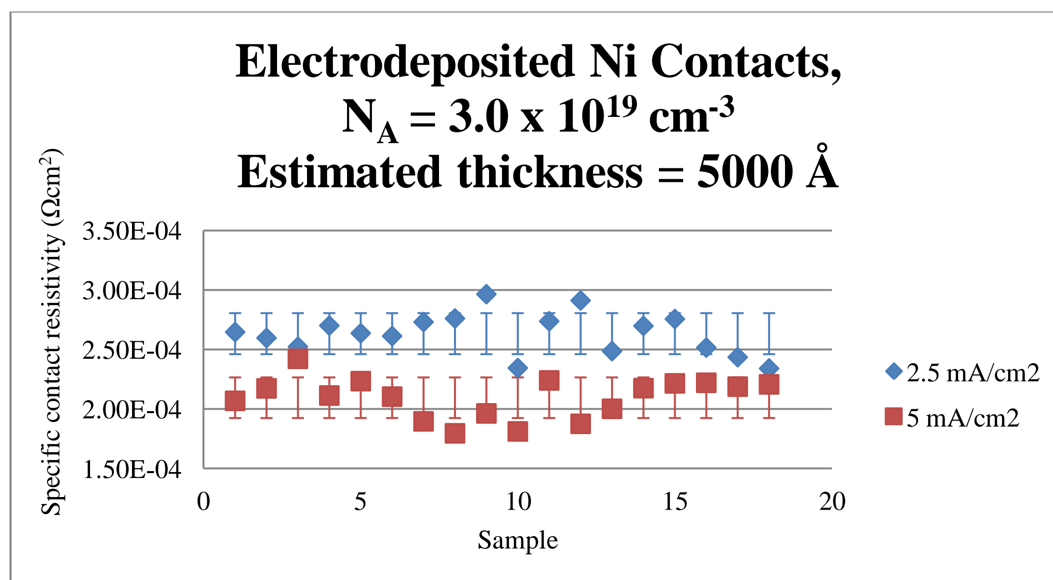

Figure 4.31 Specific contact resistivities of contacts to p-GaAs (N_A = 3.0 x 10^{19} cm^{-3}) with nickel contacts electrolytically deposited with a target thickness of 5000 Å

A comparison of specific contact resistivities measured on contacts deposited with target thickness of both 2500 Å and 5000 Å at a current density of 2.5 mA/cm^2 is displayed in Figure 4.32. There is no clear difference in contact resistivities obtained for samples of different thicknesses, except that there is a smaller standard deviation in the

results of contacts with target thickness of 5000 Å. Resistivity values obtained for samples 14 to 16 (target thickness 2500 Å) appear to be outliers, based on standard deviation error bars, and will not be considered in the discussion of the results.

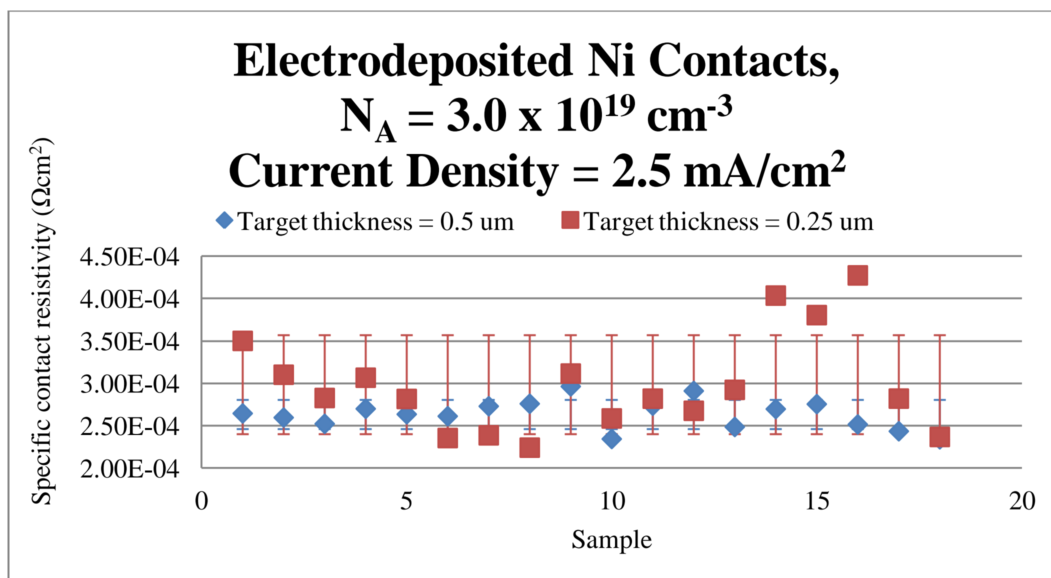

Figure 4.32 Specific contact resistivities of contacts to p-GaAs ($N_A = 3.0 \times 10^{19}$ cm^{-3}) with nickel contacts electrolytically deposited at a current density of 2.5 mA/cm^2

A comparison of specific contact resistivities measured on contacts deposited with target thickness of both 2500 Å and 5000 Å at a current density of 5 mA/cm^2 is displayed in Figure 4.33. There is no clear difference in contact resistivities obtained for samples of different thicknesses, except that there is a smaller standard deviation in the results of contacts with target thickness of 5000 Å. Resistivity values obtained for samples 1, 4, and 6 (target thickness 2500 Å) appear to be outliers, based on standard deviation error bars, and will not be considered in the discussion of the results.

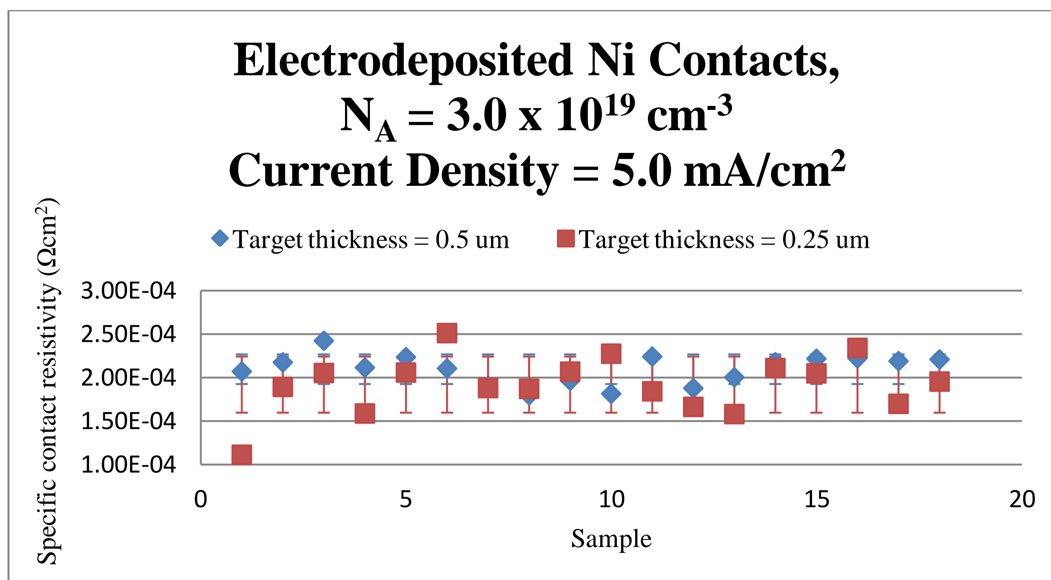

Figure 4.33 Specific contact resistivities of contacts to p-GaAs ($N_A = 3.0 \times 10^{19}$ cm^{-3}) with nickel contacts electrolytically deposited at a current density of 5 mA/cm2

Samples deposited at 2.5 mA/cm^2 to a target thickness of 2500 Å were annealed and measured for specific contact resistivity. The results are displayed in Figure 4.34. The "pre-anneal" values plotted are the average of the contact resistivity values measured pre-anneal of those samples annealed at the corresponding temperatures. The specific contact resistivity is seen to increase after annealing at both short and long times.

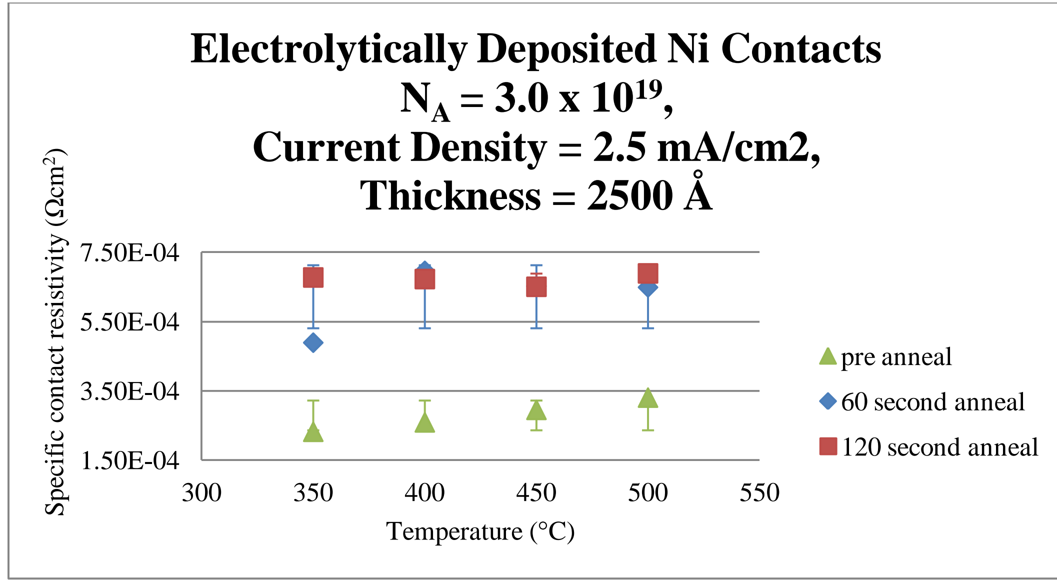

Figure 4.34 Specific contact resistivities of contacts to p-GaAs ($N_A = 3.0 \times 10^{19}$ cm^{-3}) with nickel contacts electrolytically deposited at a current density of 2.5 mA/cm2 and subsequently annealed by RTA

4.2 Surface Topography

4.2.1 Thermally Evaporated Samples (Non-Nickel), by Doping Level

4.2.1.1 $N_A = 4.0 \times 10^{16}$ cm^{-3}

Figure 4.35 shows a micrograph of Au/Zn/Au contacts deposited on the wafer of the lowest doping level and annealed for 60 seconds at 400ºC. The image was taken under a 5kV accelerating voltage at a magnification of 10,000X. The image reveals a polycrystalline structure with a grain size of approximately 125 nm. Figure 4.36 shows a Au/Zn/Au contact to the same material, annealed for 60 seconds at 450ºC. In this case, there is a polycrystalline structure is characterized by 90 nm grains; the structure is interrupted randomly by flower-like formations about 1 µm in diameter. All grain sizes reported here were estimated using image processing software ImageJ.

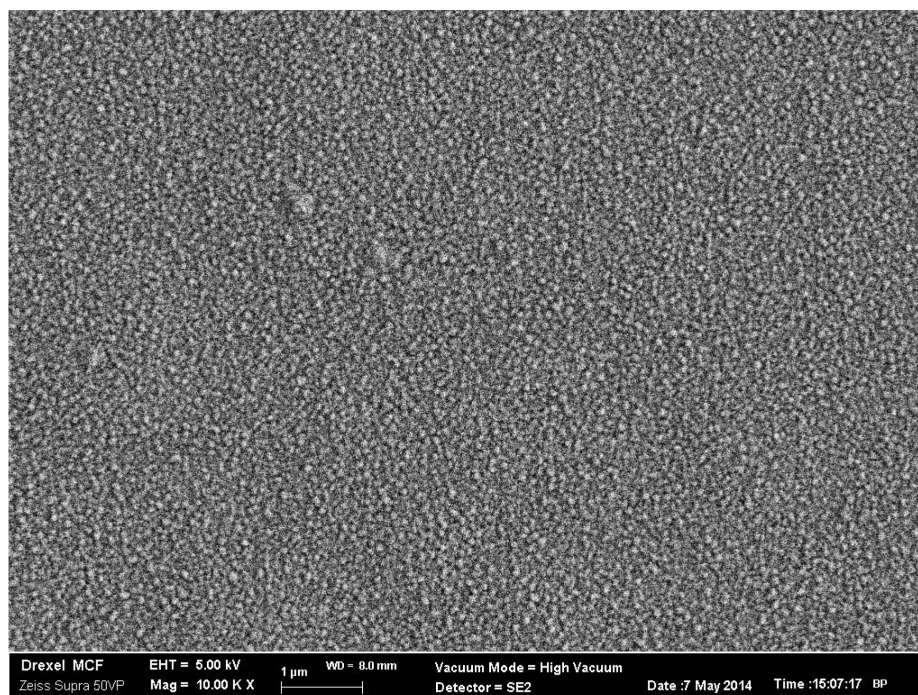

Figure 4.35 SEM micrograph of Au/Zn/Au contact to p-GaAs ($N_A = 4.0 \times 10^{16}$ cm^{-3}) after 60 seconds of RTA at 400ºC

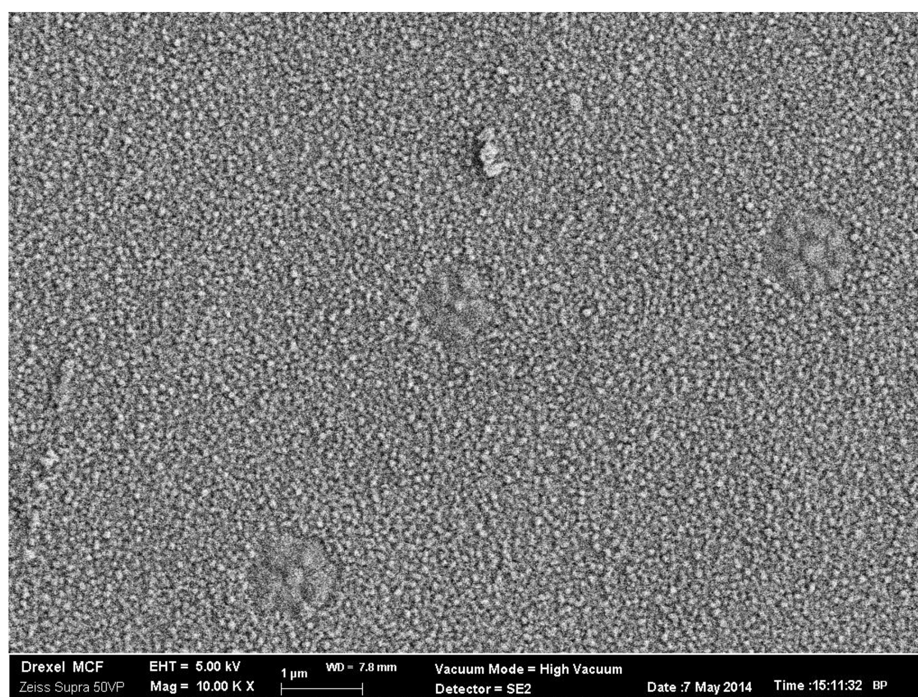

Figure 4.36 SEM micrograph of Au/Zn/Au contact to p-GaAs ($N_A = 4.0 \times 10^{16}$ cm^{-3}) after 60 seconds of RTA at 450ºC

Figure 4.37 shows a micrograph of Cr/Zn/Au contacts vacuum deposited on this wafer and annealed for 30 seconds at 500ºC. The image was taken under a 5kV accelerating voltage at a magnification of 10,000X. The image reveals a polycrystalline structure with grains approximately 120 nm in size. Figure 4.38 shows a Cr/Zn/Au contact to the same material, annealed for 30 seconds at 550ºC. In this case, the grain size is again 120 nm, but the surface is full of voids, indicating a partial decohesion of the metallization. The voids are better viewed at a magnification of 1,000X, pictured in Figure 4.39.

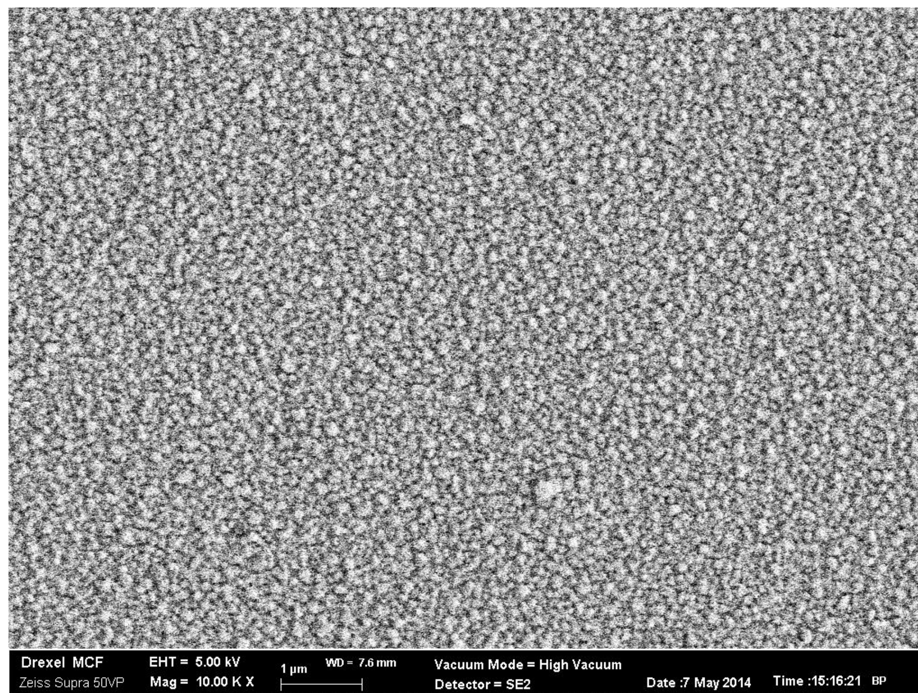

Figure 4.37 SEM micrograph of Cr/Zn/Au contact to p-GaAs (N_A = 4.0 x 10^{16} cm^{-3}) after 30 seconds of RTA at 500ºC

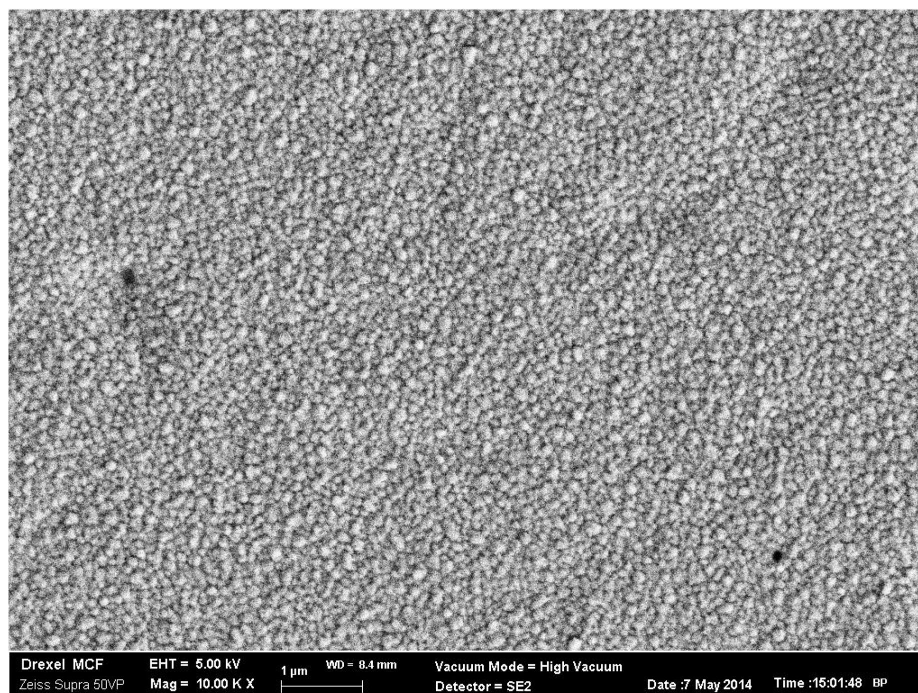

Figure 4.38 SEM micrograph of Cr/Zn/Au contact to p-GaAs ($N_A = 4.0 \times 10^{16}$ cm^{-3}) after 30 seconds of RTA at 550ºC (10,000X)

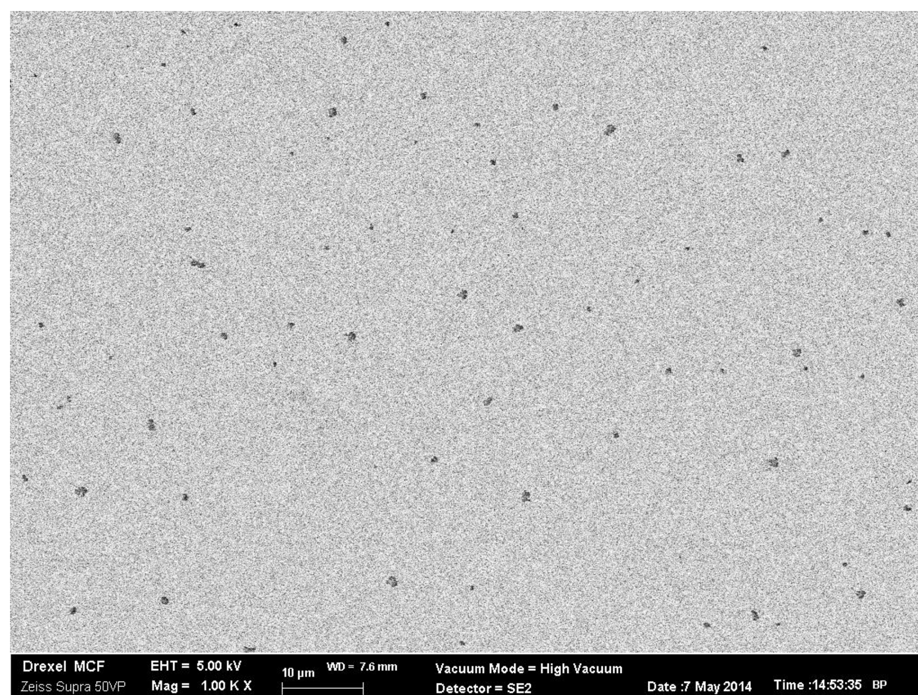

Figure 4.39 SEM micrograph of Cr/Zn/Au contact to p-GaAs ($N_A = 4.0 \times 10^{16}$ cm^{-3}) after 30 seconds of RTA at 550ºC (1,000X)

A contact formed to this material of the Cr/Au metallization is pictured in Figure 4.40. These contacts did not achieve ohmic behavior. Pictured is a contact annealed for 60 seconds at 450ºC. The surface is amorphous, characterized by randomly distributed pits and protrusions.

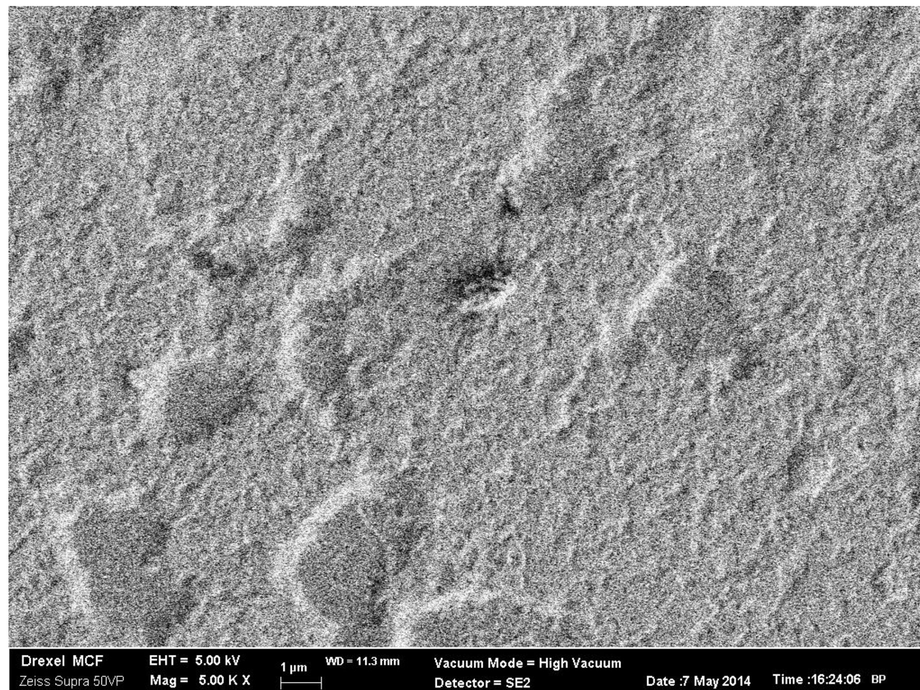

Figure 4.40 SEM micrograph of Cr/Au contact to p-GaAs ($N_A = 4.0 \times 10^{16}$ cm^{-3}) after 60 seconds of RTA at 450ºC (5,000X)

4.2.1.2 $N_A = 1.0 \times 10^{19}$ cm^{-3}

Figure 4.41 shows a micrograph of Cr/Zn/Au contacts vacuum deposited on this wafer and annealed for 30 seconds at 500ºC. The image was taken under a 5kV accelerating voltage at a magnification of 5,000X. The image reveals a polycrystalline surface with an average grain size of 120 nm. The image indicates an apparent

decohesion of the metallization and an opening of holes through which the interface can be seen. Figure 4.42 shows a Cr/Zn/Au contact to the same material, annealed for 30 seconds at 550ºC. Once again, a polycrystalline structure with grain size of 120 nm is observed.

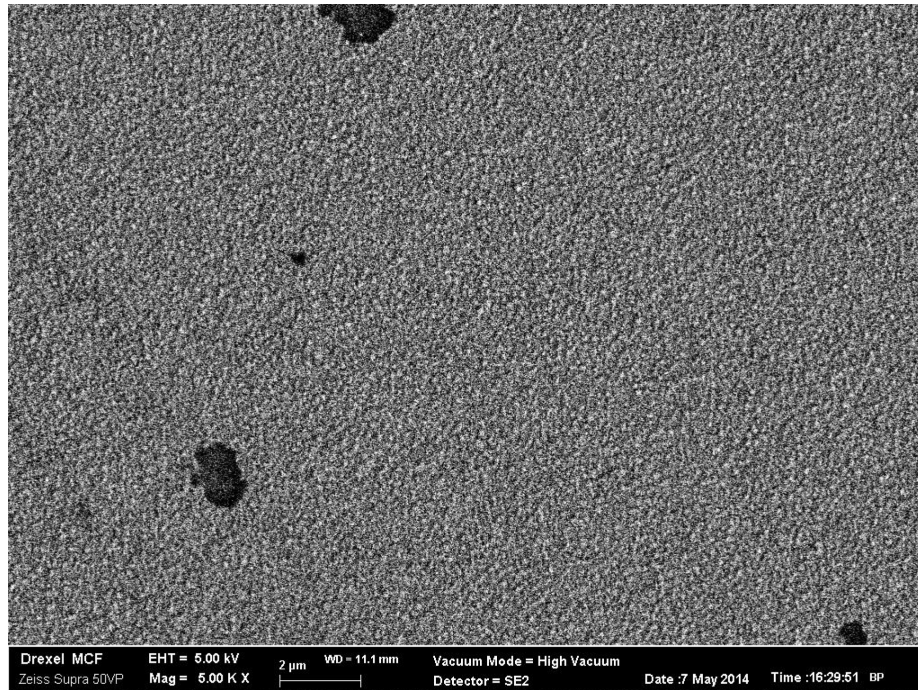

Figure 4.41 SEM micrograph of Cr/Zn/Au contact to p-GaAs (N_A = 1.0 x 10^{19} cm^{-3}) after 30 seconds of RTA at 500ºC (5,000X)

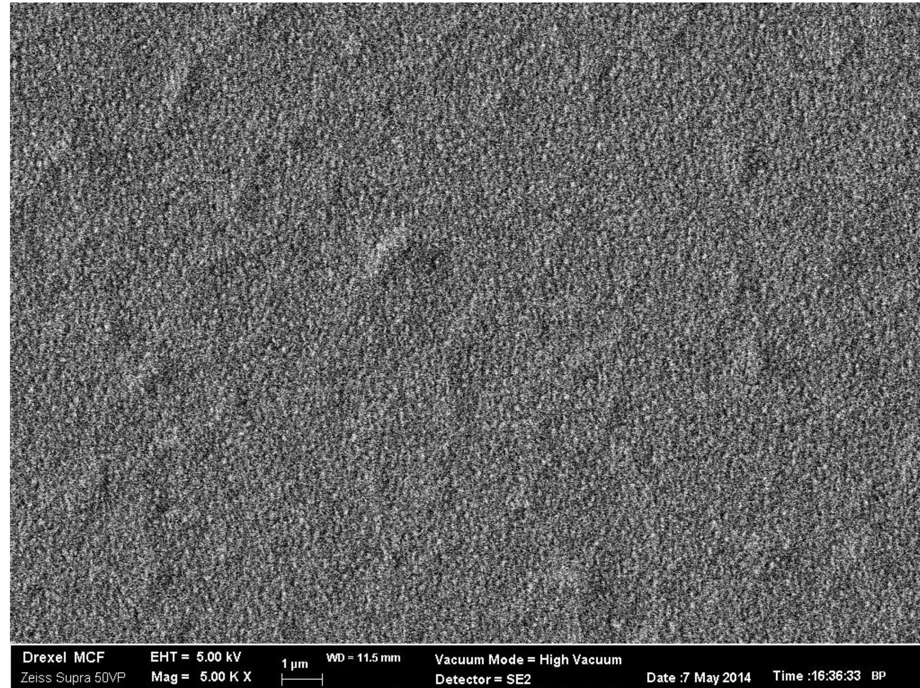

Figure 4.42 SEM micrograph of Cr/Zn/Au contact to p-GaAs ($N_A = 1.0 \times 10^{19}$ cm^{-3}) after 30 seconds of RTA at 550ºC (5,000X)

4.2.1.3 $N_A = 4.7 \times 10^{19}$ cm^{-3}

Figure 4.43 shows a micrograph of Au/Zn/Au contacts deposited on the wafer of the second highest doping level and annealed for 60 seconds at 450ºC. The image was taken under a 5kV accelerating voltage at a magnification of 10,000X. The image reveals a polycrystalline structure with a grain size of approximately 100 nm. Figure 4.44 shows a Au/Zn/Au contact to the same material, annealed for 60 seconds at 500ºC. In this case, there is a polycrystalline structure characterized by 90 nm grains.

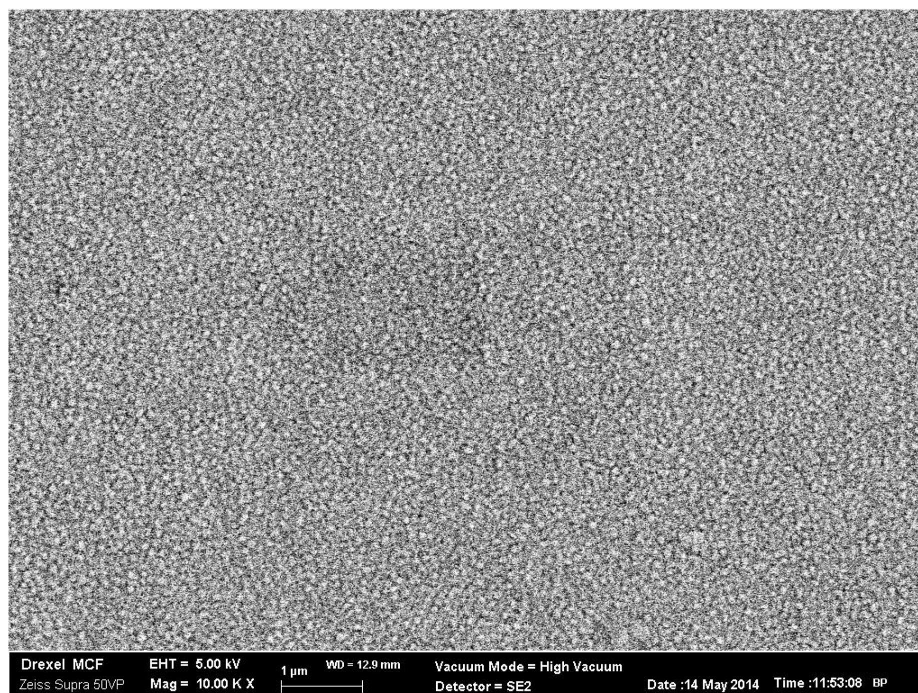

Figure 4.43 SEM micrograph of Au/Zn/Au contact to p-GaAs ($N_A = 4.7 \times 10^{19}$ cm^{-3}) after 60 seconds of RTA at 450ºC (10,000X)

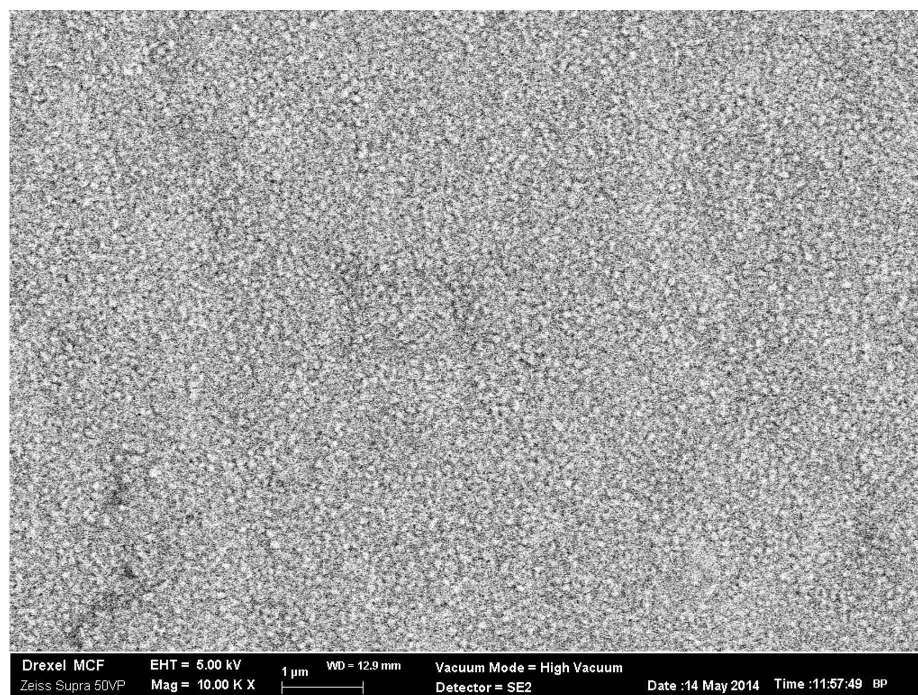

Figure 4.44 SEM micrograph of Au/Zn/Au contact to p-GaAs ($N_A = 4.7 \times 10^{19}$ cm^{-3}) after 60 seconds of RTA at 500ºC (10,000X)

Figure 4.45 shows a micrograph of Cr/Au contacts deposited on this wafer and annealed for 60 seconds at 400ºC. The image was taken under a 5kV accelerating voltage at a magnification of 10,000X. The image reveals a rough amorphous surface. Figure 4.46 shows a Cr/Au contact to the same material, annealed for 60 seconds at 450ºC. In this case, there is again an amorphous surface, but with voids throughout.

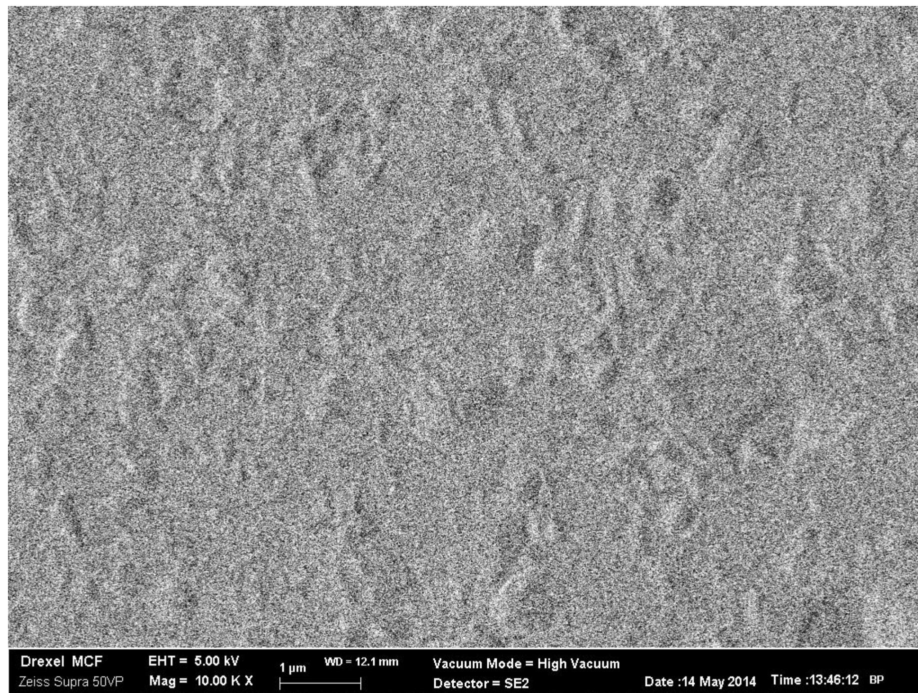

Figure 4.45 SEM micrograph of Cr/Au contact to p-GaAs ($N_A = 4.7 \times 10^{19}$ cm^{-3}) after 60 seconds of RTA at 400ºC (10,000X)

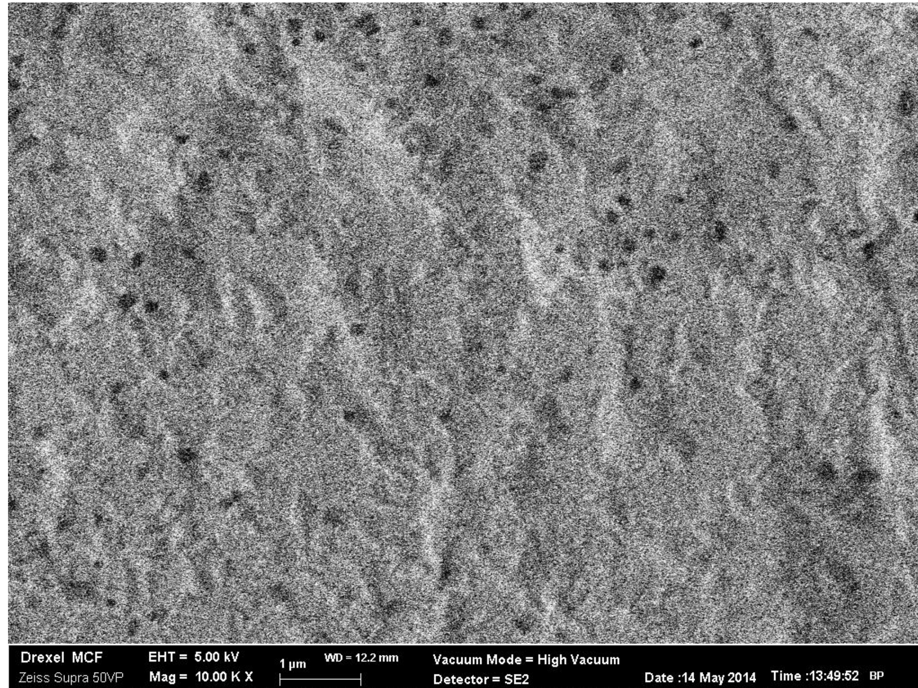

Figure 4.46 SEM micrograph of Cr/Au contact to p-GaAs (N_A = 4.7 x 10^{19} cm^{-3}) after 60 seconds of RTA at 450ºC (10,000X)

4.2.1.4 $N_A = 1.7 \times 10^{20}$ cm^{-3}

The substrate of the highest doping was characterized by process-induced surface roughness before metal deposition. Across the surface of the wafer appeared raised parallel lines. This feature can be seen in Figure 4.47, which shows an as-deposited Cr/Zn/Au contact at a magnification of 1,000X. This pre-existing roughness did not interfere with the successful metal deposition or ohmic contact formation to this wafer.

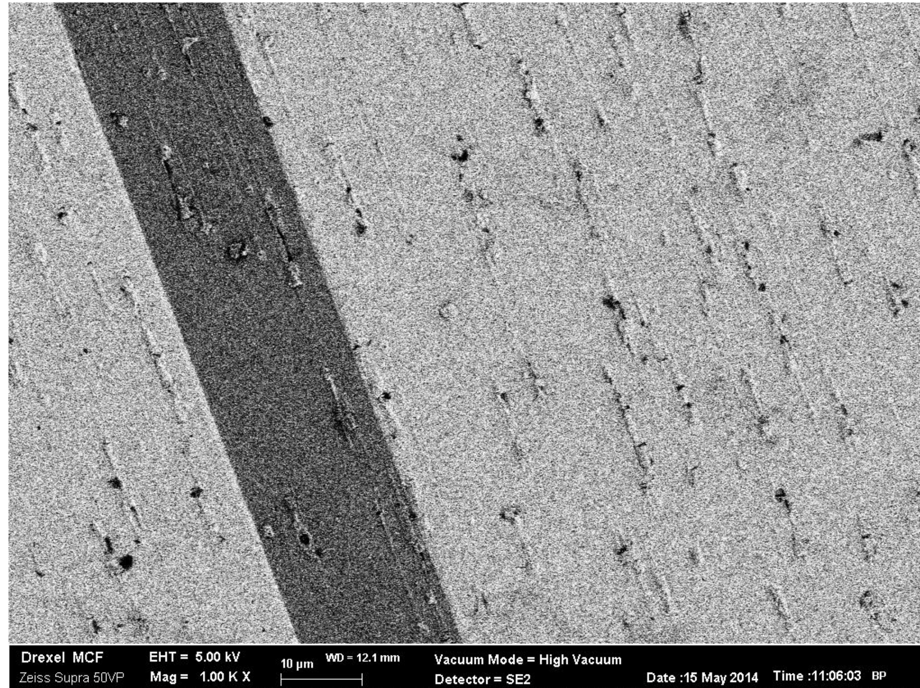

Figure 4.47 SEM micrograph of Cr/Zn/Au contact to p-GaAs ($N_A = 1.7 \times 10^{20}$ cm^{-3}), as deposited (1,000X)

Figure 4.48 shows a micrograph of Au/Zn/Au contacts deposited on this wafer and annealed for 60 seconds at 450ºC. The image was taken under a 5kV accelerating voltage at a magnification of 10,000X. The image reveals a polycrystalline structure with a grain size of approximately 90 nm. Figure 4.49 shows a Au/Zn/Au contact to the same material, annealed for 60 seconds at 500ºC. In this case, there is once again a polycrystalline structure characterized by 90 nm grains; overall, the surface appears smoother after annealing at 500°C.

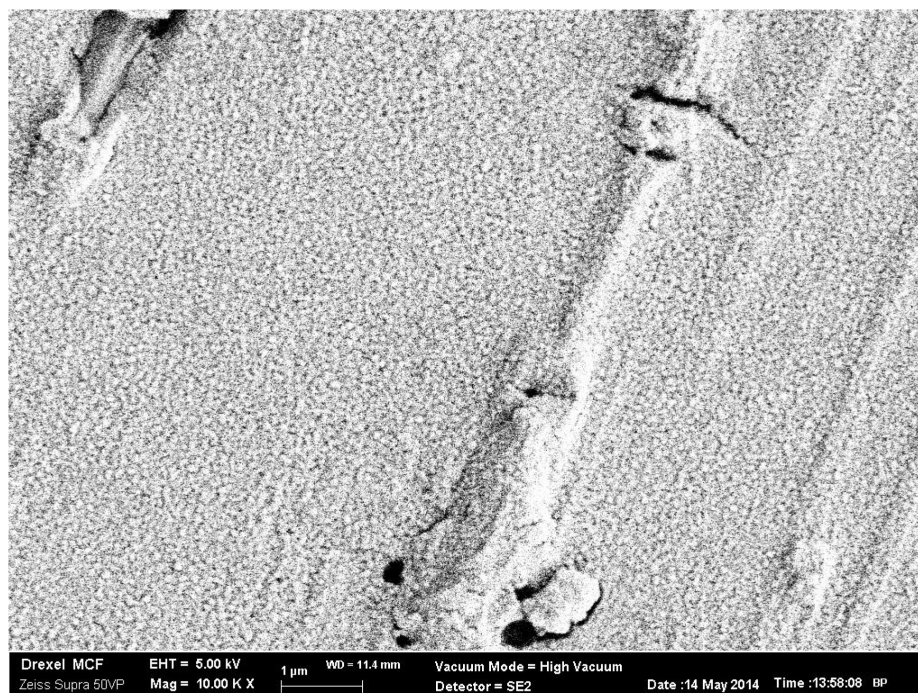

Figure 4.48 SEM micrograph of Au/Zn/Au contact to p-GaAs ($N_A = 1.7 \times 10^{20}$ cm^{-3}), after 60 seconds of RTA at 450°C (10,000X)

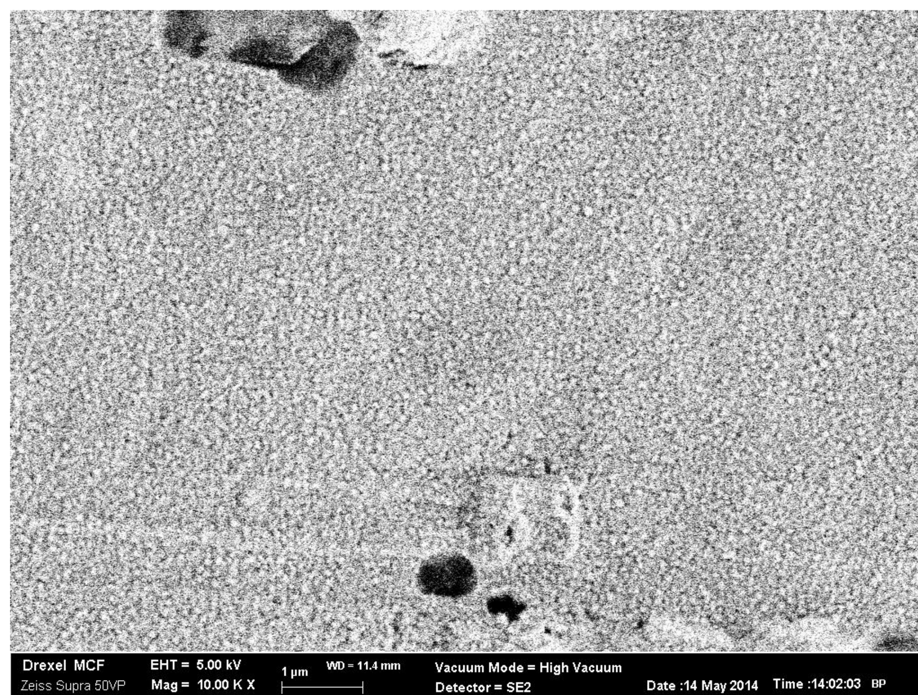

Figure 4.49 SEM micrograph of Au/Zn/Au contact to p-GaAs ($N_A = 1.7 \times 10^{20}$ cm^{-3}), after 60 seconds of RTA at 500°C (10,000X)

Figure 4.50 shows a micrograph of Cr/Zn/Au contacts vacuum deposited on this wafer and annealed for 30 seconds at 500ºC. The image was taken under a 5kV accelerating voltage at a magnification of 5,000X. The image reveals a polycrystalline surface with a grain size of approximately 140 nm. Figure 4.51 shows a Cr/Zn/Au contact to the same material, annealed for 30 seconds at 550ºC. Once again, a polycrystalline structure with grain size of 135 nm is observed. After annealing at 550°C, voids were formed around the already present roughness of the wafer due to decohesion of the metallization.

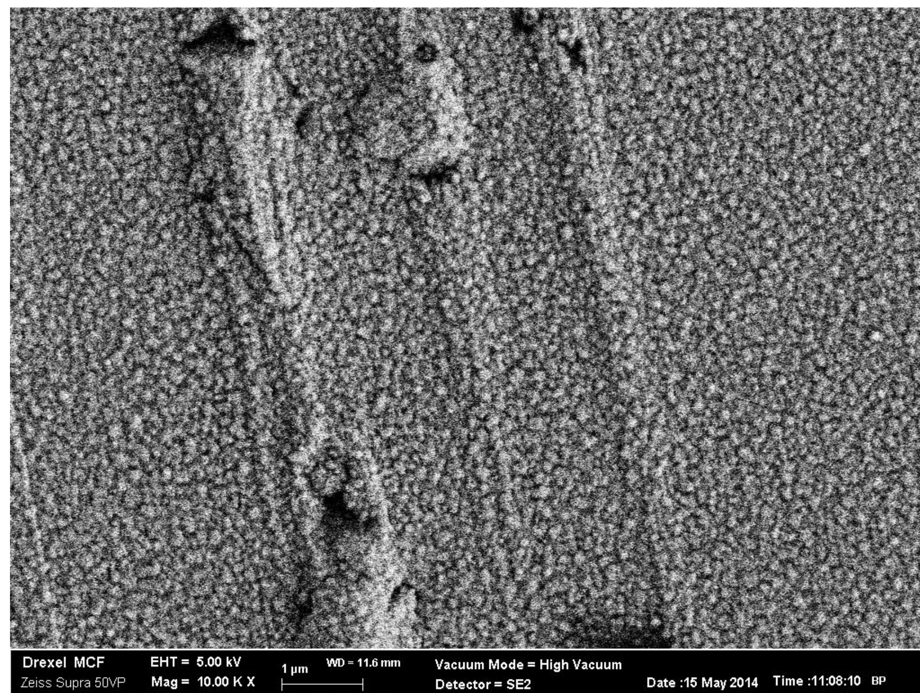

Figure 4.50 SEM micrograph of Cr/Zn/Au contact to p-GaAs ($N_A = 1.7 \times 10^{20}$ cm^{-3}), after 30 seconds of RTA at 500°C (10,000X)

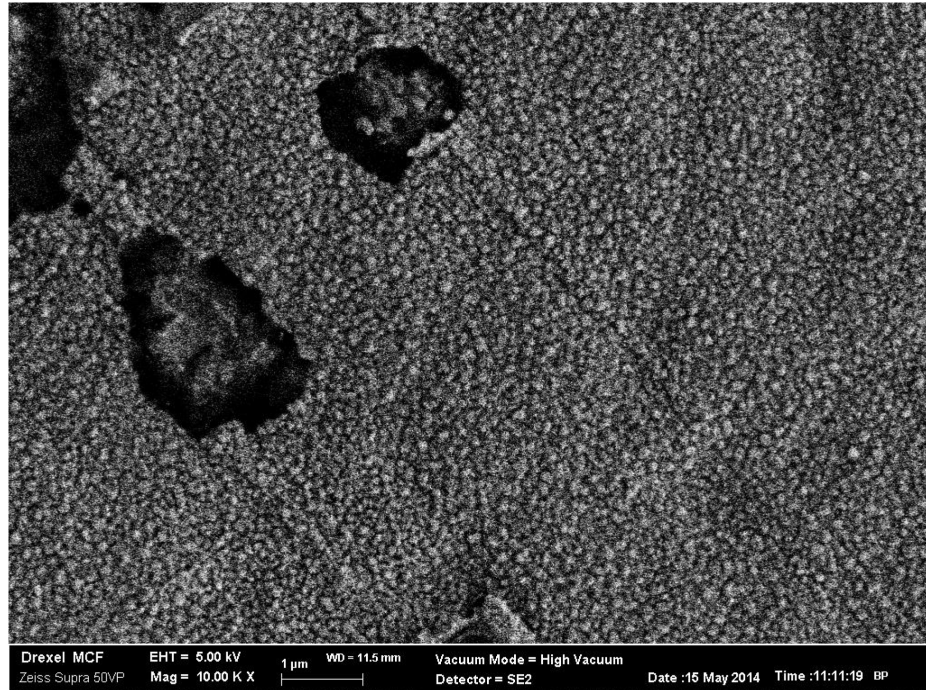

Figure 4.51 SEM micrograph of Cr/Zn/Au contact to p-GaAs ($N_A = 1.7 \times 10^{20}$ cm^{-3}), after 30 seconds of RTA at 550°C (10,000X)

Figure 4.52 shows a micrograph of Cr/Au contacts deposited on this wafer and annealed for 60 seconds at 450ºC. The image was taken under a 5kV accelerating voltage at a magnification of 5,000X. The image reveals an amorphous surface with voids formed around the roughness of the wafer surface. Figure 4.53 shows a Cr/Au contact to the same material, annealed for 60 seconds at 450ºC. In this case, there is again an amorphous surface, with voids throughout and circular raised areas approximately 6-8 µm in diameter.

Figure 4.52 SEM micrograph of Cr/Au contact to p-GaAs (N_A = 1.7 x 10^{20} cm^{-3}), after 60 seconds of RTA at 450°C (5,000X)

Figure 4.53 SEM micrograph of Cr/Au contact to p-GaAs (N_A = 1.7 x 10^{20} cm^{-3}), after 60 seconds of RTA at 500°C (5,000X)

4.2.2 Electrolytically Deposited Samples

4.2.2.1 $N_A = 5.3 \times 10^{18}$ cm^{-3}

Figure 4.54 shows a micrograph of a Ni contact, as-deposited on the more lowly doped wafer, by electrolysis at 5 mA/cm^2. The image was taken under a 5kV accelerating voltage at a magnification of 5,000X. The image reveals a polycrystalline structure (grain size of 110 nm) with larger surface deposits up to 7 nm in size. Figure 4.55 shows a Ni contact to the same material, annealed for 60 seconds at 350ºC. The surface of the contact is covered with precipitates with an average size of 115 nm. Some of the larger surface deposits are still visible, but not as pronounced as in the as-deposited sample. An elecrtolytically deposited Ni contact to the same wafer and annealed for 60 seconds at 400°C can be seen in Figure 4.56. Precipitates of approximately 130 nm are distributed across the contact surface. Larger surface deposits appear to have been mostly incorporated into the surface.

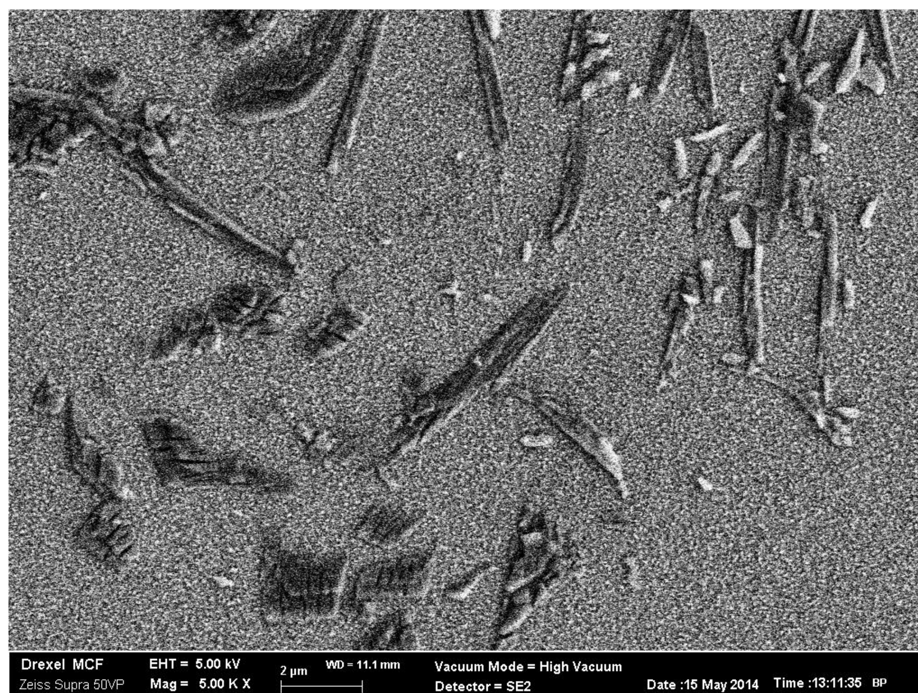

Figure 4.54 Nickel contacts, as-deposited by electrolytic deposition at 5 mA/cm^2 to p-GaAs (N_A = 5.3 x 10^{18} cm^{-3}) (5,000X)

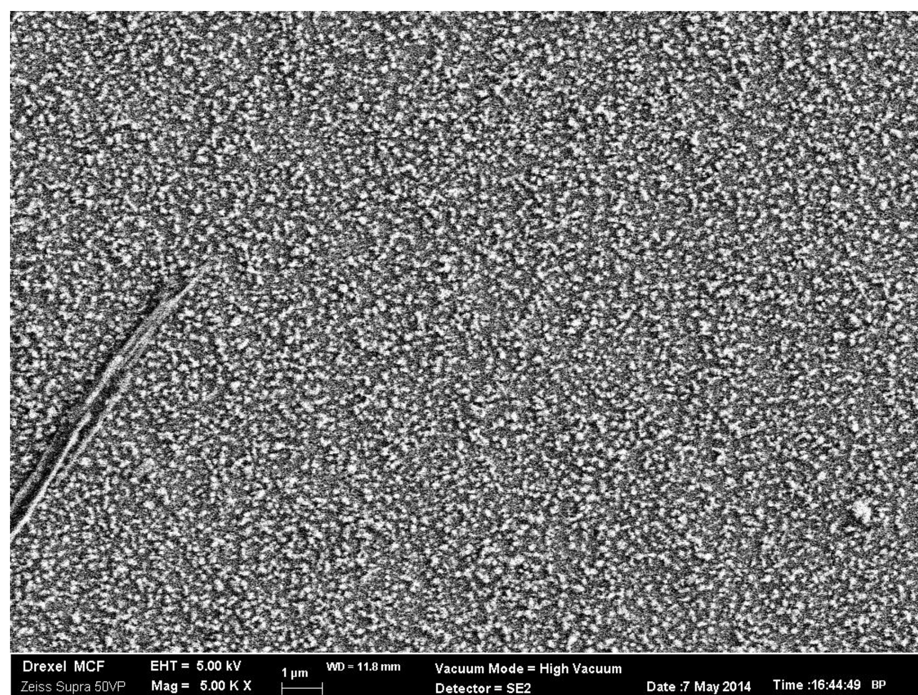

Figure 4.55 Nickel contacts by electrolytic deposition at 5 mA/cm^2 to p-GaAs (N_A = 5.3 x 10^{18} cm^{-3}) after 60 seconds of annealing at 350°C (5,000X)

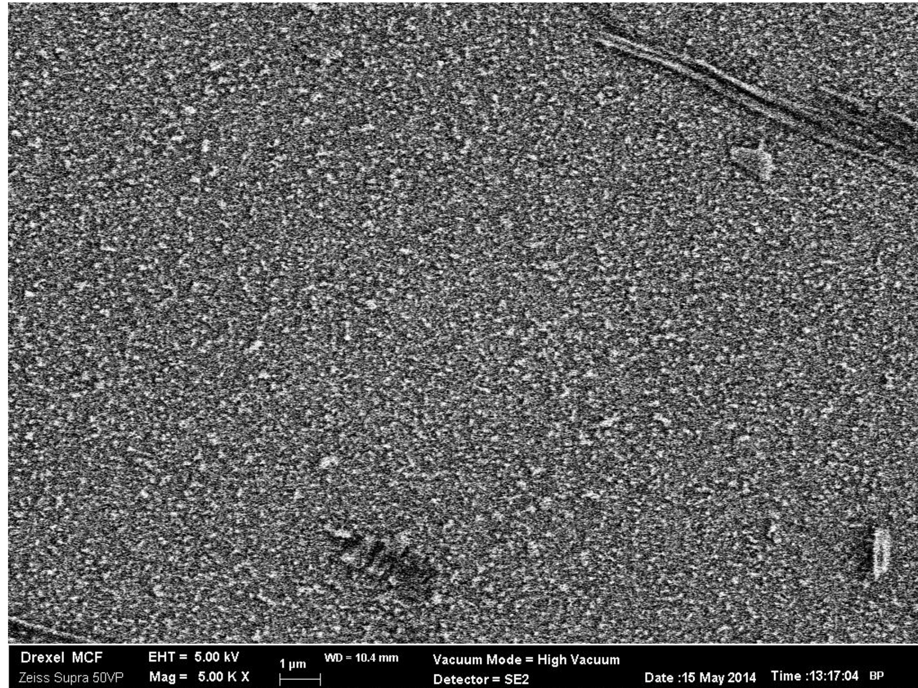

Figure 4.56 Nickel contacts by electrolytic deposition at 5 mA/cm^2 to p-GaAs (N_A = 5.3 x 10^{18} cm^{-3}) after 60 seconds of annealing at 400°C (5,000X)

4.2.2.2 $N_A = 3.0 \times 10^{19}$ cm^{-3}

Figure 4.57 shows a micrograph of a Ni contact, as-deposited on the more highly doped wafer by electrolysis at 2.5 mA/cm^2. The image was taken under a 5kV accelerating voltage at a magnification of 5,000X. The image reveals a polycrystalline structure with 150 nm grains. Figure 4.58 shows a Ni contact to the same material, deposited at 5 mA/cm^2. The resulting polycrystalline structure is characterized by a grain size of 135 nm.

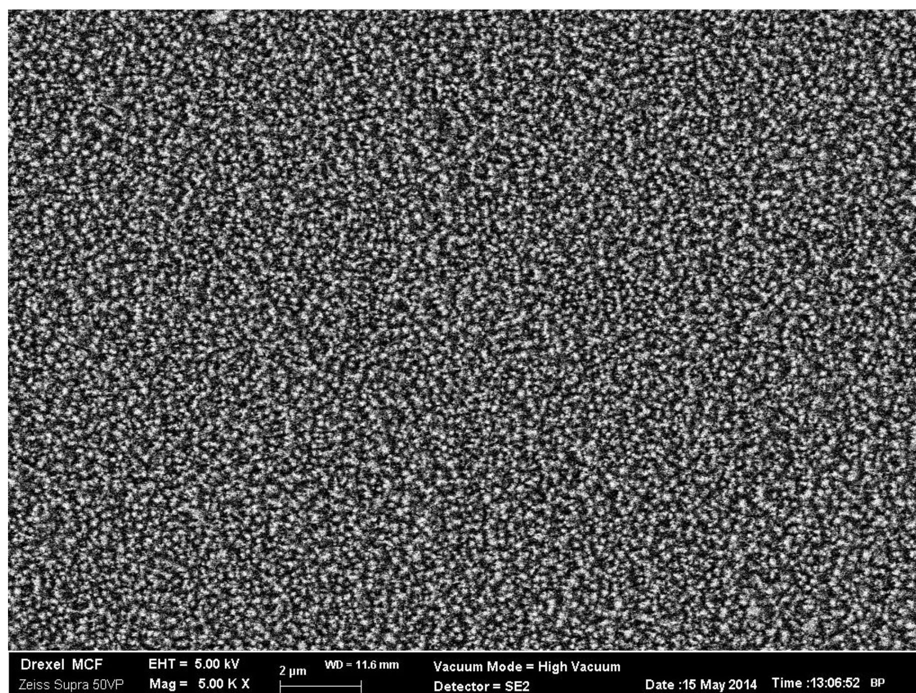

Figure 4.57 Nickel contacts, as-deposited by electrolytic deposition at 2.5 mA/cm^2 to p-GaAs (N_A = 3.0 x 10^{19} cm^{-3}) (5,000X)

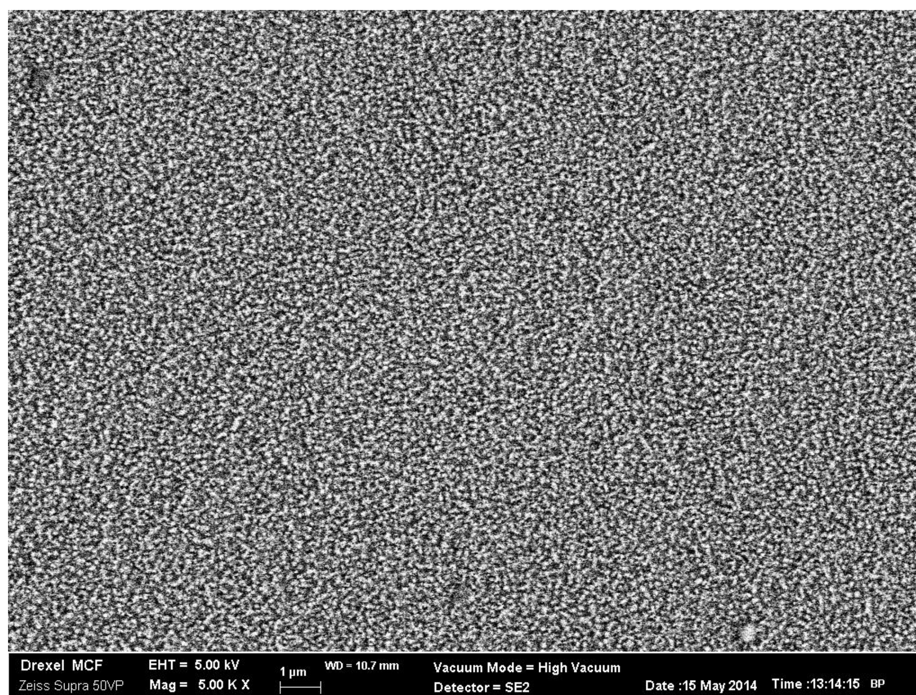

Figure 4.58 Nickel contacts, as-deposited by electrolytic deposition at 5 mA/cm2 to p-GaAs (N_A = 3.0 x 10^{19} cm^{-3}) (5,000X)

4.3 Contact Surface Composition

A qualitative elemental analysis was performed on some sample surfaces by energy-dispersive X-ray spectroscopy (EDS) to verify that the deposited metals were present on the appropriate substrate surfaces. To ensure possible identification of the proper K_α and L_α peaks, an accelerating voltage of 25 kV was used for the analysis. No standard was measured before the sample analysis occurred. Of the non-nickel thermally evaporated contacts, combinations of Au/Zn/Au, Cr/Au, and Cr/Zn/Au metallizations deposited on wafers of the three highest doping levels were analyzed. Only on the wafer of the highest doping level was EDS performed on contacts of all three metallizations. The spectra measured on these contacts yield similar results to those on the others, and for this reason will be the only ones presented.

Figure 4.59 shows an X-ray spectra for two points on a Au/Zn/Au contact to the wafer with $N_A = 1.7 \times 10^{20}$ cm^{-3}. These spectra were measured on an as-deposited sample, and do not differ much from those measured on annealed samples. The proportion of the Zn to Au peaks is in agreement with the amounts deposited.

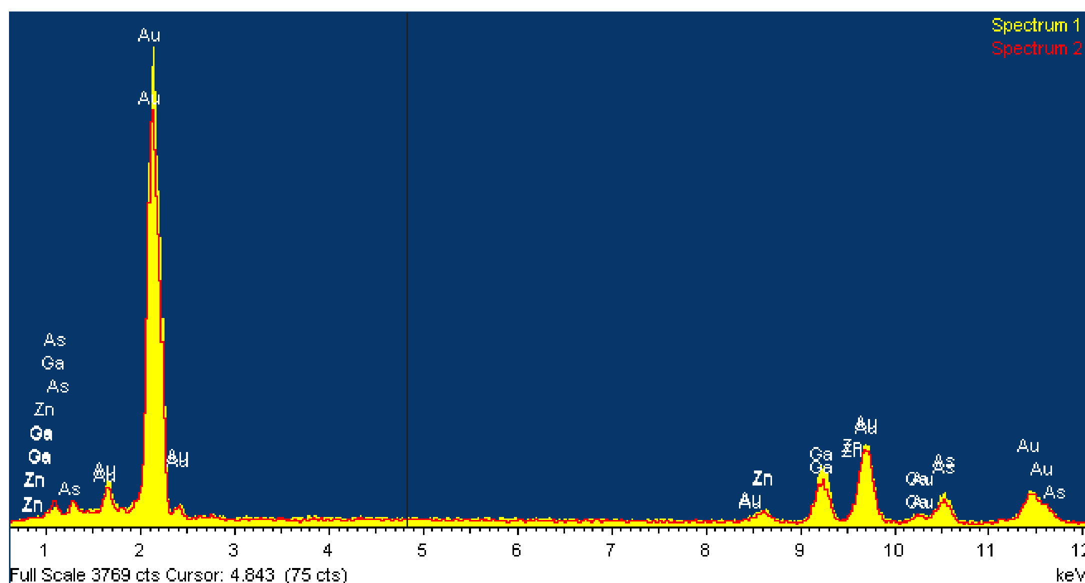

Figure 4.59 X-ray spectra measured by EDS on thermally evaporated Au/Zn/Au contact to p-GaAs (N_A = 1.7 x 10^{20} cm^{-3})

The X-ray spectra and accompanying micrograph resulting from the measurement on Cr/Au contacts to this wafer are displayed in Figure 4.60. It is suggested from the results that the precipitates formed on the surface after annealing at 500°C are composed mostly of Au. Cr is more present on the contact surface, in between the precipitates. The same can be said of contacts of thermally evaporated Cr/Zn/Au metallization to this wafer, after annealing at 550°C. The spectra and accompanying micrograph of this contact are presented in Figure 4.61. In this case, it appears as though an overlayer composed mostly of Au with some Zn was formed, with voids to the GaAs surface containing very small amounts of Cr and Zn.

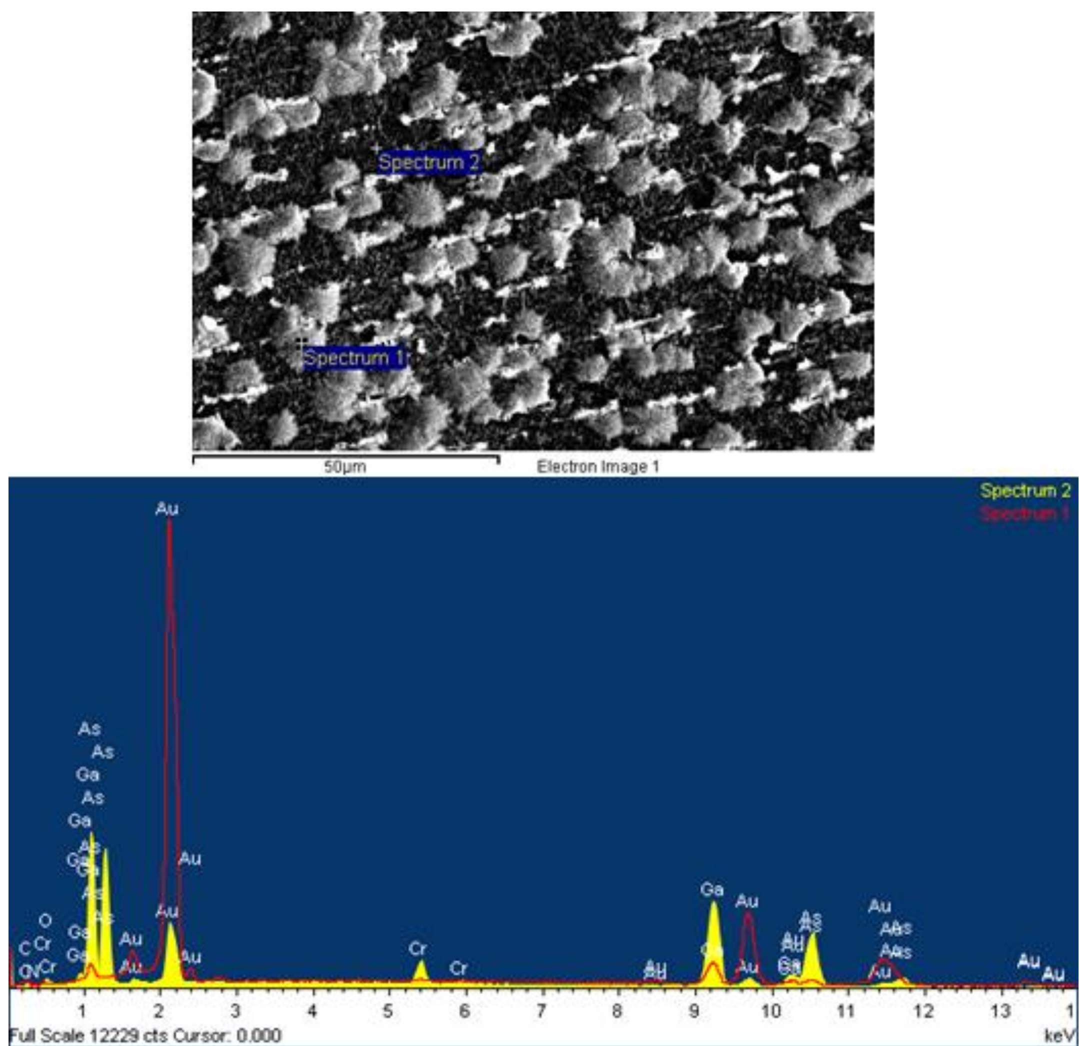

Figure 4.60 X-ray spectra measured by EDS on thermally evaporated Cr/Au contact to p-GaAs ($N_A = 1.7 \times 10^{20}$ cm^{-3}) at positions indicated in the accompanying SEM micrograph

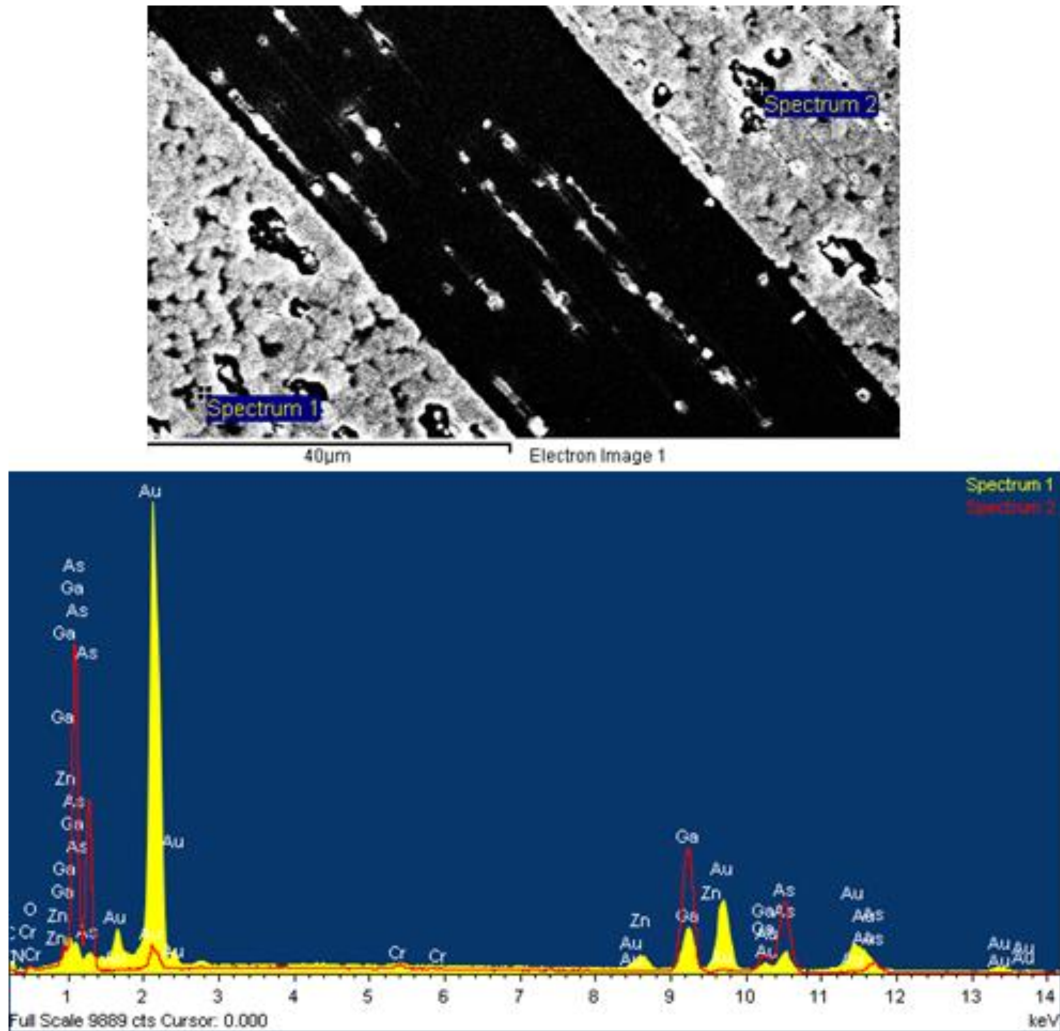

Figure 4.61 X-ray spectra measured by EDS on thermally evaporated Cr/Zn/Au contact to p-GaAs (NA N_A = 1.7×10^{20} cm^{-3}) at positions indicated in the accompanying SEM micrograph

4.4 Discussion

The discussion will begin concerning the thermally evaporated contacts to wafers with doping levels of: N_A = 4.0×10^{16}, 1.0×10^{19}, 4.7×10^{19}, and 1.7×10^{20} cm^{-3}. Contacts to lowly doped wafers ($N_A \leq 1 \times 10^{19}$ cm^{-3}) required annealing before the minimum specific contact resistivity was obtained, and, in some cases, before ohmic contacts were realized at all. This is because, prior to heat treatment, the dominant current flow mechanism is thermionic emission over a relatively high energy barrier. Upon

annealing, the surface carrier concentration of the GaAs increased as a result of doping by Zn or Cr. This further doping of the wafer caused the dominant current flow mechanism to change to tunneling through the barrier, which became so thin that it was essentially transparent to carrier flow, enabling ohmic contact formation.

Predictably, contacts characterized by the lowest specific contact resistivities were deposited onto the most highly doped wafers ($N_A > 1 \times 10^{19}$ cm^{-3}). High doping promoted carrier tunneling through the barrier region, as the depletion layer was thinned with increasing impurity concentration. In these samples, the carrier concentration was high enough that unalloyed ohmic contacts were realized with all metallizations, with the exception of Au/Zn/Au contacts to wafers with $N_A = 1.7 \times 10^{20}$ cm^{-3}. It is possible that the portion of the wafer upon which the Au/Zn/Au metallization scheme was deposited was less heavily doped than the rest of the wafer, due to inherent nonuniformity in carrier concentration across the surface; this anomaly may also have been caused by pre-existing surface roughness on this wafer. After annealing, ohmic contacts were realized with this metallization, and were characterized with specific contact resistivities comparable to those achieved on annealed contacts of the same metallization to the wafer of doping $N_A = 4.7 \times 10^{19}$ cm^{-3}.

After annealing of the contacts to more highly doped wafers, the specific contact resistivities increased in value. This observation is atypical of contacts of these metallizations, based on previous studies. A number of things could be occurring at the metal/semiconductor interface to cause this increase in contact resistivity. As previously mentioned, atomic interdiffusion and compound formation occurs when metal atoms are

deposited onto a semiconductor substrate, and these atoms are known to disrupt the substrate by releasing one or both of the semiconductor species into the metal overlayer. In many cases, chemical reactions that are occurring at the metal/semiconductor interface are desirable to create an ohmic contact; however, some adverse effects may arise upon heat treatment. Delamination of the metal from the substrate is one such adverse effect that commonly occurs after heat treatment at too high temperatures, or for too long times; such metal delamination would understandably cause a rise in contact resistivity. [14]

When ohmic contacts were realized with the as-deposited Cr/Au metallization, they were characterized by the lowest measured specific contact resistivity of all of the metallizations, on the respective wafers. As these contacts have been historically applied to this material, it was expected that they would exhibit a low specific contact resistivity. The binary Au-Cr phase diagram shows that an FCC structure exists at room temperature and at the composition determined by the deposit thickness (0.175 mol% Cr), indicating the formation of Au-Cr solid solution. Chromium is known to be chemically stable on GaAs up to 400°C, with interfacial reactions becoming more pronounced after annealing at 500°C [41]. Referring to the X-ray spectra obtained by EDS of the as-deposited Cr/Au sample, the presence of Ga on the contact surface is higher than that of As. This lack of As at the surface could indicate an accumulation of As at the interface of the metal and semiconductor; however, this has not been verified by experimental testing. This type of interfacial As accumulation has been observed by Liliental-Weber et al. to decrease with annealing as the As outdiffuses through Cr grain boundaries; this loss of excess As accumulation at the interface is correlated to an increased barrier height upon low temperature annealing [5]. This behavior can be rationalized when viewing the respective

Pauling electronegativities of the materials involved. Since As is more electronegative (Pauling electronegativity 2.0) than Cr (Pauling electronegativity 1.6), it is assumed that the driving force for outdiffusion of As is high, compared to that of Ga (Pauling electronegativity 1.7) [41]. Additionally, as Au and As only have a slight mutual solid solubility, it is assumed that the Au acted primarily to displace As in the substrate, and combine with Ga, further promoting the outdiffusion of As and its subsequent volatilization at the surface [42].

In cases where only the other two metallizations made ohmic contacts (low doping), Au/Zn/Au contacts exhibited the lower resistances; however, Cr/Zn/Au contacts did exhibit specific contact resistivities comparable to those of Au/Zn/Au and Cr/Au. In the case of Cr/Zn/Au, it is probable that the initial Cr layer acted mainly to improve contact adhesion while still allowing for Zn penetration into the GaAs substrate, with the top Au layer acting as a cover prohibiting the loss of Zn by Au/Zn interdiffusion. At room temperature, Au and Zn react to form various AuZn phases until 300°C, when a uniformly distributed Au_3Zn phase is realized; thus, mass Zn penetration into the GaAs substrate does not occur until annealing is performed above 350°C [43]. The highly conductive Au layers also must serve to reduce the sheet resistance of the contact, hence the lower specific contact resistivity in Au/Zn/Au metallizations compared with Cr/Zn/Au. Due to the similarity in specific contact resistivities between Cr/Zn/Au and Au/Zn/Au contacts, it is assumed that the initial thin Cr layer does not contribute much to the conductivity in the film.

The cleanliness of the semiconductor substrate has a great effect on the electrical properties of the metal contact. Impurities present on the semiconductor surface prior to metal deposition have been shown to influence the orientation relationship between the metal grains and the semiconductor. Orientation relationships are also greatly influenced by the presence of oxides on the semiconductor surface. Studies of Cr films on GaAs have shown that Cr readily reacts with both Ga and As, as well as with native GaAs oxides; annealing of these films on GaAs substrates containing impurities resulted in a substantial increase in Schottky barrier height. The increase in barrier height is attributed to void formation in the metallization which allows As escape during the annealing. [14] Oxygen diffusion to the interface has also been shown to increase barrier heights. This effect occurs when the metals used have a low free energy, as is the case with Au and Ni, and don't react with the oxide. [44]

The thermally evaporated Ni contacts were characterized by specific contact resistivities on the order of those of the other, more standard metallization schemes. No direct comparison can be made, as the wafer doping levels were slightly different, but an approximate comparison shows very similar results. For example, contact resistances of those Ni contacts deposited on the wafer with $N_A = 3.0 \times 10^{19}$ cm^{-3} were in between contact resistances measured on contacts deposited onto wafers of 1.0×10^{19} cm^{-3} and 4.7×10^{19} cm^{-3}.

Interfacial relationships between GaAs and vacuum deposited Ni were studied by Lahav et al [45]. The group reports the formation of Ni_2GaAs at 200-350°C, and its subsequent decomposition at 450°C. This phase decomposition is attributed to NiAs

precipitation and transformation to NiGa, and is associated with a decrease in Schottky barrier height and a transition to ohmic behavior. As the contacts studied in this work were ohmic as deposited, it is assumed that this reaction occurred at temperatures greater than 350°C to lower the barrier height, thus reducing specific contact resistivity.

Electrolytically deposited Ni contacts had comparable resistivities to those of the Ni contacts thermally evaporated, exhibiting the practicality of replacing thermal evaporation with electrolytic deposition for contact fabrication. Ohmic contacts were realized as-deposited on all electrolytically deposited samples. After annealing, contacts deposited on the wafer with $N_A = 5.3 \times 10^{18}$ cm^{-3} exhibited a lower specific contact resistivity, with the lowest values being achieved after annealing at 450°C. What has probably occurred at this temperature is a lowering of the barrier height, associated with the decomposition of the Ni_2GaAs phase. Lahav et al. mentioned the high reactivity of Ni with GaAs at low temperatures and discussed the possibility of a change in current flow mechanism (e.g. from thermionic field emission to field emission) to be caused by Ni in-diffusion and Ga out-diffusion [45]. It is possible that this diffusion occurred during deposition of contacts to the wafer with $N_A = 3.0 \times 10^{19}$ cm^{-3}, leading to as-deposited ohmic contacts.

CHAPTER 5

CONCLUSION AND FUTURE RECOMMENDATIONS

The aim of this research was to investigate different metallization schemes to form ohmic contacts to novel intermediate band solar cells. The current front ohmic contacts to this material are fabricated of a Cr/Au metallization scheme thermally evaporated under a high vacuum. This research was designed to investigate different metallizations (Au/Zn/Au, Cr/Zn/Au, and Ni) and different fabrication techniques (thermal evaporation and electrolytic deposition).

Ohmic contacts were achieved in all cases studied in this work. The Cr/Zn/Au metallization was of particular interest, as this metallization scheme has not been so extensively studied as Au/Zn/Au has. The Cr/Zn/Au contacts performed similarly to those of both Cr/Au and Au/Zn/Au. Low specific contact resistivities were obtained with this metallization without annealing for highly doped wafers. This is encouraging, but more work must be done to lower the contact resistances of the as-deposited metallization even further. In this work, the already used as-deposited Cr/Au contacts remained of the lowest specific contact resistivity. Should a different contact scheme be desired, both Au/Zn/Au and Cr/Zn/Au could be considered as substitutes for Cr/Au; however, an annealing process would be required to obtain low specific contact resistivities with these metallizations deposited on lowly doped wafers.

Nickel contacts were also of interest in this research; electrolytic deposition of Ni was especially interesting as a more economical deposition technique. Ni successfully

deposited onto p-GaAs wafers both by thermal evaporation and by electrolytic deposition, and formed ohmic contacts in both cases. Specific contact resistivities measured on these contacts were low enough to make Ni a candidate for replacing the current metallization scheme. Additionally, resistivities of contacts deposited by electrolytic deposition were comparable to those of contacts deposited by thermal evaporation, indicating that electrolytic deposition may be considered as a contact fabrication technique for these cells. Electrolytic deposition may be introduced to the cell fabrication process rather easily, and would save time and money in the production process. Additionally, depositing contacts by electrolysis would save on material costs, as less starting material would be required to cover the contact area, due to the more direct nature of deposition by this method, compared with that of thermal evaporation.

An experimental study of interfacial reactions between the metal contacts and the GaAs substrate could lead to a better understanding of the changes in specific contact resistivities of these contacts before and after heat treatment. Once the reactions occurring at the metal/semiconductor interfaces are better understood, the heat treatment can be adjusted to allow for the formation of phases and compounds which promote a low contact resistance.

The study of metal/semiconductor interfacial regions can be accomplished by transmission electron microscopy, which would allow for the determination of new phase formation, orientation relationships, and stoichiometry changes. Photoemission investigations may also be carried out to understand interfacial phenomena including chemical reactions, out-diffusion of substrate species, and adatom-induced substrate

disruption. Low-energy electron diffraction can be utilized to obtain structural information. [14] Rutherford backscattering spectrometry can reveal the presence of interfacial phase formation on a micron scale. Chemical reactions and diffusion at metal-semiconductor interfaces can be studied with X-ray photoelectron spectroscopy. Scanning tunneling microscopy can employ lateral scanning to reveal variations in electronic properties related to overlayer and surface morphology features. [46] Secondary ion mass-spectroscopy profiling can reveal whether there exists an accumulation of oxygen at the interface.

All contacts in this work were deposited onto p-GaAs wafers specifically for contact resistance measurement by TLM. Future research should concern deposition of the same contacts to wafers in a solar cell pattern; after, efficiency testing should be performed on these cells. Accelerated aging tests may also be performed, to ensure that the contact materials do not degrade the solar cell devices.

List of References

[1] Next Generation Photovoltaics: High efficiency through full spectrum utilization, Institute of Physics Publishing, Bristol, UK, 2004.

[2] J. Tsao, N. Lewis, G. Crabtree, Sandia National Laboratories, 2006, pp. 24.

[3] A. Martí, N. López, E. Antolín, E. Cánovas, C. Stanley, C. Farmer, L. Cuadra, A. Luque, Thin Solid Films, 511-512 (2006) 6.

[4] D.K. Schroder, D.L. Meier, Electron Devices, IEEE Transactions on, 31 (1984) 637-647.

[5] Z. Liliental-Weber, M.A. O'Keefe, Journal of Vacuum Science & Technology B, 7 (1989) 1022-1026.

[6] V.L. Rideout, Solid-State Electronics, 18 (1975) 541-550.

[7] T.C. Shen, G.B. Gao, H. Morkoç, Journal of Vacuum Science & Technology B, 10 (1992) 2113-2132.

[8] L. Cuadra, A. Martí, A. Luque, Thin Solid Films, 451-452 (2004) 6.

[9] A. Luque, A. Martí, C. Stanley, N. López, L. Cuadra, D. Zhou, J.L. Pearson, A. McKee, Journal of Applied Physics, 96 (2004) 903-909.

[10] W. Schottky, Phys., 113 (1939) 47.

[11] N. Braslau, Journal of Vacuum Science & Technology A, 4 (1986) 3085-3090.

[12] A. Piotrowska, E. Kaminska, Thin Solid Films, 193–194, Part 1 (1990) 511-527.

[13] R.H. Williams, Surface Science, 251-252 (1991) 9.

[14] L.J. Brillson, Contacts to semiconductors, Noyes, William Andrew Publishing, Park Ridge, NJ, 1993.

[15] A.G. Baca, C.I.H. Ashby, Institution of Engineering and Technology, pp. 179-202.

[16] F. Ren, Chemistry, Polytechnic University, Ann Arbor, 1991, pp. 117.

[17] A. Piotrowska, A. Guivarc'h, G. Pelous, Solid-State Electronics, 26 (1983) 179-197.

[18] N. Inoue, T. Higashino, K. Tanahashi, Y. Kawamura, Journal of Crystal Growth, 227–228 (2001) 123-126.

[19] L. Gert, W. Cory, Google Patents, 2006.

[20] W. Schokley, A. Goetzberger, R.M. Scarlett, Air Force Atomic Laboratory, Wright-Patterson Air Force base, Ohio, 1964, pp. 152.

[21] H.H. Berger, Solid-State Electronics, 15 (1972) 145-158.

[22] Y. Lu, T. Kalkur, C.P. de Araujo, Journal of The Electrochemical Society, 136 (1989) 3123-3129.

[23] D.E. Kren, A.A. Rezazadeh, P.K. Rees, Electronics Letters, 28 (1992) 1248-1250.

[24] E. Kamińska, A. Piotrowska, E. Mizera, E. Dynowska, Thin Solid Films, 246 (1994) 143-150.

[25] J.F. Thiery, H. Fawaz, A. Leroy, G. Salmer, Journal of Vacuum Science & Technology B, 13 (1995) 2130-2133.

[26] G. Stareev, H. Künzel, G. Dortmann, Journal of Applied Physics, 74 (1993) 7344-7356.

[27] C.-H. Wu, S.-M. Liao, K.-C. Chang, Materials Science and Engineering: B, 117 (2005) 205-209.

[28] K. Prasad, Materials Science and Engineering: B, 27 (1994) L21-L23.

[29] A. Lennon, Y. Yao, S. Wenham, Progress in Photovoltaics: Research and Applications, 21 (2013) 1454-1468.

[30] J. Lee, H. Kwon, S. Lee, Electron. Mater. Lett., 7 (2011) 349-352.

[31] D.M. Mattox, ASM Handbook Online, ASM International, 1998, pp. 556-572.

[32] H.H. Wehmann, S. Aytac, A. Schlachetzki, Solid-State Electronics, 26 (1983) 149-153.

[33] M. Harris, S.M. Hubbard, M. Kassis, S. Polly, C.G. Bailey, P. Jarosz, Photovoltaic Specialists Conference (PVSC), 2009 34th IEEE, 2009, pp. 002096-002101.

[34] M. Schlesinger, M. Paunovic, Modern Electroplating (5th Edition), Wiley, Hoboken, NJ, USA, 2011.

[35] G.A. DiBari, Metal Finishing, 100, Supplement 1 (2002) 257-274.

[36] S. Benhenda, N. Ben Jemaa, M. Bourir, Components, Packaging, and Manufacturing Technology, Part A, IEEE Transactions on, 17 (1994) 303-308.

[37] M. Holm, T.J. O'Keefe, Journal of Applied Electrochemistry, 30 (2000) 1125-1132.

[38] J. Ward, A. Duda, D.J. Friedman, J. Geisz, W. McMahon, M. Young, National Renewable Energy Laboratory, 2013.

[39] R. Castanedo, R. Asomoza, G. Jiménez, S. Romero, J.L. Peña, Journal of Vacuum Science & Technology A, 4 (1986) 814-817.

[40] J.-K. Ho, C.-S. Jong, C.C. Chiu, C.-N. Huang, C.-Y. Chen, K.-K. Shih, Applied Physics Letters, 74 (1999) 1275-1277.

[41] T.S. Huang, M.S. Yang, Journal of Applied Physics, 70 (1991) 5675-5683.

[42] T.C. Thomas, R.S. Williams, Journal of Materials Research, 1 (1986) 352-360.

[43] E. Kamińska, A. Piotrowska, A. Barcz, J. Adamczewska, Solid-State Electronics, 29 (1986) 279-286.

[44] J.W. Lathrop, Proceedings of the Flat-Plate Solar Array Project Research Forum on Photovoltaic Metallization Systems, Space Photovoltaic Research and Technology, Pine Mountain, Georgia, 1991.

[45] A. Lahav, M. Eizenberg, Y. Komem, Journal of Applied Physics, 60 (1986) 991-1001.

[46] L.J. Brillson, Surface Science, 299–300 (1994) 909-927.